1-1-2012

Investigation of the absorptive potential of polymeric nanoparticles across the lungs and their development for efficient systemic delivery following pulmonary administration

Abdul khader Mohammad
Wayne State University,

Recommended Citation

Mohammad, Abdul khader, "Investigation of the absorptive potential of polymeric nanoparticles across the lungs and their development for efficient systemic delivery following pulmonary administration" (2012). *Wayne State University Dissertations.* Paper 552.

INVESTIGATION OF THE ABSORPTIVE POTENTIAL OF POLYMERIC NANOPARTICLES ACROSS THE LUNGS AND THEIR DEVELOPMENT FOR EFFICIENT SYSTEMIC DELIVERY FOLLOWING PULMONARY ADMINISTRATION

by

ABDUL KHADER MOHAMMAD

DISSERTATION

Submitted to the Graduate School

of Wayne State University,

Detroit, Michigan

in partial fulfillment of the requirements

for the degree of

DOCTOR OF PHILOSOPHY

2012

MAJOR: PHARMACEUTICAL SCIENCES
(Pharmaceutics)

Approved by:

Advisor Date

DEDICATION

Dedicated to my parents Janab Mohammad Ashraf Sahab and Sayyida Qamar Sultana Sahiba

ACKNOWLEDGEMENTS

It is with a profound sense of gratitude that I thank Dr. Joshua Reineke, my advisor. This space would certainly not be enough to write about how he has guided and shaped me through this academic journey. His constant encouragement, guidance, and unflinching support have been extremely instrumental in the evolution of my personality through the years. His patience in teaching me several techniques first hand and discussions with regards to research have helped me tremendously. His accessibility any time of the day has hugely helped me navigate this difficult journey with relative ease. I can categorically say that without his encouragement and support, I would not evolve into the person that I am today. I have learnt a great deal from his excellent mentorship during these years. His mentorship and encouragement have taught me to think independently and strive for scientific excellence. Thank you Dr.Reineke, for everything I learnt from you with regards to science, research, and many other things that are not found in books. You have influenced me in an enormous way and I am sure that I will continue to be influenced by the things I learnt from you for the rest of my career. I will ever be indebted to you for all I learnt from you directly and indirectly.

To my committee members, Dr. Anjan Kowluru, Dr. David Oupicky, Dr. Guangzhao Mao, and Dr. Judith Whittum-Hudson, thank you for your critical analysis, suggestions and advice. Your critical evaluation of my work had only made it better and put me through a process of learning and taught me how to take criticism and address it. Thank you all for investing so much of your precious time and effort in polishing me and help me better my science. I would like to thank Dr. Randall Commissaris for helping me out with statistics for my data.

To Dr.George Corcoran, Chair, Dept. of pharmaceutical sciences, thank you for giving me the wonderful opportunity to work in this department. Under you meticulous leadership, the department has experienced a tremendous transformation and growth probably unprecedented in other departments. Your welcoming attitude and warmth always made me feel good.

I would like to thank the past postdoctoral fellows in my lab Dr. Mingguang Li and Dr. Qinghe Zhao for their camaraderie, intellectual input and suggestions regarding my research. I would also like to thank Lenah for providing help with some experiments.

It was my absolute pleasure knowing Dr.Ismail and Dr.Balaji during the course of my study. My friendship with them has grown strong over the years and I will cherish the time we spent together and hope to consolidate our friendship in the years to come. A very special thanks for both of you for being instrumental in my next step.

I would also like to express my appreciation to Dr. Sandro da Rocha and Dr. Olivia Merkel for their suggestions with regard to my research in our lung group meetings.

Last but not the least, I would like to respectfully express my deepest appreciation and gratitude to my loving parents, siblings and family. Their limitless love, support, and patience have been a source of strength throughout my endeavors. Their innumerable sacrifices throughout my life have been instrumental in carrying me to this point in my academic endeavor. I owe every one of my achievements and successes to my wonderful parents and siblings. I would never ever have been able to achieve what I did in my life if it was not for their love, care, sacrifice, and unflinching support in times of great adversity and otherwise. Finally, it goes without saying that if it was not for the special mercy of the almighty I would not have accomplished anything ever.

TABLE OF CONTENTS

Chapter 1

Chapter 2

Chapter 3

Chapter 4

Chapter 5

LIST OF TABLES

LIST OF FIGURES

LIST OF ABBREVIATIONS

d_{ae}	Aerodynamic diameter
CME	Clathrin mediated endocytosis
LDH	Lactate dehydrogenase
ALND	Axillary lymph node dissection
SLND	Sentinel lymph node dissection
SNL	Sentinel lymph nodes
NSABP	National Surgical Adjuvant Breast and Bowel Project
ALN	Axillary lymph node
CTL	Cytotoxic T lymphocyte responses
ALN	Axillary lymph nodes
PLGA	Poly (lactic-co-glycolic) acid
PN	Polystyrene nanoparticles
GPC	Gel permeation chromatography
HPLC	High Performance Liquid Chromatography
AVMA	American Veterinarian Medical Association
IACUC	Institutional Animal Care and Use Committee
OLAW	Office of Laboratory Animal Welfare
DLS	Dynamic light scattering
BLN	Brachial lymph nodes
MLN	Mesenteric lymph node

CLN	Cervical lymph nodes
BAL	Bronchoalveolar lavage
RI	Refractive index
H&E	Hematoxylin and eosin
TEM	Transmission electron microscopy
LN	Lymph nodes
RES	Reticuloendothelial system
PIN	Phase inversion nanoencapsulation
T_g	Glass transition temperature
PSH	Polyoxyethylene sorbitol hexaoleate
M_w	Weight-average molecular weight
M_n	Number-average molecular weight
M_p	Peak-average molecular weight
PDI	Polydispersity index
PEG	Poly (ethylene glycol)
CDF	3, 4-difluorobenzo curcumin
FBS	Fetal bovine serum
THF	Tetrahydrofuran
PVA	Polyvinyl alcohol
DMSO	Dimethyl sulfoxide
MTT:	3-(4,5-dimethylthiazol-2-yl)-2,5-diphenyltetrazolium bromide:
PBS	Phosphate buffered saline
CDFNP	CDF-loaded nanoparticle formulation F2

IC_{50}	Minimum inhibitory concentration required to kill 50% of viable cells

CHAPTER 1

1. Introduction

This chapter begins with a discussion of the anatomy and physiology of the lungs, and then reviews the transport of drugs (small molecules and macromolecules) from the lungs into systemic circulation. It then addresses the applicability of nanoparticles in pulmonary drug delivery and covers in detail the different mechanisms available for endocytosis of nanoparticles. In addition, this section covers the potential of nanoparticles in clinically relevant diseases such as the treatment of metastatic breast cancer with nodal involvement.

1.1 Anatomy and physiology of the lungs

The lungs have an ancient history of use as a route of delivery for medicines intended for systemic or local use. The oldest available record of using lungs for therapeutic purpose dates back to 1500BC where Egyptians inhaled medicinal vapors. A brief history of important events in pulmonary drug delivery is provided in **table 1**.

Year	Formulation/Device	Molecule(s)	Disease
1500BC	Egyptians used ‘vapors’	Not known	Not known
1662AD	Bennet’s inhalation treatment	Not known	Tuberculosis
1802	Potter’s cigarettes	Not known	Asthma
1860	Sales-Giron’s portable nebulizer	Not known	Not known
1925	Aqueous/nebulizer	Insulin	Diabetes
1945	Aqueous/nebulizer	Penicillin	Lung infections
1951	Aqueous/nebulizer	Isoprenaline	Asthma
1955	Aqueous/nebulizer	Hydrocortisone	Asthma
1956	First metered-dose inhaler (MDI) (Freon)	Albuterol	Asthma
1960	First dry powder inhaler (DPI)	Noradrenaline	Asthma
1988	First multidose DPI	Terbutaline	Asthma
1996	First protein aqueous/nebulizer	DNAse	Cystic fibrosis
1997	First hydrofluoroalkane MDI	Albuterol	Asthma
1998	First antibiotic aqueous/nebulizer	Tobramycin	Cystic fibrosis
2006	First protein DPI	Insulin	Diabetes

Table 1: History of pulmonary drug delivery of medicines. (Adapted from ref. 5)

What makes lungs an important route for drug delivery is the fact that they have a large alveolar surface area of more than 100 m^2 [1], high solute permeability, limited proteolytic activity [2], very thin alveolar epithelium (0.2 μm), and extensive vasculature [3]. The respiratory tract can be divided into two regions: (a) the conducting region consisting of nasal cavity, pharynx, trachea, bronchi, and bronchioles; and (b) the respiratory region consisting of the respiratory bronchioles and alveoli [4]. The trachea divides into two main bronchi which further divide into bronchioles and the bifurcations that begin at trachea continue through 23 stages. The airways undergo about 16-17 bifurcations after which the alveolar region begins (**figure 1**). From **figure 2** we can see that the cellular shape and structure changes drastically from airways to the alveoli [5].

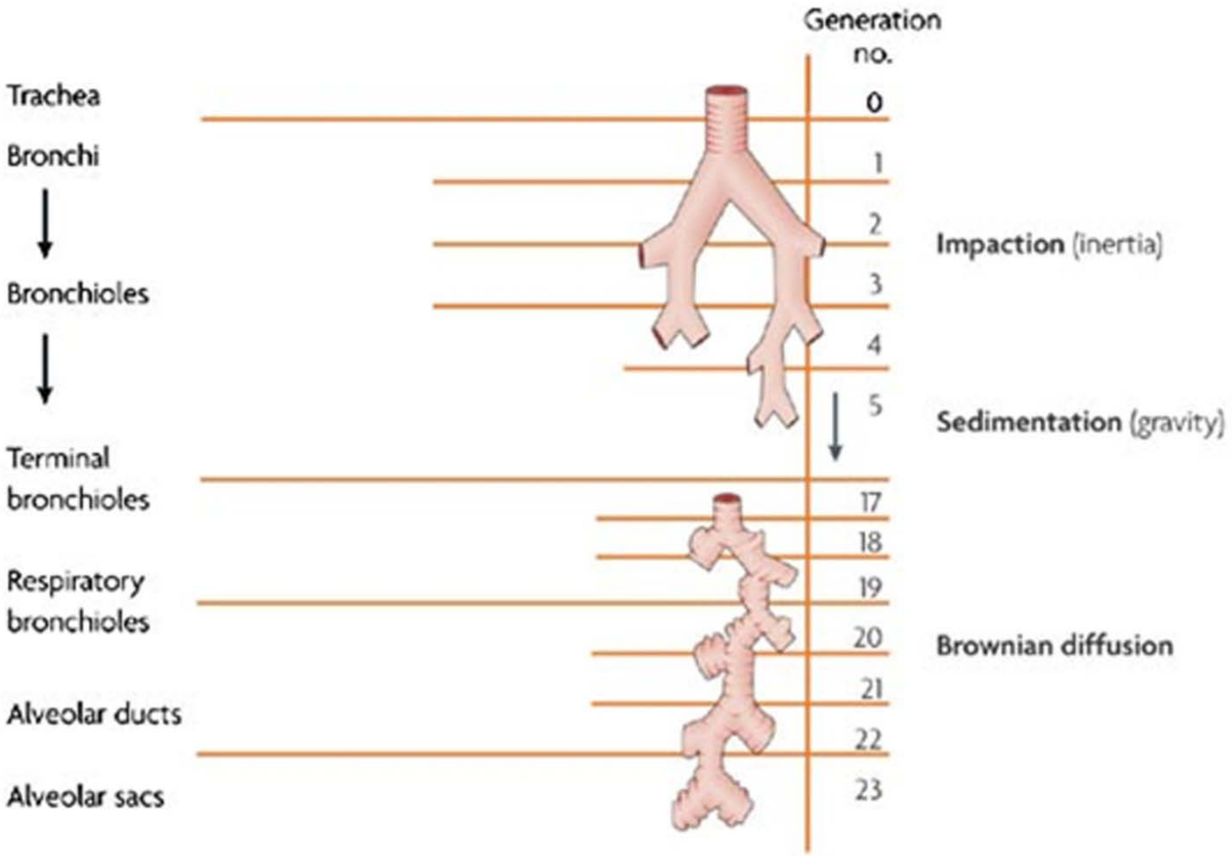

Figure 1. Schematic of airway branching in the human lung. (Adapted from ref. 5)

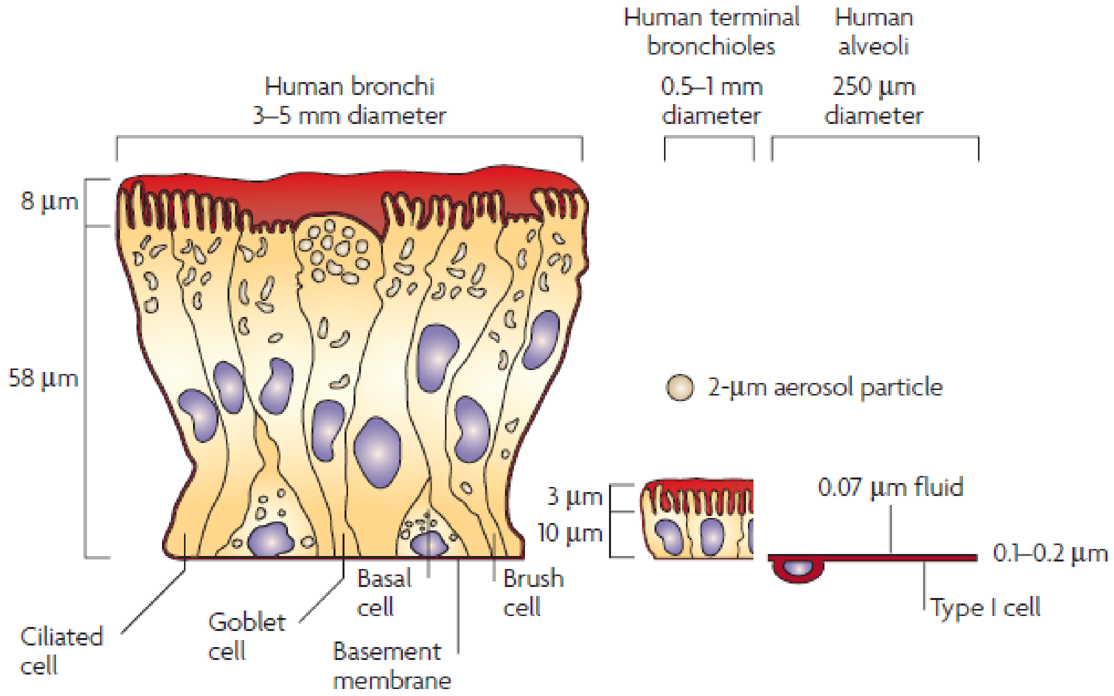

Figure 2. Schematic depicting the differences in epithelial cells at different sites in the lungs. (Adapted from ref. 5)

The airway epithelium is made up of at least four cell types including the basal cell (progenitor cell), ciliated cell, goblet cell, and the clara cell whereas the alveolar epithelium is mainly composed of type I and type II alveolar cells [2], also known as pneumocytes. In the airways, the distance covered by the air-blood barrier is about 30-40 µm whereas it decreases to approximately 500 nm (60-80 times less as compared to that in the upper airways) in the alveolar region [6]. The mucus lining of the airways is about 5-10 µm in thickness [6] which presents a formidable barrier for the transport of substances across the upper airways (trachea). In addition to the thickness of the airways, the mucociliary escalator in the airways continuously pushes particulate matter upwards to be eventually expectorated into the stomach. Particles deposited in the upper airways are swept out efficiently whereas those deposited in the deep airways are eliminated by the mucociliary escalator over a period of about 24 hours [5]. The ciliated epithelial cells cover about 30-65% of the airway epithelial cells in the human respiratory tract. Each epithelial cell has about 200 cilia of 5-6 µm in length each and a density of 6-8 per μm^2. In a normal individual the mucociliary clearance rate is about 10mm/min. The number of ciliary epithelial cells decreases as the airways become smaller. In the trachea, the ciliary epithelial cells constitute 53% of the cell population, whereas in the first airway generation they make up 45% of the cell population and in the fifth airway generation they constitute only 15% of the cell population [7]. Furthermore, the respiratory tract contains dendritic cells which are present above and beneath the basement membrane of epithelial cells [8]. They are present in higher numbers in the upper respiratory tract (600-800 per mm^2) and their number decreases significantly down the respiratory tract and reaches 75 per mm^2 in the peripheral lung. Dendritic cells in the epithelium of respiratory tract detect, process, and transport foreign antigenic material to the local lymph nodes and present them to the naïve T cells present in the paracortical region of the lymph nodes [9, 10]. The respiratory tract epithelium also contains γδ T-cells and natural killer (NK) cells as part of the innate immunity independent of dendritic cells [8]. Additionally, the airways contain B-lymphocytes, eosinophils, mast cells, and basophils which are mainly effector cells in response to hypersensitivity reactions [8].

As we move further down the respiratory tract, the alveolar region begins after about 17 bifurcations. There are an estimated 52 billion alveolar epithelial cells [11] and about 500 million alveoli in the lungs of a normal human being [12]. On average, each human alveolus has 40 type I and 67 type II cells both of which form the alveolar epithelium (**figure 3**). Though the type II cells are more in number, the area covered by type I cells is about 95% of the alveolar epithelium. Type I cells have a very thin cell body with long membranous extensions whereas type II cells possess a more cuboidal morphology. Type I alveolar cells perform the function of gaseous exchange whereas the function of type II cells is to secrete lung surfactant while also acting as progenitor for type I cells [2, 13]. Furthermore, the type II cells also play a role in ion transport and alveolar repair in response to injury [14]. The thickness of lung surfactant layer secreted by type II cells is only about 20-80 nm. The pulmonary surfactant is composed of phospholipids (80%), neutral lipids (5-10%), and proteins (8-10%) [13]. There are four main surfactant proteins SP-A, SP-B, SP-C, and SP-D. The lipophilic SP-B (~8 kD) and SP-C (~4 kD) along with the phospholipids take part in reducing the surface tension at the air-liquid interface to prevent alveolar collapse. The hydrophilic SP-A (~28-36 kD) and SP-D (~43 kD) play an important role in the immune system where they bind to various bacteria, viruses, and allergens. By binding to pathogens and particulates, these proteins modulate their interaction with lung cells in addition to modulating the inflammatory immune response [15]. Each human alveolus is continuously monitored by 12-14 macrophages which try to engulf insoluble particulate matter deposited in the alveoli [5, 12]. Particles of diameter less than 260 nm can escape phagocytosis by these macrophages whereas those with diameter between 1-3 µm are effectively phagocytosed [12]. In addition to macrophages, dendritic cells are present in several lung regions including the trachea, bronchi, alveoli, and visceral pleura [16, 17]. A recent study has shown convincing evidence that the alveolar macrophages also transport antigens to the lung draining lymph nodes [18]. This is a new revelation since it was commonly believed that only dendritic cells had migratory capacity to the lymph nodes for antigen transport. Previous studies attempting to elucidate the migratory potential of alveolar macrophages to the draining suffered serious drawbacks in that they were unable to differentiate between dendritic cells and alveolar macrophages [18]. Besides dendritic cells and alveolar macrophages, the alveolar region contains lymphocytes (CD4 cells, CD8 cells, NK cells, and B cells), neutrophils, immunoglobulins (IgG), and opsonins (surfactant, C-reactive protein, and fibronectin) [8].

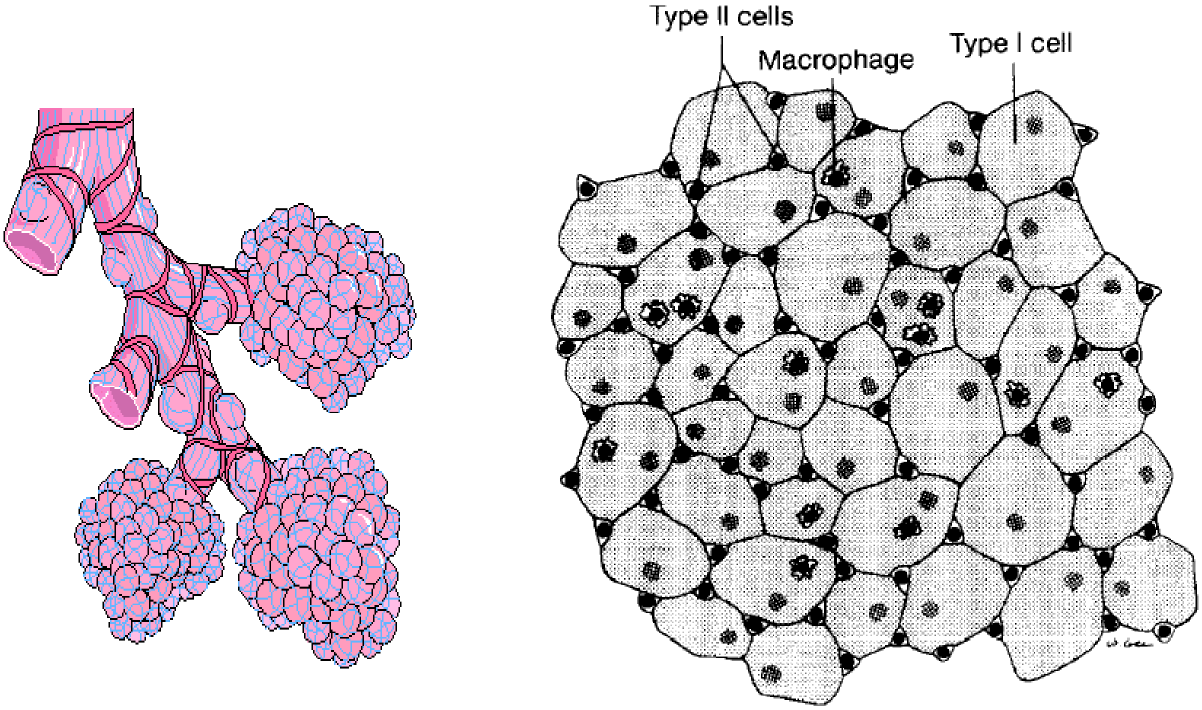

Figure 3. Schematic of a single flattened alveolus (to the right). (Adapted from ref. 2) The image on the left represents groups of alveoli; each spherical structure within the alveoli is an alveolus.

1.2 Lymphatics of the lungs

The lymphatic system which consists of lymph vessels and lymphoid organs plays an important role in maintaining normal fluid balance in tissues, immune vigilance, and adsorption of digested fats. The lymph vessels drain interstitial fluid from tissues and transport the lymph towards the venous system. Transport of fluid and macromolecules from tissues proceeds unidirectionally through a branching hierarchy in the lymph vessels. The lymphocytes and antigen presenting cells enter the lymph capillaries in the periphery and migrate to the lymph nodes via lymphatic vessels [19]. The lymph nodes perform the function of filtering, trapping, and processing cellular debris, colloidal material, bacteria, antigens, as well as other substances [20].

The lungs have a well organized system of lymphatic drainage via a superficial subpleural lymph plexus and a deep plexus of lymph vessels that accompany the bronchi [21]. The lymph vessels of lungs drain through the hilar lymph nodes (also known as bronchopulmonary lymph nodes) and from there to the tracheobronchial lymph nodes which drain in the bronchomediastinal lymph trunks on each side [21]. The mediastinal trunks usually open directly into the junction of the jugular and subclavian veins. However, sometimes the right mediastinal trunk ends in the right lymph duct and the left mediastinal trunk in the thoracic duct [22]. In such a case the right lymph duct opens into the junction of right subclavian and right internal jugular vein and the thoracic duct opens into the junction of left subclavian and left internal jugular vein [19].

1.3 Pharmacokinetics of drug absorption from the lungs

The lungs on account of their high absorptive surface area, thin alveolar epithelium, and extensive vascularization are well suited for the efficient non-invasive systemic delivery of macromolecules and small molecule drugs. In the case of small molecules, the lungs are far more permeable for absorption than the gastrointestinal tract [23]. Even for macromolecules, the lungs are much more permeable for absorption than any other non-invasive route of entry [2, 24]. Many small molecule drugs, peptides, and proteins have very rapid absorption from lungs into systemic circulation. Small peptides and proteins show absorption more rapidly from lungs as compared to subcutaneous injection.

The bioavailability of proteins and peptides from the pulmonary route is 10 to 200 times higher as compared to other non invasive routes. In the case of small molecules, lipophilic drugs are absorbed extremely quickly where the half life of absorption is approximately 1 to 2 minutes. Hydrophilic small molecules show an absorption half life of approximately 65 minutes [25]. **Table 2** depicts the absorption potential of several hydrophilic and hydrophobic small molecules as measured by $t_{1/2}$ (time taken for absorption of half of the administered dose) after pulmonary administration by intratracheal instillation in rats. Small hydrophobic molecules are believed to be absorbed rapidly throughout the lungs by way of passive diffusion through the plasma membrane. On the other hand small hydrophilic molecules can be absorbed by specific transporters or via tight junctions of the epithelial cells [2]. An interesting observation from **table 2** is that erythromycin despite its high log P value shows relatively slower absorption from lungs as compared to lipophilic drugs with lower log P values. This can be explained by the fact that erythromycin and other macrolides were shown to interact with phospholipids [26-29], therefore such interactions with lung lipids may slow absorption of the macrolide class of antibiotics [5] and/or drugs with similar lipophilic character. Apart from the strong pulmonary absorption potential of small molecule drugs, the lungs contain only a fraction of the metabolizing enzymes present in the gut and liver which are encountered in the case of oral delivery [30, 31].

For small peptides such as insulin it is not clear whether it is absorbed by paracellular transport or caveolin mediated endocytosis [2]. However, it is widely believed by scientists in the field that paracellular transport is dominant [5]. The deposition in deep lungs of small peptides and insulin seems to produce optimal absorption as compared to deposition in the upper airways. However, for the high molecular weight (150 kD) immunoglobulins of the IgG class evidence

Class	Compound	Molecular weight (Da)	Log P	$t_{1/2}$ (min)	k (min^{-1})
Lipid Insoluble	Guanidine	59	-3.56	6.3	0.110
	Urea	60	-2.11	4.7	0.147
	AIB (α-aminobutyric acid)	103	-2.54	57	0.012
	Erythritol	122	-2.29	35	0.020
	N-methylnicotinamide	136	0	50	0.014
	Mannitol	182	-3.1	60	0.012
	p-Aminohippuric acid	194	-0.89	41	0.017
	3-o-methyl-D-glucose	194	-1.69	58.7	0.012
	Decamethonium	258	-4.78	90	0.008
	Sucrose	342	-3.7	84	0.008
	Cyanocobalamin (Vitamin B12)	1355	3.57	190	0.0036
	Heparin	6,000-20,000	4.31	552	0.0013
	Dextran	75,000	-	1670	0.0004
Lipid soluble	Amitrole	84	-0.86	1.3	0.533
	Isoniazid	137	-0.7	1.9	0.365
	Salicylic acid	138	2.26	1.0	0.693
	Barbital	184	0.65	0.93	0.745
	Sulphaguanidine	218	-1.22	41	0.017
	Pentobarbital	226	2.1	1.0	0.693
	Phenobarbital	232	1.47	1.0	0.693
	Ethambutol	232	-0.41	40	0.017
	Procainamide	235	-0.55	2.3	0.301
	Sulphamethoxypyridazine	280	0.32	1.0	0.693
	Sulphadimethoxine	310	1.63	1.0	0.693
	Hydrocortisone	362.5	1.61	1.0	0.693
	Dexamethasone	392.5	1.83	1.7	0.408
	Tetracycline	444	-1.3	14	0.050
	Erythromycin	734	3.06	6.3	0.110
	Digitoxin	765	1.85	0.3	2.310
	Digoxin	781	1.26	1.0	0.693

Table 2: The effect of molecular weight and lipophilicity on the rate of absorption of small molecules following intratracheal instillation in rats. (Adapted from ref. 22) Note: The $t_{1/2}$ value is the measured time for absorption of 50% of the initial dose; k is the apparent first order rate constant; and log P is the octanol-water partition coefficient. The log P values were predicted using Syracuse Research Corporation's KowWin software.

indicates that deposition in the larger airways (where there is receptor-mediated transcytosis for IgG) is best for absorption [32].

The pulmonary delivery of proteins in polymeric nanoparticles provides a sustained release in lungs and thereby in the systemic circulation. This approach provides a reduction in dosage frequency, and better patient compliance especially for therapeutics such as insulin that are traditionally injected intramuscularly [3]. Studies have shown prolonged hypoglycemic effect in animals after pulmonary administration of insulin encapsulated in polymeric nanoparticles [33, 34]. Moving beyond animal studies, the safety and efficacy of inhaled insulin was evaluated in more than 2700 patients with type 1 or type 2 diabetes [35-37]. Several studies have shown that inhaled insulin effectively controls blood glucose levels comparable to subcutaneously administered fast-acting insulin in type 1 and type 2 diabetics [5]. On the whole, pulmonary delivery of drug encapsulated polymeric nanocarriers seems to be very efficient in achieving better pharmacokinetics for a wide gamut of therapeutics.

1.4 Nanoparticles in pulmonary delivery

Nanoparticles have gained increasing attention for pulmonary drug delivery due to several characteristics like targeted deposition, bioadhesion, sustained drug release, and reduced dosing frequency [3]. Drug encapsulated polymeric and non-polymeric nanoparticles can be administered to the lungs for both systemic and local use [1]. Nanocarriers for pulmonary drug delivery include degradable polymeric nanoparticles, liposomes, nanotubes etc. Degradable polymeric nanoparticles can be fabricated using natural polymers like albumin, gelatin, alginate, collagen, cyclodetrin, chitosan etc. or synthetic polymers such as polyesters (poly (lactic-co-glycolic) acid, poly (lactic acid), and poly (glycolic acid) etc.,), polyanhydrides (poly(sebacic anhydride), poly(adipic anhydride), poly(sebacic acid-*co*-1,3-bis(*p*-carboxyphenoxy) propane) etc.,), and polyacrylates (poly(n-propyl acrylate) and poly(n-butyl acrylate)). Synthetic polymers have the property to sustain the drug release over a period of days to months whereas natural polymers degrade and release the drug in a shorter duration [38].

Degradable polymeric nanoparticles have been extensively used in pulmonary delivery of several important proteins/peptides and drugs [39]. For deposition of particles successfully in the deep lungs the aerodynamic diameter (d_{ae}) of the particles should be between 1 to 3 µm. Particles with d_{ae} greater than 5-10 µm are deposited in the oropharyngeal region and are likely to be swallowed [6]. Particles of size less than 100 nm are transported by diffusional displacement and deposit efficiently in peripheral airways [40]. Particles of size less than 150 nm have been shown to efficiently translocate across the alveolar epithelium and enter systemic circulation [41]. When designing particulate systems for lung administration, it is important to note that particles made of hygroscopic material or water-soluble particles absorb moisture in the lungs therefore changing the particle size, which in turn affects the deposition pattern and efficiency. Encapsulating therapeutics in degradable nanoparticles offers protection to the therapeutic from peptidases and other degradative milieu in the lungs such as lung surfactant. Moreover, encapsulation of therapeutic in nanoparticles allows for the cellular uptake of the nanoparticles especially in the case of gene/siRNA delivery. Furthermore, polymeric nanoparticles allow for prolonged delivery of the therapeutic thereby reducing the frequency of administering the therapeutic which in turn results in patient compliance. All these advantages make biodegradable polymeric nanocarriers suitable and necessary for pulmonary drug delivery of a gamut of therapeutics. Polymeric nanoparticles can be fabricated using several methods such as single/double emulsion method, nanoprecipitation, spray drying, and phase inversion nanoencapsulation.

1.4.1 Cellular uptake of nanoparticles

Nanoparticles gain entry into cells by a process called endocytosis wherein the nanoparticle interacts with the cell membrane and is then engulfed in the invaginations present at the membrane. The invaginations are pinched off of the membrane to form vesicular structures known as endosomes. These endosomes then transport the nanoparticle/cargo to other intracellular structures. Clathrin-mediated endocytosis and caveolin-mediated endocytosis are the two main endocytotic mechanisms for nanoparticle entry into cells [42]. Apart from these two major pathways, there are several other endocytotic mechanisms depicted in **figure 4**.

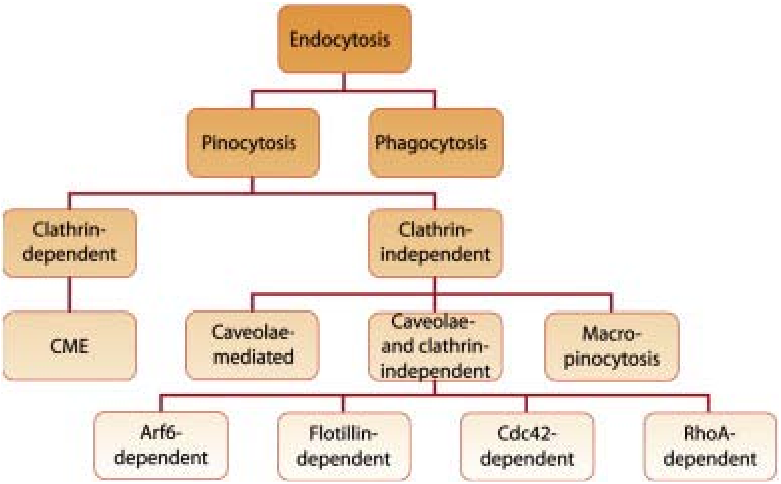

Figure 4. Classification of the several different endocytotic mechanisms based on the proteins involved in the initiatory process of endocytosis. (Adapted from ref. 42)

Clathrin mediated endocytosis (CME) plays crucial role in important physiological processes such as nutrient uptake and intercellular communication in all mammalian cells. Clathrin-dependent endocytosis is the major mechanism responsible in the internalization of macromolecules and plasma membrane constituents in most cell types. Clathrin is a three-leg protein that assembles on the cytosolic side of the plasma membrane thereby aiding the deformation of the membrane into a pit of around 150 nm size. Once the cargo is internalized by the clathrin coated vesicle, it is transferred to the early endosomes which have an acidic pH (~6). These early endosomes then mature into late endosomes which have more acidic pH (~5) as compared to early endosomes. The late endosomes fuse with prelysosomal vesicles that contain acid hydrolases thereby generating a severe environment that degrades the internalized cargo [43]. Therefore, drug delivery systems that are intended for uptake by CME have to be designed with the capability to escape the degradative process in the endosomes to be released in the cytosol. For instance, polyethyleneimine, a cationic polymer used in the delivery of nucleotides has the capability to escape the endosomes by a process termed as the 'proton-sponge effect'.

Apart from CME, caveolae mediated endocytosis is another major pathway for endocytosis of materials into cells. Caveolae are flask shaped invaginations of the plasma membrane that have a size around 50-100 nm. They are abundantly present in endothelial cells constituting about 10-20% of cell surface. The caveolae contain an array of dimeric protein caveolin and are also abundant in cholesterol and sphingolipids. Once the particles are internalized in the invaginations, the GTPase dynamin causes the fission of caveolae from the membrane thereby producing a vesicle which in this case does not contain any degradative enzymes unlike clathrin coated vesicles. Therefore, this pathway may be exploited for purpose of drug delivery for sensitive therapeutics such as peptides, proteins, and nucleic acids thereby circumventing the lysosomal degradation pathway [43]. Despite the small sizes of clathrin and caveolin coated invaginations, a study has demonstrated that for polystyrene nanoparticles of size less than 200 nm CME was involved in their internalization. However, surprisingly, for larger particles as big as 500 nm size, the caveolae mediated endocytosis was the major internalization pathway [44]. The internalization of material via caveolae mediated endocytosis occurs at a much slower rate as compared to that of CME [45]. Both the alveolar epithelial cells and the pulmonary capillary endothelial cells have an abundance of caveolar structures [46]. Therefore, nanoparticles could potentially exploit this endocytosis mechanism for their translocation across the alveolar epithelial cells into systemic circulation.

1.4.2 Risk assessment of nanoparticles

The nanoparticles translocate to distant organs from the lungs and generate adverse effects [47]. Apart from systemic effects, they also result in local toxicity to the lungs. However, most of the knowledge about pulmonary toxicity of nanoparticles is based on the inhaled nanoparticles such as carbon black, diesel particulate matter, titanium dioxide, and silica nanoparticles which are considered as ultrafine nanoparticles of size less than 100 nm [48]. Nanoparticles have shown to exert a greater inflammatory potential per unit mass as compared to particles of larger sizes in rat lungs [49]. Nanoparticles primarily induce toxic effects via generation of reactive oxygen species resulting in oxidative stress [50].

It has been shown that inhaled iridium particles may translocate from lungs into systemic circulation resulting in severe vascular effects [51, 52]. On the other hand there is evidence showing that the toxicity of metallic microparticles was similar to that of metallic nanoparticles [53]. This demonstrates that the toxicity may not exclusively be as a result of particle size alone. Polymeric nanoparticles have also been tested for pulmonary toxicity. In one study, nanoparticles were fabricated using biodegradable polymers poly(butyl)cyanoacrylate and poly(hexyl)cyanoacrylate and their toxicity was assessed on human pulmonary epithelial cells. With both these nanoparticles, an increase in lactate dehydrogenase (LDH) activity was observed [54]. In another study with poly (lactic-co-glycolic) acid (PLGA) nanoparticles, it has been shown that they induce much less inflammation as compared to polystyrene nanoparticles of similar size upon administration to lungs [55]. Taken together these results suggest that metallic nanoparticles pose a higher risk for pulmonary toxicity and that the nanoparticle size might not be the only factor that plays a key role in toxicity. Furthermore, PLGA nanoparticles are more amenable for pulmonary delivery on account of their less inflammatory potential and also due to the fact that they are completely degradable.

1.5 Metastatic breast cancer

Breast cancer, a complex disease which is highly heterogeneous at both the molecular and clinical level is also the leading cause of cancer deaths in women world-wide [56]. Five major molecular subtypes of breast cancer namely basal-like, luminal A, luminal B, $HER2^+/ER^-$, and normal breast like have been identified based on extensive gene expression profiling of tumors [57-59]. As a result of the molecular differences, the clinical outcomes and responses to treatment are distinct for each subtype with basal-like tumors having the worst prognosis and luminal A-type having the best prognosis [60]. As per a recent statistic from breastcancer.org, in the year 2011 an estimated 230, 480 new cases of invasive (metastatic) breast cancer and 57,650 new cases of non-invasive breast cancer were expected to be diagnosed in women in the United States [61]. As per statistics from American cancer society, in the year 2012 there would be an estimated 226, 870 new cases of breast cancer and an estimated 39,510 deaths resulting from breast cancer [62]. The main cause of death from breast cancer is not due to the primary tumor but due to metastatic spread of the tumor to distant sites [63]. The heterogeneity of metastatic breast cancer is such that it can range from solitary metastatic lesion to widespread metastases into multiple organs [64]. **Figure 5** depicts breast cancer progression which starts with ductal hyperproliferation which then advances into in situ and invasive carcinomas, and finally resulting in metastatic spread [56]. It has also been shown in a mouse model that mesenchymal stem cells within the cancer stroma greatly enhance the metastatic spread of breast cancer cells. They have been found to do so by releasing a chemokine CCL5 that enhances the motility, invasion, and metastasis of the breast cancer cells [65]. Despite advancements in therapy, about 25-40% of patients with breast cancer develop metastasis which is largely incurable [66].

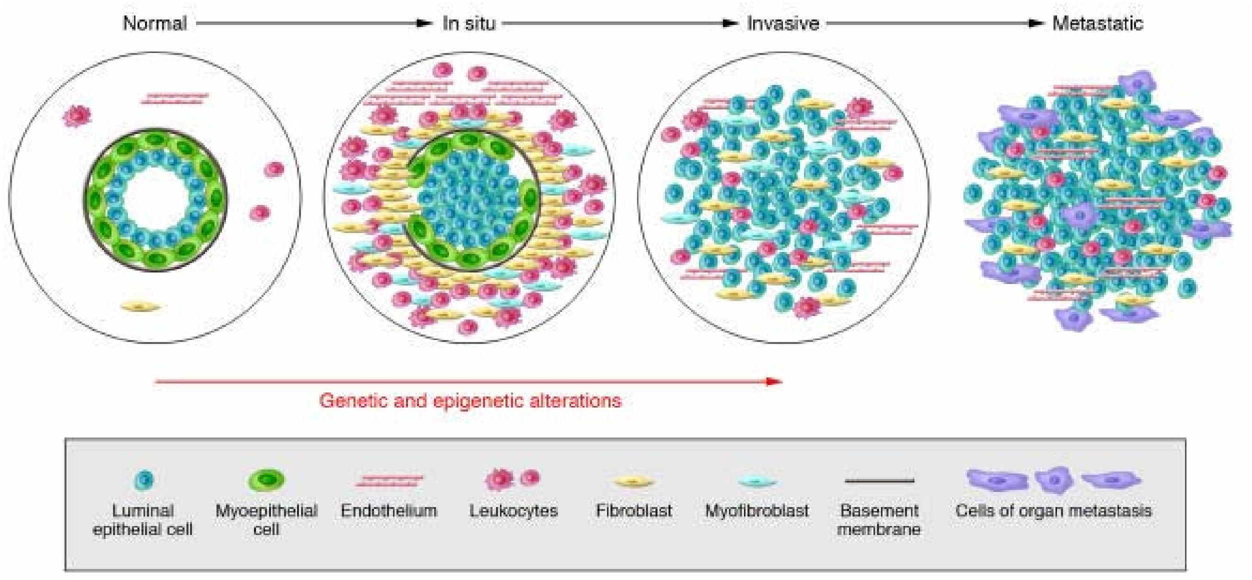

Figure 5. A schematic of a hypothetical model of breast tumor progression showing ductal changes associated with tumor progression (Adapted from ref .43).

Of the various prognostic factors related to breast cancer survival rates, the Nottingham study clearly highlights that in addition to tumor size, survival is also significantly dependent on the total number of nodes involved in metastasis [67, 68]. The conventional standard in cancer staging and determination of prognosis for nearly the past century has involved the removal of sentinel and axillary lymph nodes [67-69]. Sentinel lymph nodes are defined as the lymph nodes that are first to receive lymph from the vicinity of the primary tumor [68, 69]. Indeed, it was discovered way back in the 1830’s that lymphatic drainage from the breast follows into the subareolar plexus and ends in the axilla, which paved the way for further investigation of the lymphatic network revealing additional lymphatic routes [70]. Approximately one third of breast cancer patients are reported to receive axillary lymph node dissection (ALND) as an initial treatment followed by radiation or other adjuvant therapies [67, 68, 71].

In the Iowa Women's Health Study, several important risk factors, including obesity, tumor grade and comorbidity are identified as contributors to complications following ALND, however, these risk factors are not necessarily present in all cases of reported complications following ALND [71, 72]. A major complication that occurs after ALND is lymphedema, which has been determined to damage normal lymphatic transport [69, 71, 72]. The volume of circulating lymph therefore exceeds the capability of the resected lymphatic network, resulting in an accumulation of fibrotic tissue, protein, edema and chronic inflammation within the limb [71, 72]. Furthermore, the disrupted lymph flow can lead to retrograde lymphatic drainage to the liver via the internal mammary chain [70]. The pathology associated with ALND extends to reports of decreased quality of life and psychological implications, including anxiety, depression, distorted body image and decreased libido in women who have undergone ALND [72, 73]. Although lymphedema has been reported as both acute and chronic pathology, it is well demonstrated in the ALMANAC trial that incidence of lymphedema and associated morbidity is significantly reduced 1, 3, 6 and 12 months following sentinel lymph node dissection (SLND) versus ALND [72, 73]. Furthermore, women who underwent SLND and later underwent ALND reported significantly greater morbidity and disability in the arm as compared to women who underwent SLND alone [72, 73]. Taken together, ALND is associated with significant incidence of lymphedema related arm morbidities and extends into shoulder and muscular injury and clinical presentations including, limited range of motion of the limb, centralized pain consisting of tingling, numbness and other sensory defects as well as an increased risk of developing infections [67-69, 71-75]. With advancements in diagnostic technology, including the use of lymphoscintigraphy to delineate tumor involvement in lymphatic flow, evidence is emerging that suggests that sentinel lymph nodes (SNL) accurately represent the state of axillary lymph node involvement in 95.5% of patients with non-SNL evidence of cancer [68]. The removal of involved lymph nodes that are determined to receive lymphatic drainage from a tumor using radioactive dye lymphoscintigraphy affords conservation of breast tissue and obviates the extensive surgical interventions that have previously been widely practiced [67, 69, 74].

According to the National Surgical Adjuvant Breast and Bowel Project (NSABP) B-32 trial, which focused primarily on the effectiveness of SLND, only a 2% difference was found to exist in overall survival of patients that underwent SLND or ALND in SNL-negative involvement [69]. This finding was further substantiated in a recent study investigating SLN micrometastases, indicating that 38-67% of lymph nodes involved are identified as SLNs and a plausible treatments with such tumors is SLND alone and preservation of ALNs [76]. However, for patients presenting with multifocal tumors SNLs do not serve as an accurate assessment of axillary lymph node (ALN) involvement, as these tumors are likely to involve extensive routes of the breast lymphatic network [68, 69, 74]. SLN has emerged as a clinically useful procedure that is gaining worldwide notoriety as a standard method of lymph node analysis in node negative SNLs identified by lymphoscintigraphy, however optimization for the method of identification of SLN involvement and the accuracy with which it predicts ALN involvement is still debated [74, 76]. This study has impacted the conventional treatment of breast cancer, which typically involved mastectomy, ALND as well as extensive adjuvant therapy: chemotherapy, radiation and long term Tamoxifen therapy [67, 69, 74]. Improvement in methods used to detect sentinel lymph node involvement has major implications in the enhancement of the quality of care for millions of breast cancer patients [69, 74]. However, as an alternative approach, passively targeting the axillary lymph nodes from lungs in cases of node-positive metastatic breast cancers could offer a solution to the multiple complex pathologies associated with ALND. This approach could not only result in effective treatment but also a significant improvement in quality of life of the patients.

1.6 CDF and doxorubicin for metastatic breast cancer treatment

Doxorubicin, introduced nearly four decades ago has generally been considered the most active drug for metastatic breast cancer. In patients with metastatic breast cancer who have received prior alkylating agent chemotherapy, doxorubicin was found to produce excellent response rates. At doses between 60 to 75 mg/m^2 the response rate was between 25 to 33% [77]. Furthermore, it was discovered that at low to moderate doses, doxorubicin and other anti cancer agents have the ability to stimulate the immune system against cancer [78]. Doxorubicin when administered to mice in moderate doses led to the potentiation of cytotoxic T lymphocyte responses (CTL) to syngeneic tumors in addition to increasing the antitumor action of cytotoxic macrophages [79]. Difluorinated curcumin (CDF), a curcumin analogue has been shown to possess inhibitory activity against several cancer cell lines. Additionally, it acts as a chemosensitizer in several cancer cell lines, thereby potentiating the activity of chemotherapeutic agents in cancer chemotherapy. Therefore, exploiting the multi faceted abilities of doxorubicin and CDF in combination and delivering them to the axillary lymph nodes (by encapsulating the drugs in nanoparticles) might offer an alternative for effective treatment in metastatic breast cancer with nodal involvement.

1.7 Hypothesis and specific aims

Hypothesis

Nodal involvement in metastatic breast cancer is well documented. There is overwhelming evidence of cancer spread to axillary lymph nodes (ALN) in metastatic breast cancer. Therefore, killing the cancer cells in ALN by way of passively targeting the ALN from lungs will be an effective strategy in combating metastatic breast cancer. In light of this idea, I **hypothesize** that CDF encapsulated polymer nanoparticles can be passively targeted to lymph nodes via lungs.

Specific aims

1. To study the effect of size of polystyrene nanoparticles on their pulmonary biodistribution

It is well established that nanoparticle size plays an important role in their *in vivo* biodistribution. There is a lot of information available about the effect of nanoparticle size on its biodistribution after intravenous administration. However, there are very few studies that quantitatively investigate the effect of polymeric nanoparticle size on pulmonary biodistribution from a drug delivery perspective. Furthermore, the uptake of nanoparticles occurs by many potential mechanisms including phagocytosis, clathrin-mediated endocytosis, caveolin-mediated endocytosis, and non-endocytotic pathways. It is hypothesized that these different uptake mechanisms may affect the biodistribution of nanoparticles based on their size. Therefore, polystyrene nanoparticles of size 50 nm, 100 nm, 250 nm, and 900 nm will be used to investigate the effect of nanoparticle size on their pulmonary biodistribution in mice.

2. To develop an assay to determine the nanoparticle biodistribution and biodegradation *in vivo*

Degradable polymeric nanoparticle biodistribution studies are usually performed by either physical encapsulation of a fluorescent dye or by means of conjugating the dye with the polymer. In this situation, there is a high chance of misinterpreting the results due to the fact that fluorescence of the dye alone can be misread as that of the whole nanoparticle. Furthermore, performing biodistribution studies for longer periods of time would not be possible due to the fact that the dye would be released over time both from the encapsulated formulation and from the conjugate. In such a situation, the nanoparticle is no more associated with the dye and therefore the fluorescence of the dye cannot be used as an indicator to track the nanoparticle system anymore. Another approach that is used is radiolabeling of the polymer backbone. However, this will only give biodistribution data of nanoparticles. The *in vivo* tissue degradation of polymeric nanoparticles has not been investigated yet. Drug release from nanoparticles is dependent on diffusion as well as polymer degradation. Therefore, determining the *in vivo* biodistribution of polymeric nanoparticles simultaneously with their *in vivo* degradation will help in designing better drug delivery systems with a highly predictable drug release profile in tissues. For this purpose, the biodegradable polymer PLGA will be used to formulate nanoparticles. These PLGA nanoparticles will then be administered intravenously in order to simultaneously determine their *in vivo* biodistribution and biodegradation in tissues.

3. To develop CDF-encapsulated PLGA nanoparticles for use in the treatment of metastatic breast cancer

Difluorinated-curcumin (CDF), an analogue of curcumin has been shown to be a chemosensitizer and also potent inhibitor for several types of cancer cells. Since nanoparticles are well known to provide special characteristics such as improved bioavailability and half life, extended release of the drug, intracellular delivery etc., CDF will be encapsulated in PLGA nanoparticles and tested for its activity in cancer cell lines, especially a breast cancer cell line.

1.8 References

1. Smola M, Vandamme T, Sokolowski A. Nanocarriers as pulmonary drug delivery systems to treat and to diagnose respiratory and non respiratory diseases. International Journal of Nanomedicine 2008;3:1-19.

2. Patton JS. Mechanisms of macromolecule absorption by the lungs. Adv Drug Deliv Rev 1996;19:3-36.

3. Sung JC, Pulliam BL, Edwards DA. Nanoparticles for drug delivery to the lungs. Trends Biotechnol 2007;25:563-570.

4. Lam JK, Liang W, Chan HK. Pulmonary delivery of therapeutic siRNA. Adv Drug Deliv Rev 2012;64:1-15.

5. Patton JS, Byron PR. Inhaling medicines: delivering drugs to the body through the lungs. Nat Rev Drug Discov 2007;6:67-74.

6. Rytting E, Nguyen J, Wang X, Kissel T. Biodegradable polymeric nanocarriers for pulmonary drug delivery. Expert Opin Drug Deliv 2008;5:629-639.

7. Groneberg DA, Witt C, Wagner U, Chung KF, Fischer A. Fundamentals of pulmonary drug delivery. Respiratory Medicine 2003;97:382-387.

8. Nicod LP. Lung defences: an overview. European Respiratory Review, 2005;14:45-50.

9. McWilliam AS, Holt PG. Immunobiology of dendritic cells in the respiratory tract: steady-state and inflammatory sentinels? Toxicol Lett 1998;102-103:323-329.

10. Nicod LP, Cochand L, Dreher D. Antigen presentation in the lung: dendritic cells and macrophages. Sarcoidosis Vasc Diffuse Lung Dis 2000;17:246-255.

11. Stone KC, Mercer RR, Gehr P, Stockstill B, Crapo JD. Allometric relationships of cell numbers and size in the mammalian lung. Am J Respir Cell Mol Biol 1992;6:235-243.

12. Yang W, Peters JI, Williams RO, 3rd. Inhaled nanoparticles--a current review. Int J Pharm 2008;356:239-247.

13. Fernandes CA, Vanbever R. Preclinical models for pulmonary drug delivery. Expert Opin Drug Deliv 2009;6:1231-1245.

14. Chuquimia OD, Petursdottir DH, Rahman MJ, Hartl K, Singh M, Fernandez C. The Role of Alveolar Epithelial Cells in Initiating and Shaping Pulmonary Immune Responses: Communication between Innate and Adaptive Immune Systems. PLoS One 2012;7:e32125.

15. Schleh C, Rothen-Rutishauser B, Kreyling WG. The influence of pulmonary surfactant on nanoparticulate drug delivery systems. Eur J Pharm Biopharm 2011;77:350-352.

16. Sertl K, Takemura T, Tschachler E, Ferrans VJ, Kaliner MA, Shevach EM. Dendritic cells with antigen-presenting capability reside in airway epithelium, lung parenchyma, and visceral pleura. J Exp Med 1986;163:436-451.

17. de Heer HJ, Hammad H, Kool M, Lambrecht BN. Dendritic cell subsets and immune regulation in the lung. Semin Immunol 2005;17:295-303.

18. Kirby AC, Coles MC, Kaye PM. Alveolar macrophages transport pathogens to lung draining lymph nodes. J Immunol 2009;183:1983-1989.

19. Skandalakis JE, Skandalakis LJ, Skandalakis PN. Anatomy of the lymphatics. Surg Oncol Clin N Am 2007;16:1-16.

20. Morrow PE. Lymphatic drainage of the lung in dust clearance. Ann N Y Acad Sci 1972;200:46-65.

21. Craven J. The lungs and their relations. Anaesthesia & intensive care medicine 2008;9:459-461.

22. Harold E. Lungs: blood supply, lymphatic drainage and nerve supply. Anaesthesia & Intensive Care Medicine 2008;9:462-463.

23. Schanker LS. Drug absorption from the lung. Biochem Pharmacol 1978;27:381-385.

24. Patton JS, Nagarajan S, Clark AR. Pulmonary Absorption and Metabolism of Peptides and Proteins. Respiratory Drug Delivery VI 1998;17-24.

25. Patton JS, Fishburn CS, Weers JG. The Lungs as a Portal of Entry for Systemic Drug Delivery. Proceedings of the American Thoracic Society 2004;1:338-344.

26. Tyteca D, Schanck A, Dufrene YF, Deleu M, Courtoy PJ, Tulkens PM, et al. The macrolide antibiotic azithromycin interacts with lipids and affects membrane organization and fluidity: studies on Langmuir-Blodgett monolayers, liposomes and J774 macrophages. J Membr Biol 2003;192:203-215.

27. Montenez JP, Van Bambeke F, Piret J, Brasseur R, Tulkens PM, Mingeot-Leclercq MP. Interactions of macrolide antibiotics (Erythromycin A, roxithromycin, erythromycylamine [Dirithromycin], and azithromycin) with phospholipids: computer-aided conformational analysis and studies on acellular and cell culture models. Toxicol Appl Pharmacol 1999;156:129-140.

28. Montenez JP, Van Bambeke F, Piret J, Schanck A, Brasseur R, Tulkens PM, et al. Interaction of the macrolide azithromycin with phospholipids. II. Biophysical and computer-aided conformational studies. Eur J Pharmacol 1996;314:215-227.

29. Van Bambeke F, Montenez JP, Piret J, Tulkens PM, Courtoy PJ, Mingeot-Leclercq MP. Interaction of the macrolide azithromycin with phospholipids. I. Inhibition of lysosomal phospholipase A1 activity. Eur J Pharmacol 1996;314:203-214.

30. Ji CM, Cardoso WV, Gebremichael A, Philpot RM, Buckpitt AR, Plopper CG, et al. Pulmonary cytochrome P-450 monooxygenase system and Clara cell differentiation in rats. Am J Physiol 1995;269:L394-402.

31. Tronde A, Norden B, Marchner H, Wendel AK, Lennernas H, Bengtsson UH. Pulmonary absorption rate and bioavailability of drugs *in vivo* in rats: structure-absorption relationships and physicochemical profiling of inhaled drugs. J Pharm Sci 2003;92:1216-1233.

32. Codrons V, Vanderbist F, Ucakar B, Preat V, Vanbever R. Impact of formulation and methods of pulmonary delivery on absorption of parathyroid hormone (1-34) from rat lungs. J Pharm Sci 2004;93:1241-1252.

33. Kawashima Y, Yamamoto H, Takeuchi H, Fujioka S, Hino T. Pulmonary delivery of insulin with nebulized DL-lactide/glycolide copolymer (PLGA) nanospheres to prolong hypoglycemic effect. J Control Release 1999;62:279-287.

34. Zhang Q, Shen ZC, Nagai T. Prolonged hypoglycemic effect of insulin-loaded polybutylcyanoacrylate nanoparticles after pulmonary administration to normal rats. International Journal of Pharmaceutics 2001;218:75-80.

35. Quattrin T, Belanger A, Bohannon NJ, Schwartz SL. Efficacy and safety of inhaled insulin (Exubera) compared with subcutaneous insulin therapy in patients with type 1 diabetes: results of a 6-month, randomized, comparative trial. Diabetes Care 2004;27:2622-2627.

36. Hollander PA, Blonde L, Rowe R, Mehta AE, Milburn JL, Hershon KS, et al. Efficacy and safety of inhaled insulin (exubera) compared with subcutaneous insulin therapy in patients with type 2 diabetes: results of a 6-month, randomized, comparative trial. Diabetes Care 2004 ;27:2356-2362.

37. DeFronzo RA, Bergenstal RM, Cefalu WT, Pullman J, Lerman S, Bode BW, et al. Efficacy of Inhaled Insulin in Patients With Type 2 Diabetes not Controlled With Diet and Exercise. Diabetes Care 2005;28:1922-1928.

38. Panyam J, Labhasetwar V. Biodegradable nanoparticles for drug and gene delivery to cells and tissue. Adv Drug Deliv Rev 2003;55:329-347.

39. Mansour HM, Rhee YS, Wu X. Nanomedicine in pulmonary delivery. Int J Nanomedicine 2009;4:299-319.

40. Lippmann M, Yeates DB, Albert RE. Deposition, retention, and clearance of inhaled particles. Br J Ind Med 1980;37:337-362.

41. Chow AH, Tong HH, Chattopadhyay P, Shekunov BY. Particle engineering for pulmonary drug delivery. Pharm Res 2007;24:411-437.

42. Sahay G, Alakhova DY, Kabanov AV. Endocytosis of nanomedicines. J Control Release 2010;145:182-195.

43. Hillaireau H, Couvreur P. Nanocarriers' entry into the cell: relevance to drug delivery. Cellular and Molecular Life Sciences 2009;66:2873-2896.

44. Rejman J, Oberle V, Zuhorn IS, Hoekstra D. Size-dependent internalization of particles via the pathways of clathrin- and caveolae-mediated endocytosis. Biochem J 2004;377(Pt 1):159-169.

45. Bareford LM, Swaan PW. Endocytic mechanisms for targeted drug delivery. Adv Drug Deliv Rev 2007;59:748-758.

46. Gumbleton M. Caveolae as potential macromolecule trafficking compartments within alveolar epithelium. Advanced Drug Delivery Reviews 2001;49:281-300.

47. Oberdorster G, Maynard A, Donaldson K, Castranova V, Fitzpatrick J, Ausman K, et al. Principles for characterizing the potential human health effects from exposure to nanomaterials: elements of a screening strategy. Part Fibre Toxicol 2005;2:8.

48. Azarmi S, Roa WH, Lobenberg R. Targeted delivery of nanoparticles for the treatment of lung diseases. Adv Drug Deliv Rev 2008;60:863-875.

49. Steimer A, Haltner E, Lehr C-M. Cell Culture Models of the Respiratory Tract Relevant to Pulmonary Drug Delivery. Journal of Aerosol Medicine 2005;137-182.

50. Nel A, Xia T, Mädler L, Li N. Toxic Potential of Materials at the Nanolevel. Science 2006;311:622-627.

51. Hoet PH, Nemmar A, Nemery B. Health impact of nanomaterials? Nat Biotechnol 2004 22:19.

52. Semmler M, Seitz J, Erbe F, Mayer P, Heyder J, Oberdörster G, et al. Long-Term Clearance Kinetics of Inhaled Ultrafine Insoluble Iridium Particles from the Rat Lung, Including Transient Translocation into Secondary Organs. Inhalation Toxicology 2004;16:453-459.

53. Cha KE, Myung H. Cytotoxic effects of nanoparticles assessed in vitro and *in vivo*. J Microbiol Biotechnol 2007;17:1573-1578.

54. Brzoska M, Langer K, Coester C, Loitsch S, Wagner TO, Mallinckrodt C. Incorporation of biodegradable nanoparticles into human airway epithelium cells-*in vitro* study of the suitability as a vehicle for drug or gene delivery in pulmonary diseases. Biochem Biophys Res Commun 2004;318:562-570.

55. Dailey LA, Jekel N, Fink L, Gessler T, Schmehl T, Wittmar M, et al. Investigation of the proinflammatory potential of biodegradable nanoparticle drug delivery systems in the lung. Toxicol Appl Pharmacol 2006;215:100-108.

56. Polyak K. Breast cancer: origins and evolution. J Clin Invest 2007;117:3155-3163.

57. Perou CM, Sorlie T, Eisen MB, van de Rijn M, Jeffrey SS, Rees CA, et al. Molecular portraits of human breast tumours. Nature 2000;406:747-752.

58. Hu Z, Fan C, Oh DS, Marron JS, He X, Qaqish BF, et al. The molecular portraits of breast tumors are conserved across microarray platforms. BMC Genomics 2006;7:96.

59. Sorlie T, Wang Y, Xiao C, Johnsen H, Naume B, Samaha RR, et al. Distinct molecular mechanisms underlying clinically relevant subtypes of breast cancer: gene expression analyses across three different platforms. BMC Genomics 2006;7:127.

60. Sorlie T, Perou CM, Tibshirani R, Aas T, Geisler S, Johnsen H, et al. Gene expression patterns of breast carcinomas distinguish tumor subclasses with clinical implications. Proc Natl Acad Sci U S A 2001;98:10869-10874.

61. U.S. Breast Cancer Statistics. 2012 March 4, 2012 [cited 2012]; Available from: http://www.breastcancer.org/symptoms/understand_bc/statistics.jsp

62. American Cancer Society. Atlanta: American Cancer Society; 2012: Cancer Facts & Figures 2012.

63. Weigelt B, Peterse JL, van 't Veer LJ. Breast cancer metastasis: markers and models. Nat Rev Cancer 2005;5:591-602.

64. Pagani O, Senkus E, Wood W, Colleoni M, Cufer T, Kyriakides S, et al. International guidelines for management of metastatic breast cancer: can metastatic breast cancer be cured? J Natl Cancer Inst 2010;102:456-463.

65. Karnoub AE, Dash AB, Vo AP, Sullivan A, Brooks MW, Bell GW, et al. Mesenchymal stem cells within tumour stroma promote breast cancer metastasis. Nature 2007;449:557-563.

66. Guarneri V, Conte P. Metastatic breast cancer: therapeutic options according to molecular subtypes and prior adjuvant therapy. Oncologist 2009;14:645-656.

67. Galea MH, Blamey RW, Elston CE, Ellis IO. The Nottingham Prognostic Index in primary breast cancer. Breast cancer research and treatment 1992;22:207-219.

68. Veronesi U, Paganelli G, Viale G, Galimberti V, Luini A, Zurrida S, et al. Sentinel lymph node biopsy and axillary dissection in breast cancer: results in a large series. Journal of the National Cancer Institute 1999;91:368-373.

69. Krag DN, Anderson SJ, Julian TB, Brown AM, Harlow SP, Costantino JP, et al. Sentinel-lymph-node resection compared with conventional axillary-lymph-node dissection in clinically node-negative patients with breast cancer: overall survival findings from the NSABP B-32 randomised phase 3 trial. The lancet oncology 2010;11:927-933.

70. Tanis PJ, Nieweg OE, Valdes Olmos RA, Kroon BB. Anatomy and physiology of lymphatic drainage of the breast from the perspective of sentinel node biopsy. Journal of the American College of Surgeons 2001;192:399-409.

71. Ahmed RL, Schmitz KH, Prizment AE, Folsom AR. Risk factors for lymphedema in breast cancer survivors, the Iowa Women's Health Study. Breast cancer research and treatment 2011;130:981-991.

72. Husted Madsen A, Haugaard K, Soerensen J, Bokmand S, Friis E, Holtveg H, et al. Arm morbidity following sentinel lymph node biopsy or axillary lymph node dissection: a study from the Danish Breast Cancer Cooperative Group. Breast 2008;17:138-147.

73. Hack TF, Kwan WB, Thomas-Maclean RL, Towers A, Miedema B, Tilley A, et al. Predictors of arm morbidity following breast cancer surgery. Psycho-oncology 2010;19:1205-1212.

74. Howard JH, Bland KI. Current management and treatment strategies for breast cancer. Current opinion in obstetrics & gynecology 2012;24:44-48.

75. Lin PP, Allison DC, Wainstock J, Miller KD, Dooley WC, Friedman N, et al. Impact of axillary lymph node dissection on the therapy of breast cancer patients. J Clin Oncol 1993 ;11:1536-1544.

76. Noguchi M. Current controversies concerning sentinel lymph node biopsy for breast cancer. Breast cancer research and treatment 2004;84:261-271.

77. Chan S, Friedrichs K, Noel D, Pinter T, Van Belle S, Vorobiof D, et al. Prospective randomized trial of docetaxel versus doxorubicin in patients with metastatic breast cancer. J Clin Oncol 1999;17:2341-2354.

78. Mihich E. On the immunomodulating effects of anti-cancer drugs and their therapeutic exploitation. Jpn J Clin Oncol 2000;30:469-471.

79. Mihich E. Historical overview of biologic response modifiers. Cancer Invest 2000;18:456-466.

CHAPTER 2

2.1 Introduction

The lungs possess many advantages as an administration pathway including an alveolar surface area of around 100 m^2 [1], high solute permeability, limited proteolytic activity [2], a very thin alveolar epithelium of 0.2 µm, and extensive vasculature [3]. Considerable research has been carried out in investigating and improving the pharmacokinetics of several drugs, peptides and proteins from the lungs [4-8]. In the field of pulmonary drug delivery, nanoparticles have gained increasing attention as they may provide targeted delivery, sustained release, reduced dosage frequency, and improved patient compliance [3]. Recently, it has been shown that nanoparticles with a maximum size of up to 34 nm are absorbed into the blood stream and are also translocated to the regional lymph nodes after administration to lungs [9]. However, the size range investigated may be below that of particles that would be well suited for drug delivery applications. Therefore, considering the potential of lungs for the purpose of local and systemic drug delivery, we investigated the translocation and organ distribution of relatively larger nanoparticles through the pulmonary route. To test this, the biodistribution and uptake characteristics of polystyrene nanoparticles (PN) of sizes 50 nm, 100 nm, 250 nm, and 900 nm in mice, following administration to lungs by pharyngeal aspiration, were evaluated. Polystyrene nanoparticles were used as a convenient non-degradable model system due to their high degree of monodispersity; a prime importance when evaluating the effect of particle size on biodistribution. Since PN are non-degradable, they can be used to quantitatively track the fate of PN administered *in vivo*.

It has been shown that PN in the range of 250 nm – 3 µm present an optimal size for phagocytosis, whereas, those less than 250 nm were shown to be phagocytosed less efficiently

[10]. Additionally, particles less than 200 nm in size are extensively internalized via clathrin mediated endocytosis [11]. Therefore, nanoparticle sizes in this study were selected based on the premise that different uptake mechanisms may possibly lead to varied biodistribution profiles.

The main objective of this study was to understand the effect of nanoparticle size on their uptake and biodistribution from lungs, specifically investigating the lymph deposition. Here, with a gel permeation chromatography (GPC)-based detection technique, yielding the quantitative concentration of polystyrene present in each tissue from tissue extracts, we determine the pulmonary uptake potential and biodistribution of PN.

2.2 Materials

PN of sizes 50 nm, 100 nm, 250 nm, and 900 nm were purchased from Polysciences Inc. Nanoparticle suspensions of 1% w/v concentration were used. Hematoxylin, eosin Y disodium salt, ethyl alcohol (anhydrous), xylene (histological grade), and Permount® were purchased from Fisher Scientific. Solvents were of HPLC grade or higher, and were purchased from Fisher Scientific.

2.3 Methods

2.3.1 Administration of nanoparticles to mice

Male BALB/c mice weighing between 20-25 g (Charles River Inc.) were used following acclimation for one week. Food and water were available to the animals *ad libitum*. All animal procedures adhere to American Veterinarian Medical Association (AVMA) Guidelines, Wayne State University Institutional Animal Care and Use Committee (IACUC) approval, in accordance with the Office of Laboratory Animal Welfare (OLAW) Public Health Service Policy on Humane Care and Use of Laboratory Animals, and Principals of Laboratory Animal Care. All studies were performed in animal cohort groups of 6 (n=6). Mice were anaesthetized by inhalation of 2.5% v/v isoflurane and placed on a slant board with the back resting on the board, and partially suspended with a rubber band by their incisors. The tongue was held gently in extension and a PN suspension was placed in the pharynx region using a Hamilton microliter syringe with a 22s gauge needle of length 51 mm. The tongue was continuously held in extension until several breaths had elapsed. Once the entire dosage (150 µl) had been administered, the mice were returned to their housing and laid on their side. This method has been validated in comparison to intratracheal administration and allows for greater lung deposition and higher dose-to-dose consistency [12]. To ensure that our results are not dependant on the administration method we compared pharyngeal aspiration and intratracheal instillation for a single study group. Nanoparticle suspensions were used as provided from Polysciences Inc. However, additional biodistribution studies were performed with washed nanoparticles suspended in normal saline by sonication. Particle suspensions following the wash were sized with dynamic light scattering (DLS) on a 90Plus Particle Size Analyzer (Brookhaven Instrument Corporation) and compared to the commercially available suspensions. There was no significant difference in the size characterizations of the two suspensions (**table 3**).

2.3.2 Harvesting of tissues from mice

After the administration of nanoparticles, at predetermined intervals of 1, 3, and 5 hours, various tissues were harvested. Before performing the terminal surgery, the mice were anesthetized by inhalation of 5% v/v isoflurane. The list of tissues harvested is as follows: axillary lymph nodes (ALN), brachial lymph nodes (BLN), mesenteric lymph node (MLN), cervical lymph nodes (CLN), lungs, liver, stomach, small intestine, kidneys, spleen, blood, brain, heart, bronchoalveolar lavage (BAL), and thymus. For collecting the BAL, 0.5 ml of normal saline was injected into the lungs *per os* and the inflated lungs were gently massaged and the rinsate was collected back into the syringe.

2.3.3 Tissue processing

Tissue samples were processed and analyzed by a method modified from previously described studies [13, 14]. The harvested tissues were physically homogenized using a tissue homogenizer. Following homogenization, the tissues were frozen and lyophilized to remove water. To each lyophilized tissue vial, chloroform was added and placed on a mixer for extraction over 96 hours. Following this, all the tissues were filtered using a 0.2 µm PTFE Millipore filter. The filtrate containing the polymer/tissue extracts was frozen at -80˚C overnight and lyophilized. Following this, the polymer and/or tissue extracts remain in the vial. To each vial, a known volume (0.5 ml or 1 ml) of tetrahydrofuran was added, placed on the mixer for 1 hour and then filtered into a conical GPC analysis vial using a 0.2 µm syringe filter. To verify this method of extraction for PN, three tissues (ALN, heart, spleen) were doped with a known amount of PN and processed to extract PN as mentioned above. Upon analysis by GPC, as described in section 2.3.4, the extraction yield for PN for the three tissues was 94.5, 98.2, and 90.9% (**table 4**).

2.3.4 Method of analysis

Analysis of polymer concentration from tissue extracts was performed by GPC (GPC Max VE 2001, Viscotek Corporation) equipped with a column bank consisting of three columns with size exclusion limits of 4 million, 70,000, and 5,000. A refractive index (RI) detector (VE 3580, Viscotek Corporation) was used for polystyrene detection. The area under the polystyrene peak was compared to a standard curve of GPC peaks for polystyrene samples of known concentration. This method yields absolute quantitative data and is label-free. The amount of polymer in each tissue is expressed as a percent of administered dose. As this is a quantitative method, mass balance was analyzed for all study groups and the quantity of PN residing in the lung tissue at each time point is presented.

2.3.5 Tissue histology

Five hours after administering the particles by pharyngeal aspiration, the mice were sacrificed and the harvested tissues (lungs and lymph nodes) were fixed with 4% paraformaldehyde overnight at 4°C. The lung sections were cryosectioned on a cryotome (Cryotome FSE, Thermo Scientific) into 10 μm-thick sections, which were then stained with standard hematoxylin and eosin (H&E) staining (Harris hematoxylin for 3 min followed by running tap water for 1 min, eosin Y for 5 min, 70% ethanol for 1 min, 95% ethanol for 1 min, 100% ethanol for 1 min, two rinses in 100% Xylene for 1 min each) and cover slip mounted. The stained lung and lymph node tissues were then observed under inverted bright field microscopy (Olympus 1x71, DP70).

2.3.6 Transmission electron microscopy

Portions of tissues harvested for histology were also collected for transmission electron microscopy (TEM). Tissues were dissected down to 1–2 mm^3 and fixed in 2% paraformaldeyde, 1.25% glutaraldehyde, 0.2% sucrose and 25mM HEPES buffer in 0.12M sodium cacodylate TEM buffer at 4^oC for 4 hours. Tissues were then washed in 0.12M sodium cacodylate, gradually going to room temperature. A secondary fix in 3% glutaraldehyde and 4% tannic acid (lipid mordant) in sodium cacodylate at 37 ^oC for 1 hour, was performed and rinsed with 0.12M sodium cacodylate. Osmium tetroxide and 2% sodium cacodylate were used as post-fixative stains. For application of a non electron-dense staining, samples were stained *en block* with 2% uranyl acetate followed by dehydrating tissues in graded ethanol series of 10 minutes each. Fixed tissues were transfer to conical Beem capsules (Electron Microscopy Sciences; Hatfield, PA). Propylene oxide was added quickly and enclosed with the tissue for 2 hours. Finally, Embed 812 was added in gradual ratios for 2 hours. Samples were cured at 55^{o}C for 2 or 3 days. Tissues were ultrathin sectioned using a microtome Diatome with a diamond knife, transferred to Formvar film copper grids, and post-stained with NaOH-treated 0.03% lead citrate for 5 minutes. The stained tissues were then observed under a Zeiss EM-900 TEM at 50Kv.

2.3.7 Statistical analysis

Data are expressed as mean ± SEM with cohort sizes of 6. Statistical analysis was performed using one-way ANOVA followed up by Tukey's test with OriginPro® software. The differences were defined statistically significant at $p<0.05$.

2.4 Results

2.4.1 Effect of size on the total uptake of PN

Total uptake for all PN sizes at 1, 3 and 5 hours is shown in **figure 6**. At 1 hour, the total uptake for 50 nm (5.2%) and 100 nm (6.2%) PN is low, and is higher for 250 nm and 900 nm at 14.8% and 14.7%, respectively. At the 3 hour time point, we see a reversal in trend where the 50 nm PN has the highest total uptake (24.4%) and an increase in PN size leads to a decrease in total uptake. At this time point, the total uptake for 100 nm is 11.3% and for 250 nm is 13.1%, further decreasing to 4.8% for the 900 nm PN. A similar trend can be seen at the 5-hour time point where the highest total uptake is for 50 nm PN at 20.9% and the lowest is for 900 nm PN at 7.5%. At this time point, the total uptake for 100 nm and 250 nm PN is 15.3% and 12.4%, respectively. Inset in **figure 6** is a representative histology image of the lung 5 hours after 50 nm PN administration. It can be noted that there is minimal infiltration and alveoli are intact. While it is not possible to see discrete particles at the image magnification, no aggregated clusters of nanoparticles were seen either. When the lung tissue was further investigated with TEM, discrete PN are seen without the presence of aggregates (**figure 7**). Both larger PN and small PN (representative images for 900 nm and 50 nm PN shown in **figure 7**) were internalized from the alveolar space into the interalveolar septum without observed disruption to the epithelial cell layer.

2.4.2 Effect of size on the biodistribution of PN

The biodistribution of PN of different sizes (50 nm, 100 nm, 250 nm, and 900 nm) at time points of 1, 3, and 5 hours is presented in **figures 8 – 10**. The distribution of PN in tissues is represented as % of the total administered dose. In this study, the amount of PN in lymph nodes (LN) is the cumulative amount of PN detected in each of the tissues including axillary, brachial, cervical, mesenteric lymph nodes, and thymus (a primary lymphoid organ). The highest deposition of nanoparticles was in the lymph nodes and the lymph node of highest deposition was the axillary node for each of the sizes studied. LN deposition is discussed in further detail in the subsequent section.

In the liver, the primary reticuloendothelial system (RES) organ, there is minimal presence of PN across all time points and sizes. The highest level of liver accumulation is 1.1% of the dose for 50 nm at hour 3. For all sizes, no PN were detected in the liver at 1 hour post-administration.

Further, the larger 900 nm PN were not found in the liver during any of the time points tested. In the first hour after pulmonary administration the only organ to have significant accumulation outside of the LN is the spleen. In spleen, we see a general trend of increasing PN accumulation with an increase in size, the highest being 2.2% for 900 nm PN. Distribution to all other tissue compartments was minimal (<1%) including the central blood compartment.

However, by hours 3 and 5 post-pulmonary administration, a significant amount of 50 nm PN (3.4% and 3.1%, respectively) was detected in the blood compartment. Blood distribution was low for all other sizes with the highest being 1.3%. At these time points, PN distribution was highest in the LN followed by heart and spleen, with very low amounts detected in other tissues. This was true for all sizes except for 50 nm where more PN were present in the blood than spleen. There is also a general inverse relationship to PN size across all tissues with smaller PN having higher deposition than larger PN.

To ensure that the uptake and biodistribution results reported here were not an artifact of the nanoparticle suspension media, we tested 900 nm PN after a series of washes and re-suspension in sterile saline. Sizing data for the two suspensions can be found in **table 3**. The uptake and LN distribution of the washed nanoparticles (biodistribution shown in **figure 11**) were similar to the manufacturer suspension without statistical differences. However, the washed particles did have significantly less distribution to the heart and spleen. Additionally, for a single study group (50 nm at 5 hours), intratracheal installation was compared to pharyngeal aspiration to identify any possible dependencies of our results on the method of administration. Comparison of the biodistribution following the two methods is shown in **figure 12**. The pattern of tissue distribution remained the same with the LN having the highest deposition; however, both the uptake and the LN distribution were significantly less for the intratracheal administration as discussed in further detail in section 2.5.

2.4.3 Lymph node distribution of PN

PN were deposited in greater amounts in the lymph nodes as compared to other tissues for all PN sizes and time points as can be seen in **figures 8 – 10**. The amount of PN deposited in the lymph nodes was highest for 50 nm size at 5 hours (12.3% of dose). The 100 nm PN show a trend of increasing lymph deposition with time ranging from 3.6% to 6.9% over the period of 5 hours. For the 250 nm size, there is no statistically significant difference in the amount of PN deposited in the lymph nodes at the three time points where the amount of lymph node deposition of PN ranges from 6.5 to 8.0% of dose. For the 900 nm PN, the lymph deposition is the highest at 1 hour (6.2%). Similar to the results of total PN uptake, the PN distribution to the lymph is highest for the larger PN in the first hour, but for 3 and 5 hours the trend reverses resulting in an inverse relationship with size (smaller PN have highest LN distribution).

However, when the lymphatic distribution of PN is normalized for the amount of PN uptake (i.e. the amount of PN in the lymph nodes calculated as a percentage of the total absorbed PN from the lungs) further information on LN specificity and PN size relationship is gained. From the normalized lymphatic distribution (**figure 13**), the 1 hour time point displays a general decrease in the percentage of absorbed PN depositing in LN with increased PN size though no statistical differences exist. However, at the 3-hour time point we see a general trend of increasing percentage of absorbed PN depositing in lymph nodes for each increase in PN size with no statistical significance at this time point. Furthermore, at this time point the 900 nm PN has a normalized lymph deposition of 50.3% compared to 33.4% for the 50 nm PN. The 5 hour normalized LN distribution reveals that no trend and no significant differences exist among all NP sizes.

To further investigate the LN specificity beyond the normalized data, the amount of PN per gram of tissue was plotted (**figure 14**) based on the wet tissue weight directly following tissue harvesting. For 50 nm PN at 5 hours, the amount of PN per gram of tissue in LN (3 mg/g) is more than 4-fold higher as compared to that in spleen (0.7 mg/g), which is the organ with the next highest distribution of 50 nm PN. Similarly, the amount of PN per gram of tissue in LN when compared to liver and spleen combined together is 3 times higher for 100 nm, more than 4 times higher for 250 nm, and ~4 times higher for 900 nm PN (**figure 14**). Similar results are observed at the 1 hour and 3 hour time points where the amount of PN deposition in LN is multiple fold higher as compared to the liver and spleen (**figure 14**).

Since the ALN was the tissue of highest PN distribution among the lymph nodes tested, ALN tissue was histologically examined and a representative image of ALN with 250 nm PN is shown (**figure 15**). It can be seen that a cluster of PN is present in the ALN. The PN cluster is an irregularly shaped aggregate distinct from that of the relatively larger, and round nuclei of the ALN. The PN cluster becomes more obvious in the magnified image inset in **figure 15**.

2.5 Discussion

In this work, we investigated the uptake and tissue distribution of 50 nm, 100 nm, 250 nm, and 900 nm PN following pulmonary administration. We observed that PN of the stated sizes distribute from the lungs to LN in relatively large amounts and to other major organs to a lesser extent including little distribution to RES organs. The relatively rapid and high uptake of the model PN to LN, in addition to a high LN specificity, suggests potential for LN-directed pulmonary drug delivery.

The total translocation of PN out of the lungs was found to be significant with as much as 20.9% in as little as 5 hours for the 50 nm PN (**figure 6**). The translocation of PN from the lungs to extrapulmonary organs is in accordance with the observations made by Sarlo *et al.*, where they reported the translocation of fluorescently labeled PN of sizes 20, 100, and 1,000 nm from the lungs into various organs including liver, spleen, heart, brain, and kidneys [15]. In their study, rats were subjected to an acute exposure or a repeated exposure of fluorescently labeled PN to the lungs followed by semi-quantitative analysis of fluorescent intensities in excised organs. In all cases (the quantitative results presented here and the semi-quantitative observations in the paper by Sarlo et al.) the smallest size PN (50 nm and 20 nm, respectively) had the highest extrapulmonary translocation. In addition, at the early time point of 1 hour, both studies demonstrate lower uptake for the small PN size compared to larger PN sizes. Size-dependant translocation kinetics, where smaller PN have a relatively slower initial translocation, but higher overall translocation compared to larger PN, may be a result of different internalization pathways. Our investigation of lung tissue with TEM demonstrated PN internalization from the alveolar space into the interalveolar septum (**figure 7**). Uptake mechanisms are not directly evident from these images, but are an area of current investigation. However, it is clear that PN of all sizes are being internalized from the lung alveoli as indicated from our quantitative uptake and biodistribution analysis.

Following translocation from the lung, the tissue of highest PN deposition is the LN. The amount of 50 nm PN in LN is 12.3% at 5 hours, which is more than half the total uptake (20.9%). This is a particularly significant amount of lymph node translocation of PN in a short time frame of 5 hours. Histological examination of the ALN resulted in discrete irregular aggregates of PN that are distinct from the surrounding nuclei as represented in **figure 15**. The irregular aggregated pattern does not resemble any immune cells of the lymph nodes or any other structure belonging to lymph nodes. Therefore, it can be said that the aggregates we observe in the ALN is likely to be a cluster of PN. Further, we postulate that the PN transit to the LN by route of macrophage or dendritic cell transit due to the aggregated nature of the PN in the ALN.

Previously, it was shown that polymer nanoparticles of different sizes and surface properties passively deposit in the lymph nodes (popliteal, iliac, inguinal, and renal lymph nodes) when administered under the dorsal surface of the left hind footpad in rats [16]. However, subcutaneous or intramuscular injection routes of administration have not been shown to effectively target nanoparticles to the regional lymph nodes of the thoracic cavity and neck (i.e. ALN, BLN, and CLN), which play a critical role in many diseases including breast cancer, lung cancer, and lymphadenopathies. Oussoren and Storm have shown that liposomes of 100 nm size do deposit in ALN and BLN, but at a very low amount (of less than 2% of injected dose/g of tissue) following subcutaneous administration [17]. In contrast to this, we see a very high amount of PN depositing to the ALN, BLN and CLN after pulmonary administration, ranging from 90-230% of administered dose/g of tissue (when calculated in the same manner as Oussoren and Storm). This suggests that pulmonary administration may be a preferred route to effectively deposit nanoparticles in the ALN and BLN.

An interesting observation from the LN deposition of PN is that, though the 50nm PN had the highest LN deposition (**figure 10**), the 900 nm PN had a greater percent of the absorbed PN depositing in LN (**figure 13**). This is an important observation indicating the greater fraction of the absorbed PN accumulating in the LN presents a potential for effective LN targeting, thereby significantly reducing the possibility of systemic side effects. Moreover, PN of all the sizes tested have a higher propensity to deposit in the LN as compared to other tissues.

The specificity of PN for LN over major organs, especially the RES organs (liver and spleen), is a remarkable result. From **figure 14**, at the 5 hour time point the amount of PN in LN is in the range of 1,140 – 3,027 µg /g of tissue with the highest deposition being for the 50 nm size, and lowest for the 900 nm size. Considering the small size and weight of the LN, this is a significant amount of deposition and may indicate localized therapeutic potential for biodegradable nanocarriers of similar properties to the model PN. Therefore, the significant amount of uptake from lungs in the short time period of 5 hours in addition to the high propensity of PN distribution to the LN supports the potential of nanoparticulate pulmonary drug delivery systems for systemic and lymph-targeted therapies.

The liver, spleen, and lungs constitute the RES, which is responsible in removing foreign substances from blood circulation following opsonization [18]. When administered intravenously, a great majority of polymer nanoparticles accumulate in the liver and spleen as a result of RES sequestration [15, 19-23]. Evasion of RES clearance has become a large area of interest in the drug delivery field resulting in the prevalence of ‘stealth’, PEGylated carrier systems. It has been widely reported that a great proportion of polymeric and non-polymeric nanoparticles are sequestered by the RES within a time frame of minutes to less than an hour after intravenous administration [24-26]. However, when administered to the lungs, the PN are deposited in small amounts (of less than 2% of administered dose) in the liver and spleen. This result is in accordance with the observation by Sarlo *et al*. (15), where less than 1% of the recovered dose of fluorescently labeled PN was deposited in the liver and spleen following administration to lungs by pharyngeal aspiration. The negligible amounts of PN deposited in the liver and spleen is of particular interest as it indicates the pulmonary route as another potential systemic delivery mechanism to evade RES.

PN that do distribute to the RES organs are found mostly in the spleen and the biodistribution pattern of spleen mimics the general trend of biodistribution in LN. At the 1-hour time point in spleen, we see a general trend of increase in the amount of PN with increasing size as seen in LN (**figure 8**). However, at 3 and 5 hours, we see the amount of PN in spleen decreases with an increase in size, again similar to LN at these time points (**figures 9** and **10**). We speculate that PN transit from the lung to LN, and then through the lymphatic system to the spleen. This is further substantiated by the observation of PN in higher amounts in the spleen than liver. If PN transit to the spleen were to occur through the blood circulation, we would expect to see deposition in both the liver and spleen by RES sequestration.

In order to further verify the observed biodistribution data, 50 nm PN uptake and distribution studies (the study group with highest total uptake and lymph distribution) were repeated under additional study conditions. To ensure that the suspension medium was not a factor influencing total uptake, PN were washed several times, lyophilized and resuspended by probe and bath sonication in sterile, normal saline. Size characterizations of the washed and commercial suspensions by DLS were not statistically different (**table 3**). Uptake and biodistribution results from the washed nanoparticle study group did not show any significant difference to the studies discussed above (**figure 11**). Additionally, we repeated studies using intratracheal installation despite pharyngeal aspiration already being validated by other labs [12, 15], and found very similar results, but with a slight decrease in the total uptake, which was not statistically significant (**figure 12**). This slight decrease in uptake may be due to non-even lung deposition with intratracheal administration [12]. No differences in biodistribution were observed. Histology of the lung following PN administration demonstrates that the alveolar wall was of normal thickness and there was no evidence of alveolar collapse. In the lung image, there appears to be little or no severe cell infiltration and inflammation, suggesting that the PN administration caused no severe acute damage to the lungs. In contrast, the intratracheal instillation technique of administering the payload to lungs invokes severe cell infiltration and inflammation due to invasiveness of the technique [27]. Therefore, we feel the pharyngeal aspiration technique is more suitable for studying the biodistribution of nanoparticles from lungs. Recently, the method has gained attention as a more suitable technique for studying chemically induced diseases such as asthma [28].

The quantitative nature of the GPC assay used allowed us to determine mass balance for all study groups. The mass balance of PN ranges from 80-90% of the administered dose for all sizes at 1 hour. However, it decreases with time for all sizes (**figure 16**). We attribute this decrease in mass balance to the possible redistribution of PN to tissues like muscle, bone, adipose tissue, urine, etc.: tissues that were not collected in this study. In the discussion above we took the conservative approach of only considering the particles detected in tissues when calculating uptake. However, our mass balance indicates that the potential uptake may actually be higher. **Figure 17** represents the amount of PN in the lungs at all time points for all PN sizes. Except for the 900 nm PN, there is a general trend of decrease in the PN amounts in lungs with time for all other PN (**figure 17**).

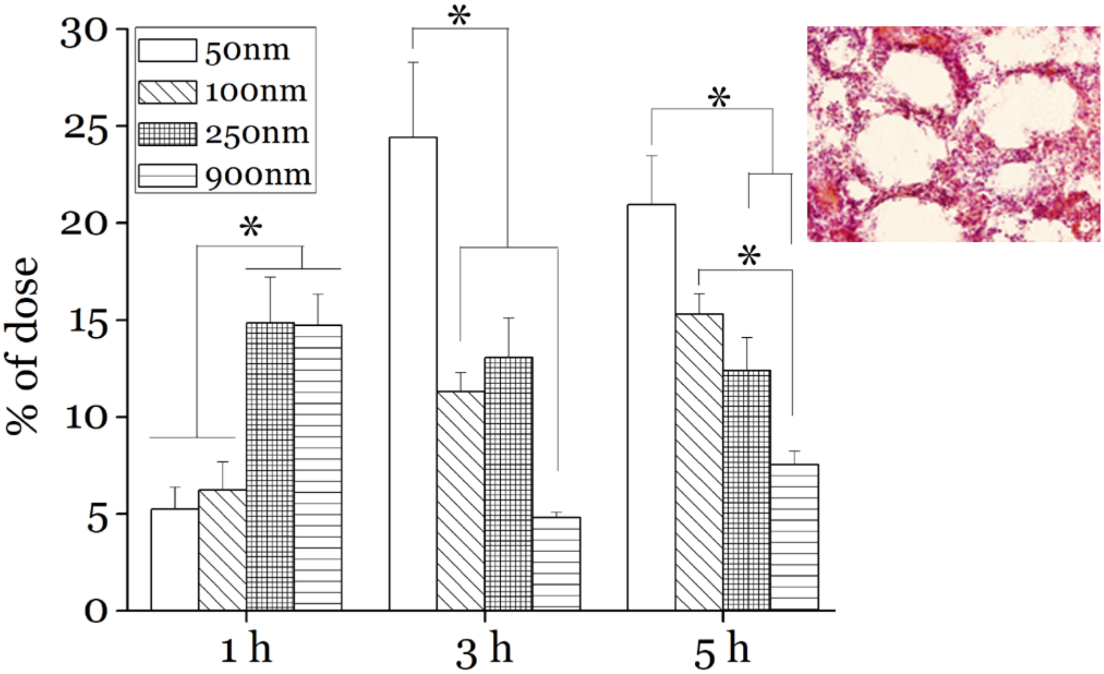

Figure 6. Extrapulmonary uptake of 50, 100, 250 and 900 nm PN at 1, 3 and 5 hours following pulmonary administration as a % of dose. * $p<0.05$ (n=6; mean ± SEM). Inset; histology of lungs after administration of 50 nm PN (630X magnification).

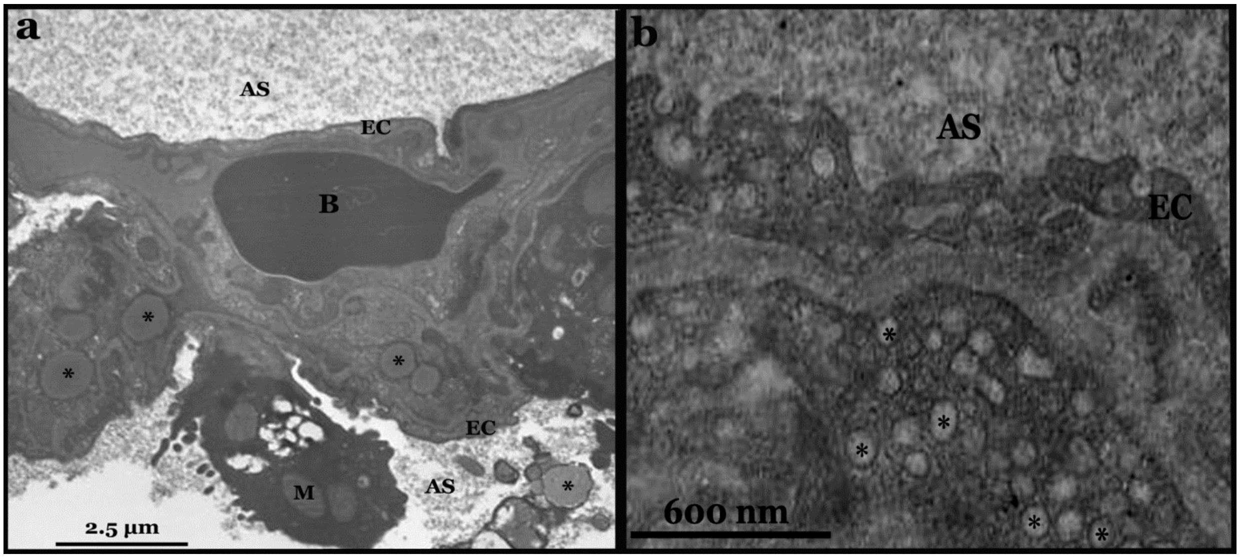

Figure 7. TEM images of lungs after 900 nm (a) and 50 nm (b) PN administration. AS, alveolar space; B, red blood cell; EC, epithelial cell layer; M, mitochondria; *, PN. Scale bars are 2.5 µm (a) and 600 nm (b).

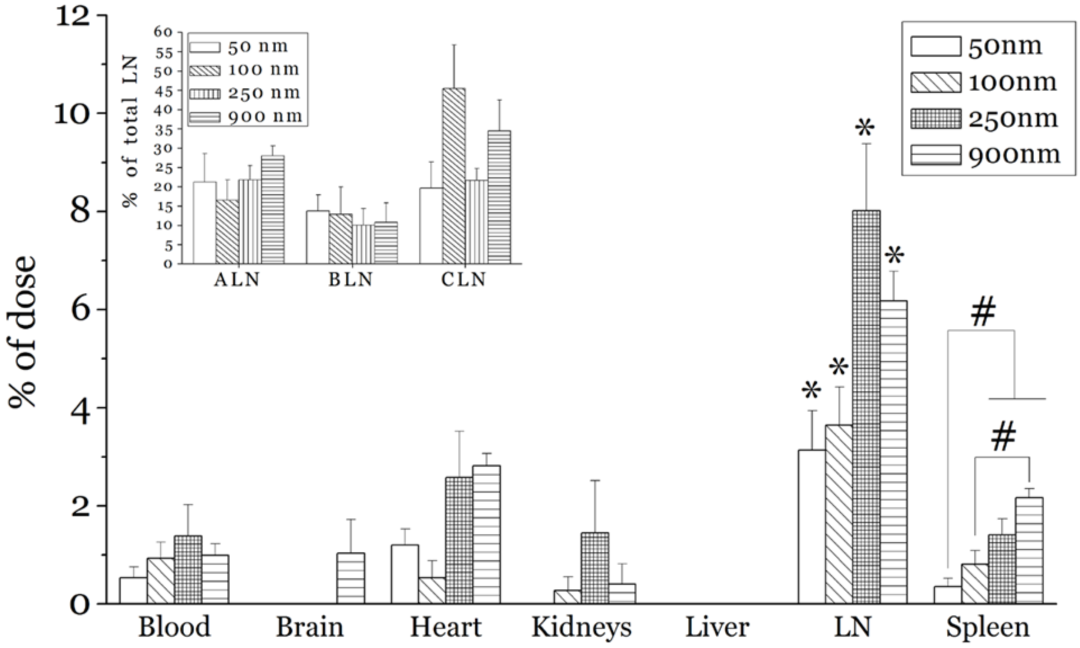

Figure 8. PN biodistribution 1-hour after pulmonary administration as a % of dose. LN, Lymph nodes; *, p<0.05 when compared to every tissue among each size; #, p<0.05 when

comparing the two tissues represented by this symbol (n=6; mean±SEM). Inset; percent PN distribution among various LN. ALN, axillary lymph nodes; BLN, brachial lymph nodes; CLN, cervical lymph nodes.

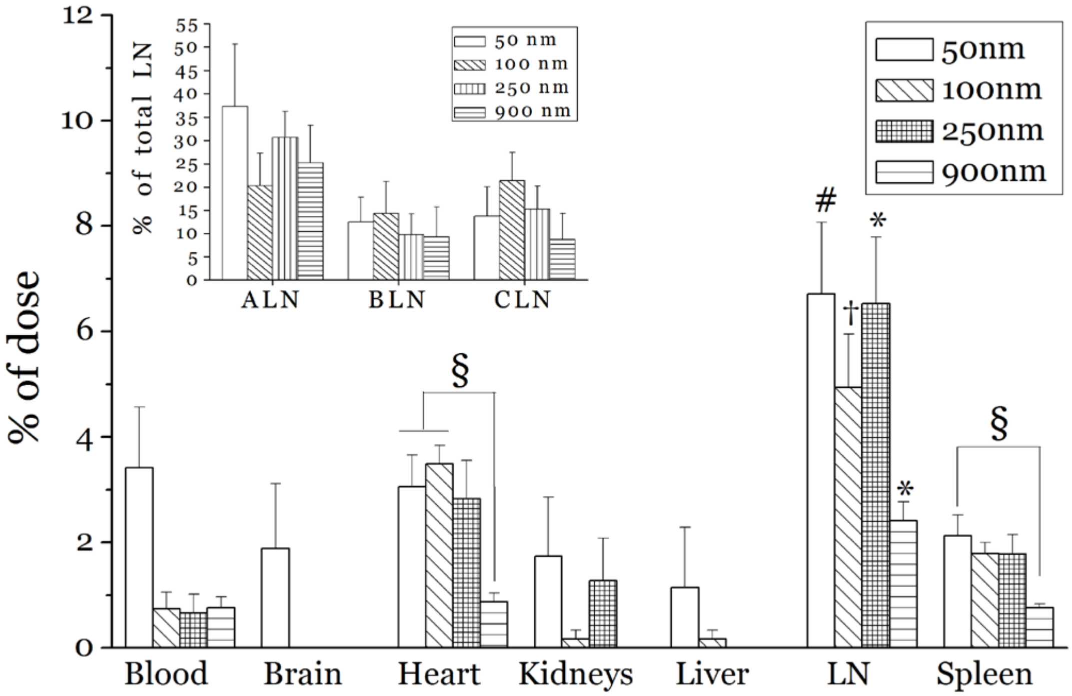

Figure 9. PN biodistribution 3-hours after pulmonary administration as a % of dose. LN-Lymph nodes; *, $p<0.05$ when compared to every tissue among each size; †, $p<0.05$ when compared to every tissue except for heart, #, $p<0.05$ when compared to every tissue except for heart and blood. §, $p<0.05$ between the two tissues represented by this symbol (n=6; mean ± SEM). Inset; percent PN distribution among various LN. ALN, axillary lymph nodes; BLN, brachial lymph nodes; CLN, cervical lymph nodes.

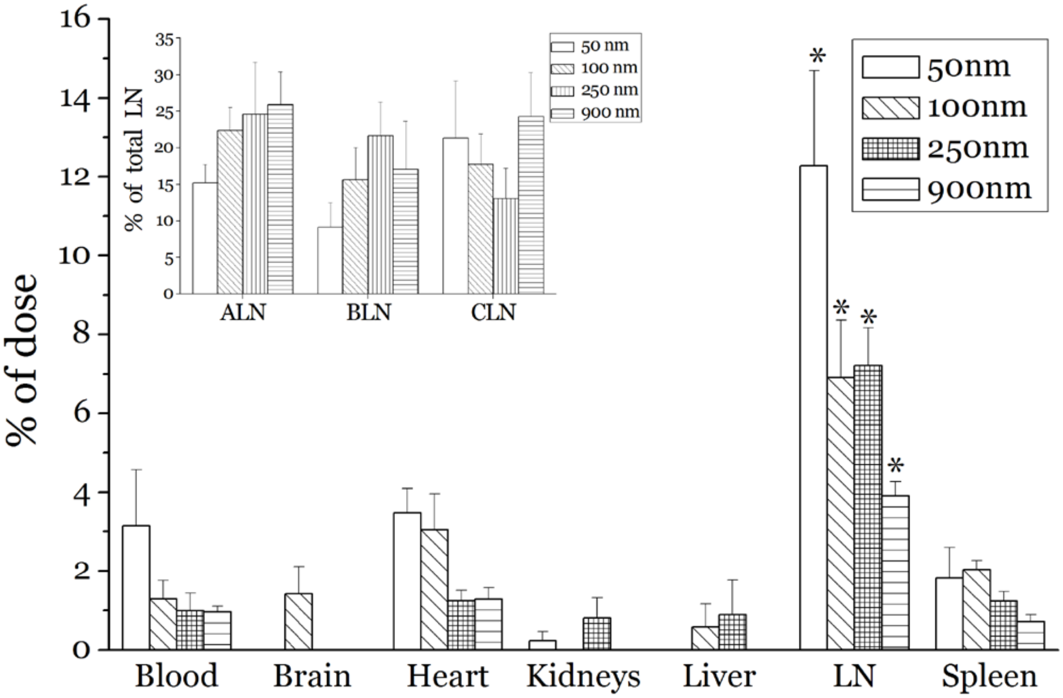

Figure 10. PN biodistribution 5-hours after pulmonary administration as a % of dose. LN-Lymph nodes; *,p<0.05 when compared to every tissue among each size (n=6; mean ± SEM). Inset; percent PN distribution among various LN. ALN, axillary lymph nodes; BLN, brachial lymph nodes; CLN, cervical lymph nodes.

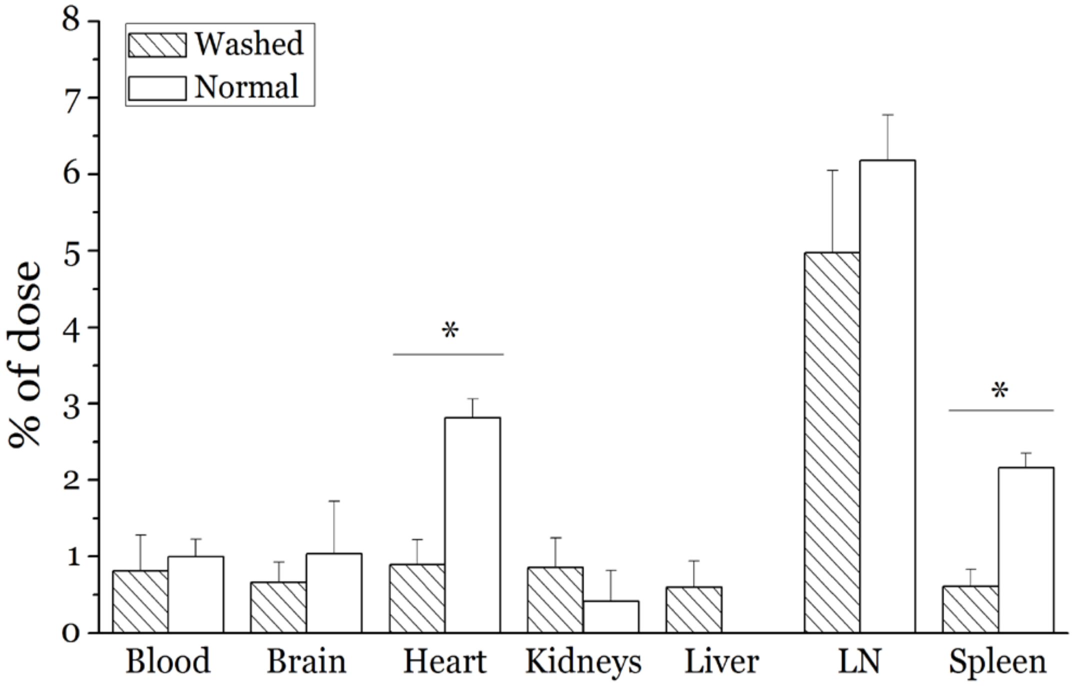

Figure 11. Biodistribution of PN (normal and washed) of 900 nm size 1 hour after administration to the lungs. LN, lymph nodes; *, $p<0.05$ between the two data sets (n=6; mean±SEM).

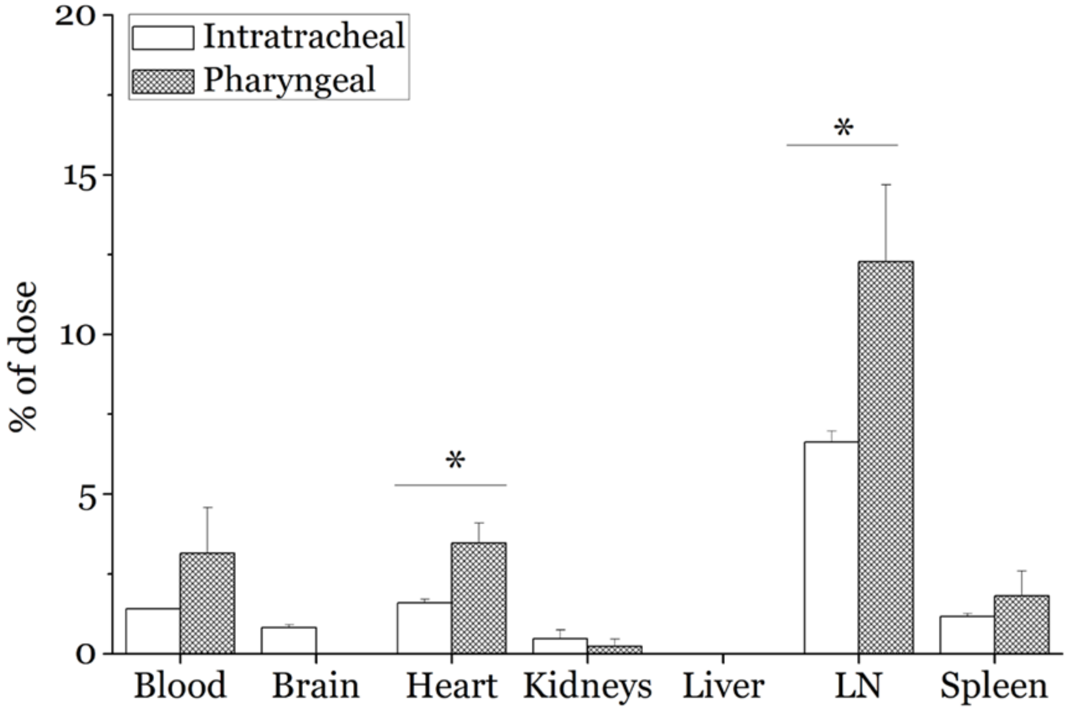

Figure 12. Comparison of the biodistribution of 50 nm PN 5 hours after administration by intratracheal instillation and pharyngeal aspiration. LN, lymph nodes; *, p<0.05 between the two data sets (n=6; mean±SEM).

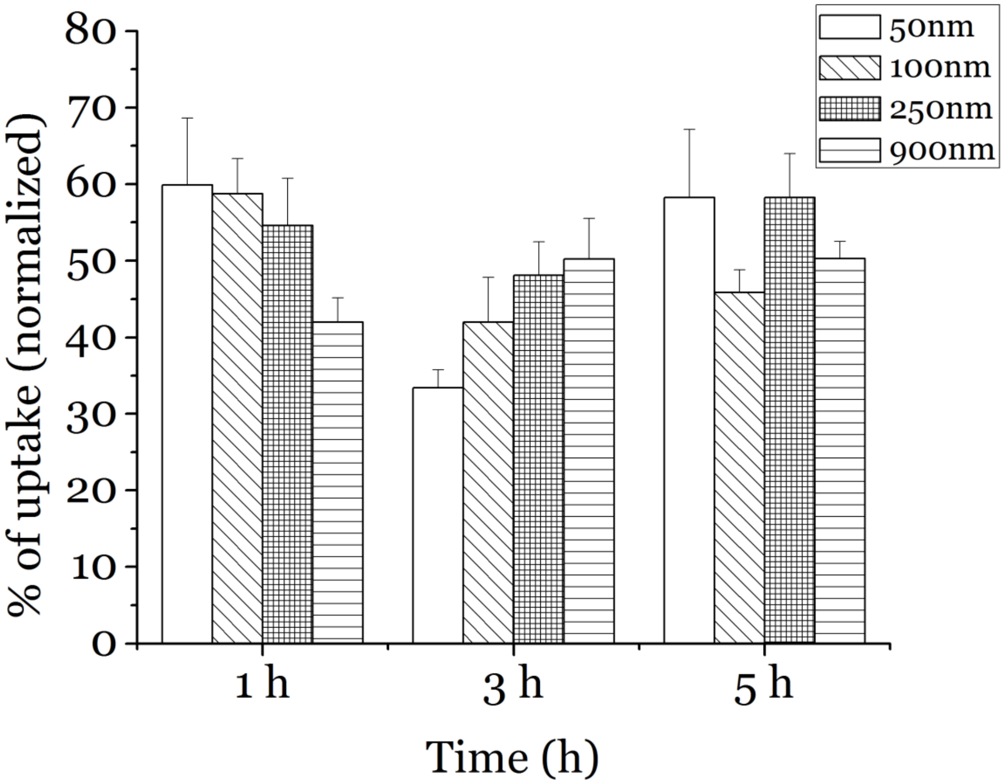

Figure 13. Normalized lymph node deposition of PN 1, 3, and 5 hours after pulmonary administration as a % of uptake (n=6; mean ± SEM).

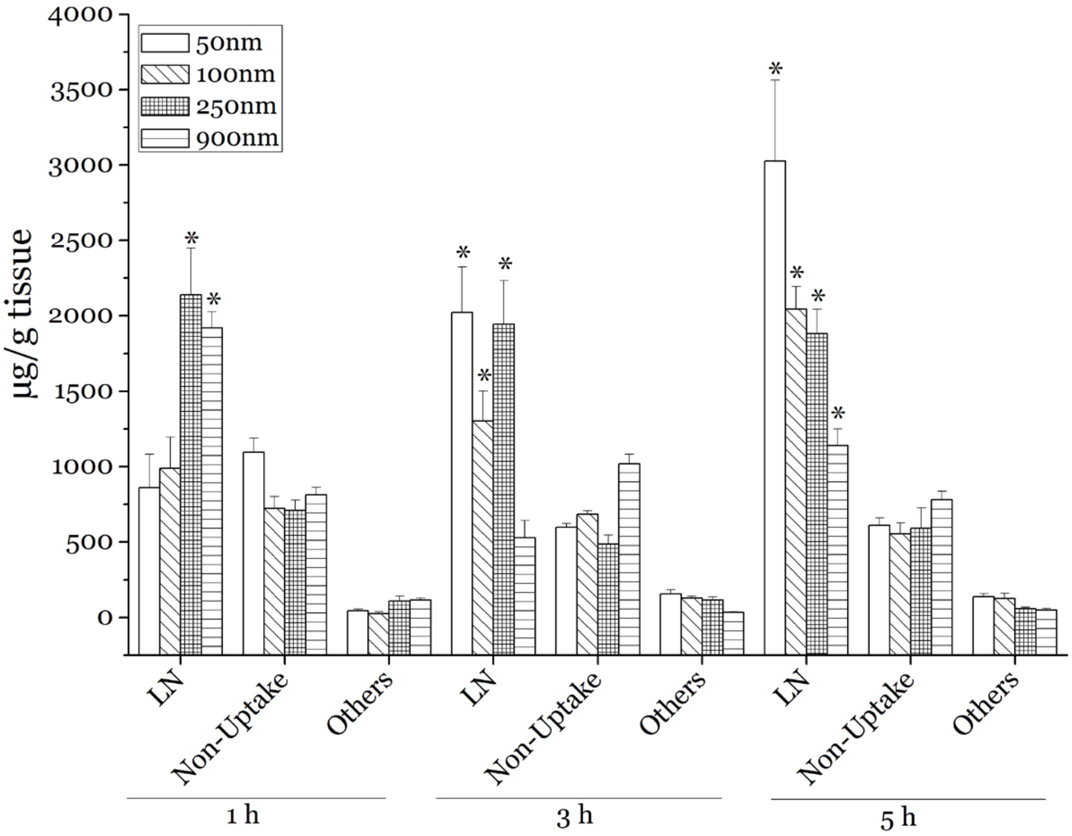

Figure 14. Lymph node (LN) specificity of PN 1, 3, and 5 hours after pulmonary administration. *, $p<0.05$ when compared to the other two sets of tissues (non-uptake and others) among each size. Amount of PN in LN is represented as µg/g of tissue compared to non-uptake (lung, lung rinse, GI) and others (all others including liver, spleen and heart) (n=6; mean ± SEM). Note: Non-uptake includes the nanoparticles deposited in lungs and GIT.

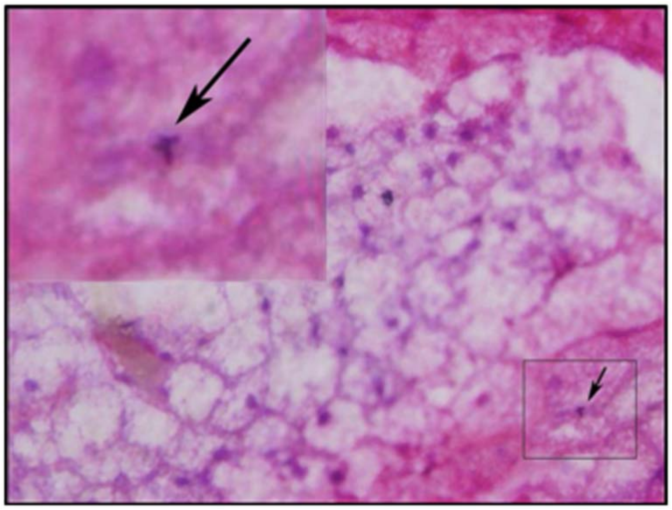

Figure 15. Histological image of the axillary lymph node (ALN) 5 hours after pulmonary administration of 250 nm PN (630X magnification). Inset; digital magnification of the cluster of PN (arrow) in the ALN. PN cluster is distinct from the bigger and more regular shaped nuclei seen throughout the image.

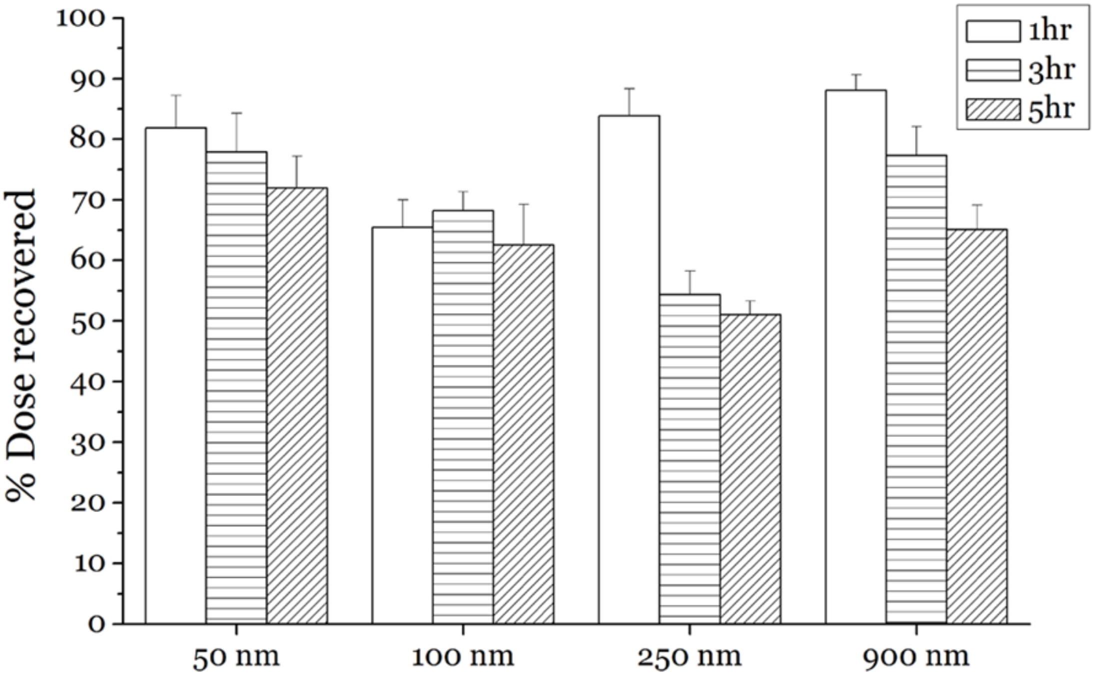

Figure 16. Mass balance for all study sets (n=6; mean ± SEM).

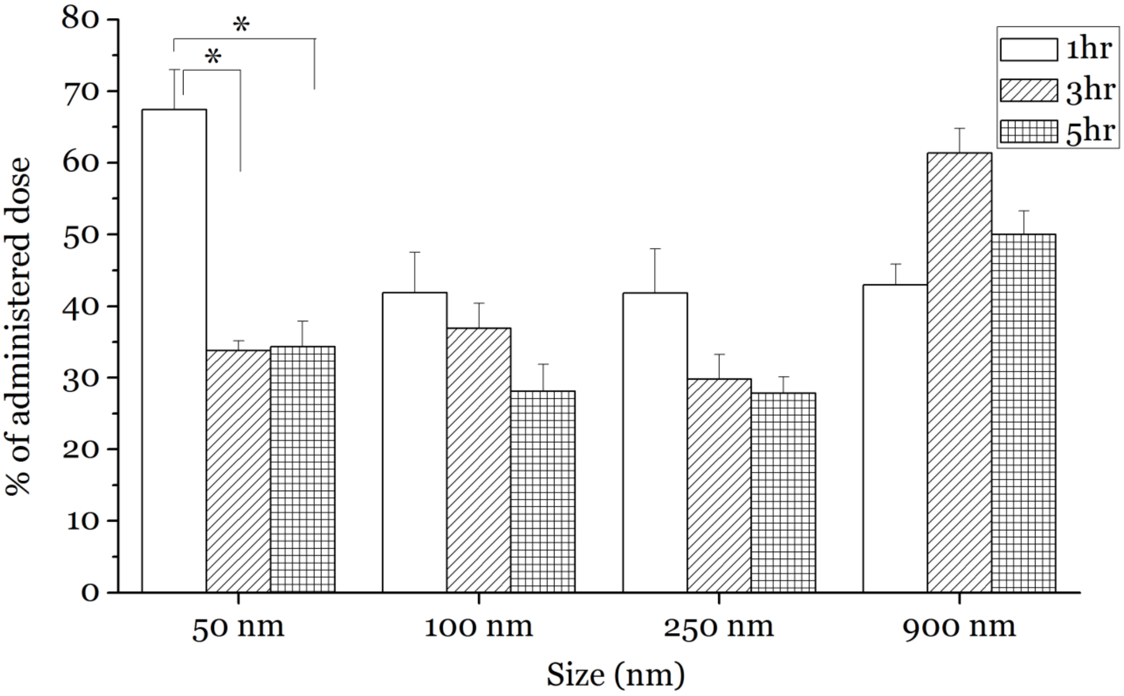

Figure 17. Amount of PN present in the lungs at all time points. *, p<0.05 between the indicated time points (n=6; mean ± SEM).

Parameters	Before washing	After washing
Size (nm)	833.3±31	788.2±89
PDI	0.102±0.039	0.052±0.03

Table 3: Size of polystyrene nanoparticles before and after washing with deionized water.

Tissue	Amount of PN added (mg)	Amount recovered (mg)	% Recovery
ALN	0.55	0.52	94.5
Heart	0.55	0.54	98.2
Spleen	0.55	0.50	90.9

Table 4: Recovery of PN from doped tissues after processing

2.6 Conclusions

This study illustrates the potential of nanoparticles administered to the lungs for systemic use in general and lymph related therapies in particular. Though clear differences in biodistribution and uptake were observed based on the nanoparticle size, other physiochemical parameters also affect the biodistribution, but are not in the scope of this work. Furthermore, when designing nanoparticles for pulmonary administration, the potential of toxicity to the lungs needs to be taken into consideration.

We observed a higher deposition of nanoparticles in the regional lymph nodes as compared to other major tissues. The importance of this result is augmented by the relatively rapid transit following lung administration (≤5 hours). Further research in this area is needed to exploit the potential of nanoparticles delivered via oral inhalation for vaccines or in the treatment of an array of lymph related disorders.

2.7 References

1. Smola M, Vandamme T, Sokolowski A. Nanocarriers as pulmonary drug delivery systems to treat and to diagnose respiratory and non respiratory diseases. International Journal of Nanomedicine. 2008;3:1-19.

2. Patton JS. Mechanisms of macromolecule absorption by the lungs. Advanced Drug Delivery Reviews. 1996;19:3-36.

3. Sung JC, Pulliam BL, Edwards DA. Nanoparticles for drug delivery to the lungs. Trends Biotechnol. 2007;25:563-70.

4. Patel LN, Wang J, Kim KJ, Borok Z, Crandall ED, Shen WC. Conjugation with cationic cell-penetrating peptide increases pulmonary absorption of insulin. Mol Pharm. 2009;6:492-503.

5. Koushik K, Dhanda DS, Cheruvu NP, Kompella UB. Pulmonary delivery of deslorelin: large-porous PLGA particles and HPbetaCD complexes. Pharm Res. 2004;21:1119-26.

6. Lee J, Oh YJ, Lee SK, Lee KY. Facile control of porous structures of polymer microspheres using an osmotic agent for pulmonary delivery. Journal of Controlled Release. 2010;146:61-7.

7. Zhang Q, Shen Z, Nagai T. Prolonged hypoglycemic effect of insulin-loaded polybutylcyanoacrylate nanoparticles after pulmonary administration to normal rats. Int J Pharm. 2001;218:75-80.

8. Kawashima Y, Yamamoto H, Takeuchi H, Fujioka S, Hino T. Pulmonary delivery of insulin with nebulized DL-lactide/glycolide copolymer (PLGA) nanospheres to prolong hypoglycemic effect. J Control Release. 1999;62:279-87.

9. Choi HS, Ashitate Y, Lee JH, Kim SH, Matsui A, Insin N, et al. Rapid translocation of nanoparticles from the lung airspaces to the body. Nat Biotechnol. 2010;28:1300-3.

10. Korn ED, Weisman RA. Phagocytosis of latex beads by Acanthamoeba. II. Electron microscopic study of the initial events. J Cell Biol. 1967;34:219-27.

11. Rejman J, Oberle V, Zuhorn IS, Hoekstra D. Size-dependent internalization of particles via the pathways of clathrin- and caveolae-mediated endocytosis. Biochem J. 2004;377:159-69.

12. Rao GV, Tinkle S, Weissman DN, Antonini JM, Kashon ML, Salmen R, et al. Efficacy of a technique for exposing the mouse lung to particles aspirated from the pharynx. J Toxicol Environ Health A. 2003;66:1441-52.

13. Florence AT, Hillery AM, Hussain N, Jani PU. Nanoparticles as carriers for oral peptide absorption: Studies on particle uptake and fate. Journal of Controlled Release. 1995;36:39-46.

14. Jani P, Halbert GW, Langridge J, Florence AT. Nanoparticle uptake by the rat gastrointestinal mucosa: quantitation and particle size dependency. J Pharm Pharmacol. 1990;42:821-6.

15. Sarlo K, Blackburn KL, Clark ED, Grothaus J, Chaney J, Neu S, et al. Tissue distribution of 20 nm, 100 nm and 1000 nm fluorescent polystyrene latex nanospheres following acute systemic or acute and repeat airway exposure in the rat. Toxicology. 2009;263:117-26.

16. Rao DA, Robinson JR. Effect of size and surface properties of biodegradable PLGA-PMA: PLA:PEG nanoparticles on lymphatic uptake and retention in rats. Journal of Controlled Release. 2008;132:e45-e7.

17. Oussoren C, Storm G. Targeting to lymph nodes by subcutaneous administration of liposomes. International Journal of Pharmaceutics. 1998;162:39-44.

18. Saxena V, Sadoqi M, Shao J. Polymeric nanoparticulate delivery system for Indocyanine green: biodistribution in healthy mice. Int J Pharm. 2006;308:200-4.

19. Yaseen MA, Yu J, Jung B, Wong MS, Anvari B. Biodistribution of encapsulated indocyanine green in healthy mice. Mol Pharm. 2009;6:1321-32.

20. Shan X, Liu C, Yuan Y, Xu F, Tao X, Sheng Y, et al. *In vitro* macrophage uptake and *in vivo* biodistribution of long-circulation nanoparticles with poly(ethylene-glycol)-modified PLA (BAB type) triblock copolymer. Colloids Surf B Biointerfaces. 2009;72:303-11.

21. Bazile DV, Ropert C, Huve P, Verrecchia T, Marlard M, Frydman A, et al. Body distribution of fully biodegradable [14C]-poly(lactic acid) nanoparticles coated with albumin after parenteral administration to rats. Biomaterials. 1992;13:1093-102.

22. Simon BH, Ando HY, Gupta PK. Circulation time and body distribution of 14C-labeled amino-modified polystyrene nanoparticles in mice. J Pharm Sci. 1995;84:1249-53.

23. Panagi Z, Beletsi A, Evangelatos G, Livaniou E, Ithakissios DS, Avgoustakis K. Effect of dose on the biodistribution and pharmacokinetics of PLGA and PLGA-mPEG nanoparticles. Int J Pharm. 2001;221:143-52.

24. Gref R, Domb A, Quellec P, Blunk T, Müller RH, Verbavatz JM, et al. The controlled intravenous delivery of drugs using PEG-coated sterically stabilized nanospheres. Advanced Drug Delivery Reviews. 1995;16:215-33.

25. Illum L, Davis SS, Muller RH, Mak E, West P. The organ distribution and circulation time of intravenously injected colloidal carriers sterically stabilized with a block copolymer--poloxamine 908. Life Sci. 1987;40:367-74.

26. Sadauskas E, Wallin H, Stoltenberg M, Vogel U, Doering P, Larsen A, et al. Kupffer cells are central in the removal of nanoparticles from the organism. Part Fibre Toxicol. 2007;4:10.

27. Zhang LJ, Xing B, Wu J, Xu B, Fang XL. Biodistribution in mice and severity of damage in rat lungs following pulmonary delivery of 9-nitrocamptothecin liposomes. Pulm Pharmacol Ther. 2008;21:239-46.

28. De Vooght V, Vanoirbeek JA, Haenen S, Verbeken E, Nemery B, Hoet PH. Oropharyngeal aspiration: an alternative route for challenging in a mouse model of chemical-induced asthma. Toxicology. 2009;259:84-9.

CHAPTER 3

3.1 Introduction

Nanoparticles hold promise as drug delivery devices due to their ability to stabilize and/or protect the encapsulated drug, control release of drugs, and enable/enhance intracellular uptake. In addition, polymeric nanoparticles can be fabricated from polymers that are biocompatible and have degradation products that can be easily cleared or may even consist of natural byproducts [1, 2]. The ability of nanoparticles to transit across cellular membrane barriers and effectively release the cargo has been demonstrated for various drugs including nucleic acids and proteins [3]. Further, nanoparticle delivery systems may reduce side-effects by improving drug delivery efficiency to affected areas (targeting) and by sustaining pharmacological effects [4]. These numerous drug delivery advantages of nanoparticles emanate, in part, from the diverse physical, chemical, and biological properties that can be achieved [5]. PLGA is a particularly important polymer for use in nanoencapsulation due to its biodegradability by hydrolysis and biocompatibility. Already approved by the FDA for use in some drug delivery applications, PLGA degrades into lactic and glycolic acid, byproducts of metabolic processes [6].

The particular method of nanoparticle fabrication and encapsulation is chosen based on the type of drug used, desired route of administration and the preferred nanoparticle properties. For polymeric nanoparticles, solvent evaporation, solvent diffusion (or removal), and nanoprecipitation are commonly utilized techniques [7]. All of these techniques often suffer from the problem of low encapsulation efficiency of hydrophilic molecules due to rapid partitioning of the drug into the external aqueous phase. This problem has been overcome by modification of these nanoparticle fabrication methods [8]. Additionally, novel encapsulation methods to improving encapsulation efficiency of hydrophilic drugs (including proteins) have been developed.

One such method, phase inversion nanoencapsulation (PIN), can produce nanoparticles in a one-step process without the use of an aqueous phase or the need for stirring and/or temperature control. Several variables, including concentration of polymer, viscosity of the polymer solution, miscibility of solvent/non-solvent, and volumetric ratio of solvent/non-solvent can be used to alter nanoparticle properties including size when created by PIN [9]. Furthermore, this method of fabrication is especially advantageous for protein encapsulation. Using the PIN method, insulin has been successfully encapsulated in polymeric nanoparticles, shown to release insulin *in vivo* in the biologically active form [10] and has been successful as an oral formulation in a diabetic rat model [11]. Using this method, Mathiowitz et. al. were able to obtain a mean particle size of 96.7 nm with the copolymer poly(fumaric-co-sebacic anhydride) [10]. However, this method of nanoparticle fabrication can be applied to a range of polymeric materials including PLGA. Therefore, we chose this method with an aim of fabricating PLGA nanoparticles of the smallest possible size.

The use of polymeric surfactants such as polyvinyl alcohol, pluronic F-68 or others is common in the conventional nanoparticle fabrication methods such as emulsion method and nanoprecipitation. Surfactants are commonly used in nanoparticle fabrication to reduce interfacial tension thereby stabilizing the nanoparticle suspension, reducing nanoparticle size and preventing aggregation. The effect of surfactant concentration on nanoparticle size is well documented in the conventional single and double emulsion methods [12, 13]. Whereas in the case of the PIN method, to the best of our knowledge there have been no published reports studying the effect of surfactants on particle size and other physiochemical properties. Therefore, we carried out this study investigating the effect of non-ionic surfactant HLB (hydrophile-lipophile balance) on nanoparticle characteristics with a particular objective of obtaining the smallest possible nanoparticle size. We investigated Span 85 (HLB 1.8), Merpol A (HLB 6), Polyoxyethylene sorbitol hexaoleate (PSH) (HLB 10), and Tween 80 (HLB 15) effects on the physical properties of the nanoparticles including size, zeta potential, surface morphology and thermal properties on PLGA nanoparticles fabricated with PIN. Additionally, we investigated the effect of surfactant concentration.

From our studies discussed in chapter 2 (specific aim 1) we have seen that nanoparticles with the smallest particle size had the highest potential of translocation out of the lungs as well as deposition in the lymph nodes. However, the nanoparticles used in that study were non degradable and they were only used as a model system as emphasized and explained in further detail in chapter 2. For the purposes of drug delivery, a degradable nanoparticle system is desired which is both biocompatible and non-toxic. PLGA is one such polymer that has been extensively used in the formulation of drug loaded nanoparticles. Therefore, we envisioned the use of PLGA polymer to encapsulate a model drug for its pulmonary delivery. This chapter discusses the several approaches that have been employed in order to obtain PLGA nanoparticles of different sizes for further use in the study of their *in vitro* and most importantly *in vivo* tissue degradation characteristics which is a focus of chapter 4 (specific aim 2). This chapter therefore is a part of specific aim 2 wherein PLGA nanoparticles are fabricated for exploration of their *in vivo* tissue degradation characteristics.

3.2 Materials

PLGA (Resomer RG 502, 50:50) with an inherent viscosity of 0.16-0.24 dL/g was obtained from Boehringer Ingelheim (Germany). Span 85, Merpol A, Tween 80 and all solvents including dichloromethane and petroleum ether were of analytical grade (Fisher Scientific, USA). Polyoxyethylene sorbitol hexaoleate (PSH), polyvinyl alcohol (PVA) were purchased from Sigma Aldrich, USA.

3.3 Methods

3.3.1 Nanoparticle fabrication by PIN method

Nanoparticles were formulated using the PIN method as describe elsewhere [10]. Briefly, a 4% w/v PLGA solution in dichloromethane (solvent phase) was prepared. The surfactants were added to the solvent phase. This polymer solution was added quickly to a bath of petroleum ether (non-solvent phase) under stirring at 1000 rpm using an overhead stirrer in a solvent:non-solvent ratio of 1:100 resulting in the rapid formation of solid nanoparticles. The dispersion was then positive-pressure filtered through a membrane filter of pore size 0.20 µm (Millipore). The nanoparticles were collected, lyophilized and stored at -20˚C until further use and characterization. Formulations were labeled S1 through S16 and each formulation was replicated thrice to account for inter batch variability. The numbers in the notation indicate the surfactant and concentration used as detailed in **table 5**. Formulation C was prepared without the use of surfactant as a comparative control.

3.3.2 Nanoparticle fabrication by emulsion method and nanoprecipitation method

Nanoprecipitation method. For the 200nm size nanoparticles, 0.9% of PLGA solution in acetone was added drop wise to an aqueous solution of 1% PVA at a stirring speed of 800 rpm overnight [14]. The nanoparticles were centrifuged at 40,000 x g for 1 hour and were then washed with 30 ml deionized water thrice following which they were resuspended in 15 ml of deionized water, frozen and lyophilized.

Emulsion method. For the 500 nm size nanoparticles a previously used method was slightly modified from a previously published method [15]. Briefly, 2 ml of 5% PLGA solution in dichloromethane was added to 30ml of 0.5% PVA and sonicated at 30 watt output for 10 minutes on an ice bath. This preparation was then added to 100 ml of deionized water under magnetic stirring at 600 rpm overnight. The preparation was centrifuged at 40,000 x g to collect the nanoparticles following which the nanoparticles were washed thrice in 30 ml deionized water. After this step, the nanoparticles were resuspended in 15 ml of deionized water, frozen, and lyophilized. The nanoparticles were resuspended in 0.9% saline before administration for animal studies.

3.3.3 Size Analysis

The formulations made by the PIN method were reconstituted with 1% Pluronic F-127 solution to make 0.1% w/v dispersion and sonicated for 30-60 seconds in a bath sonicator to disperse the nanoparticles. The dispersion was then subject to size analysis on a 90Plus Particle Size Analyzer (Brookhaven Instrument Corporation). Mean values following 10 runs for each formulation were recorded.

The nanoparticle formulations made by the emulsion method and the nanoprecipitation method were reconstituted with 0.5% PVA solution to make a dispersions of 0.1% w/v concentration which were sonicated for about 30-60 seconds in a bath sonicator to disperse the nanoparticles. The dispersions were then subject to size analysis on a 90Plus Particle Size Analyzer (Brookhaven Instrument Corporation).

3.3.4 Scanning electron microscopy

A small amount of the lyophilized formulation was mounted on a carbon adhesive tape and sputter-coated with gold using 70 mA current for 25 seconds. Images of the formulation were captured at a working distance of 9 mm and an accelerating voltage of 25 kV with a JSM-6510LV-LGS Scanning Electron Microscope (SEM). For the particles made using the nanoprecipitation method, the initial sample preparation was slightly modified instead of the usual procedure of mounting the particles onto a carbon adhesive tape. Briefly, the nanoparticles were dispersed in deionized water and a few suspension droplets were added onto a transparent cover slip. This suspension on the cover slip was allowed to evaporate overnight and then the dry film of particles were sputter coated and imaged.

3.3.5 Zeta Potential measurement

The nanoparticles made by the PIN method had poor redispersibility in water, whereas they were well dispersed when 1% Pluronic F-127 solution was used as the dispersion media. Therefore, suspensions of PLGA nanoparticles (0.1% w/v) were prepared in 1% Pluronic F-127 by bath sonication for 60 seconds. Nanoparticle suspensions were subjected to zeta potential analysis on a 90Plus Zeta Potential Analyzer (Brookhaven Instrument Corporation), which uses the electrophoretic light scattering and the laser doppler velocimetry method to determine the zeta potential. Average zeta potentials following 10 runs for each formulation were recorded.

3.3.6 Thermal analysis by DSC

The DSC measurements were carried out on a Q2000 series DSC (TA Instruments). A heat-cool-heat scan was performed over the temperature range of -40˚C to 220˚C at a rate of 10˚C/min for each cycle. Data analysis was performed using the Universal Analysis 2000 software (TA Instruments). Reported glass transition temperatures (T_g) are from the first heat.

3.4 Results

3.4.1 Phase inversion nanoencapsulation

The surfactants Span 85 (HLB 1.8), Merpol A (HLB 6), PSH (HLB 10), and Tween 80 (HLB 15) were used at concentrations of 0.25%, 0.5%, 1%, and 2% v/v as shown in **table 5**.

3.4.1.1 Effect of surfactant HLB and concentration on nanoparticle size

At a concentration of 0.25% v/v, an increase in HLB value results in an increase in the nanoparticle size from 783.6 nm to 1314.5nm. At 0.5% v/v concentration, the nanoparticle size is almost same except for HLB value of 15 where the size increases to 1713.7 nm. However, at 1% v/v concentration, the nanoparticle size increases from 751.8 nm at HLB 1.8 to 1604.8 nm at HLB 6, after which it decreases to 1172.3 nm at HLB 10 (**figure 18**).

With Span 85, there is an increase in nanoparticle size from a concentration of 0.25% to 0.5% after which the size decreases. For Merpol A, there is an increase in the size with increase in the surfactant concentration from 0.25% up to 1% after which the size remains constant. For PSH, surfactant concentration doesn’t seem to affect the nanoparticle size significantly. However for Tween 80, nanoparticle size increases with concentration wherein at 0.25% concentration the nanoparticle size is 1314.5 nm which increases to 1713.7 nm at concentration of 0.5%. At concentrations above 0.5%, the nanoparticles were not able to be dispersed for sizing. Therefore, it was not possible to analyze the nanoparticle size at these higher concentrations. This difficulty in redispersibility of nanoparticles at higher concentration may be as a result of extensive aggregation at these higher concentrations (**figure 18**).

3.4.1.2 Effect of HLB and surfactant concentration on Tg of nanoparticles

The Tg for control nanoparticles without surfactant was 36.7°C. In formulations with surfactant of HLB 1.8, the Tg was higher than that for control ranging from 39.8 to 43.13. At this

HLB, the surfactant concentration has no noticeable trend on the Tg. In formulations with surfactant of HLB 6, the Tg was higher than that for control only at the lowest concentration of 0.25% v/v. At all higher concentrations it was lesser than that for control ranging from 31.5 to 34˚C. At this HLB, an increase in the surfactant concentration resulted in a decrease in Tg. In formulations with surfactant of HLB 10, the Tg is higher than that for control ranging from 39.6 to 40.9˚C. At this HLB, the surfactant concentration didn't seem to have a significant effect on the Tg. The surfactant with HLB 15 caused a reduction in the Tg as compared to that of control. This decrease in Tg followed a concentration dependent manner where an increase in concentration resulted in decrease in Tg from 35.8˚C at 0.25% concentration to 28.7˚C at a concentration of 2% (**figure 19**).

3.4.1.3 Effect on surfactant on zeta potential

The surfactant doesn't seem to have a significant effect on the zeta potential of the nanoparticles except that formulations with surfactant had a higher zeta potential than that of control (-14.2 mV). As shown in **figure 20**, the zeta potential for nanoparticle with PSH ranges from -17.4 to -20.5 mV. There is not a significant change in the zeta potential with different concentration of surfactant used. This observation is likely to be same for formulations with all other surfactants used in the study.

3.4.1.4 Scanning electron microscopy imaging of nanoparticles

All formulations were imaged with SEM. Some representative images are shown in **figure 21**. The smallest formulation was obtained by incorporation of Span 85 at a concentration as low as 0.25% v/v. These nanoparticles are shown to be discrete spherical particles and likely have a bimodal distribution with many small particles and a few larger particles with a measured average size of 783.6nm (**figure 21B**). Representative SEM images of nanoparticle formulations made with the other three surfactants are shown in **figure 21C-F**. Formulations with low T_g (S13-S16, S5-S7) were seen to be heavily aggregated and fused (**figure 21E** and **21F**). Regardless of the surfactant used, incorporation of surfactant resulted in aggregated and fused particles to a varying degree based on the type and concentration of surfactant used. This was evident even in particles with relatively higher T_g as is shown for formulation S4, T_g of 42.7^{o}C, in **figure 21B**. The control formulation with no surfactant also had extensively fused nanoparticles (**Figure 21A**).

3.4.2 Emulsion method and nanoprecipitation method

The emulsion method yielded nanoparticles of mean size 501±31 nm with a narrow size distribution and low polydispersity index. **Figure 22A** shows an SEM image of these nanoparticles wherein the particles are spherical in shape with a smooth surface. There is very little to no fusion between the particles. These nanoparticles showed excellent redispersibility in water upon sonication.

The nanoprecipitation method yielded particles of mean size 215±18 nm with a narrow size distribution and excellent polydispersity index (~0.1). The SEM image of these particles is shown in **figure 22B**. As seen in the image, the particles appear spherical in shape and are discrete. Due to the method by which the sample was prepared, the PVA likely forms a continuous layer around the particles. This is likely an artifact of the sample preparation and does not represent any structural fusion of the particles in actuality.

3.5 Discussion

The PIN method is a rapid, simple technique of formulating polymer nanoparticles without the use of an aqueous phase lending great potential to encapsulation of hydrophilic molecules including proteins and peptides. Unlike conventional methods of encapsulation, this method eliminates the shear stress on the agents to be encapsulated, thereby improving the physical stability and integrity of sensitive macromolecules like proteins and peptides. Using this method, nanoparticles of sizes ranging from 683.2nm-1713.7nm were produced. From **figure 21**, we observe that surfactant HLB and concentration play an important role in controlling nanoparticle size. Therefore, the use of a non-ionic surfactant during PIN fabrication of PLGA nanospheres resulted in formulations with varied properties such as size, thermal properties, and morphology.

When compared to control, in general the addition of surfactants resulted in an increase in the nanoparticle size except for span 85 at 0.25, 1, and 2% v/v concentrations where the nanoparticle size is almost the same as that for control formulation. From **figure 21**, it is clear that for HLB value greater than 6, there is a marked increase in the degree of fusion of the formed nanoparticles. Therefore incorporation of non-ionic surfactants of HLB value less than 6 provides an option to manipulate the nanoparticle size and reduce fusion/aggregation of nanoparticles.

There was a general trend of particle size increase with increasing surfactant concentration. The role of surfactants in nanoparticle formulation is commonly to reduce surface tension of immiscible liquids, typically reducing the particle size that can be achieved [16]. In the PIN method, where both phase are miscible, we believe that surfactants play a similar role by reducing the initial droplet size formed resulting in the observation of reduced particle size. However, we hypothesize that surfactants also increase the curing or hardening time of the nanoparticles allowing greater opportunity of droplet interaction and coalescence prior to hardening. This may account for the observed increase in particle size with increased surfactant concentration and is further supported by the observation of fusing in some nanoparticle formulations as imaged by SEM (**figure 21F**). This hypothesis is further backed by the T_g results as will be discussed further. **Figure 21 B** and **C** show SEM images of nanoparticles prepared by incorporating the surfactants of HLB value 1.8 and 6. From these SEM images of these two formulations it appears as though the most of the nanoparticles are in the size range of less than 500 nm. However, due to the particles being fused at some degree, the hydrodynamic size as shown by DLS is greater than the actual particle size as could be evidenced by the SEM image. This suggests that the hydrodynamic diameter data for the particles might be an overestimate of the actual size of individual particles due to the fusion between particles. With regards to this observation, it would be interesting to see whether important properties of these particles such as drug release and degradation would follow a pattern mimicking that of their actual size or that of the fused structure.

As HLB value of a surfactant increases, its hydrophilic character increases. PLGA is a hydrophobic polymer and surfactants of higher HLB as a result of their hydrophilic character have a relatively lesser association with the particle surface when compared to surfactants with lower HLB. Therefore, in the case of formulations with higher HLB values (10 and 15) this might be another reason for extensive fusion of the nanoparticles as the surfactants fail to perform the function of stabilization of the nanoparticle. Studies evaluating the degree of adsorption of surfactants onto the particle surface will be able to test this hypothesis.

A critical parameter in polymeric nanoparticle formulations is the T_g as it will impact polymer degradation [17], thereby affecting the drug release. For many medical applications a T_g higher than body temperature, 37^oC, would be desired. Interestingly, for HLB values of 15 and 6, the Tg is lower than 37^oC. Whereas for HLB value of 1.8 and 10 the Tg is greater than 37^oC. Therefore, the ability to modulate Tg would be critical for many medical applications. Surfactant incorporation into polymers has long been used as a “plasticizer” to effectively reduce T_g and make rigid polymers more flexible and rubbery [18]. For half the formulations described here, the incorporation of surfactant actually substantially increased the measured T_g of the formulation ranging from 36.7^oC (nanoparticles with no surfactant) to above 40^oC as seen in **figure 19**. This may indicate that the surfactants are truly interacting at the interfacial surface and are not being fully incorporated into the polymer nanoparticles. These results support our hypothesis that some surfactants increase the cure time. This increase in cure time, or slowing of hardening, would allow polymer organization within each droplet effectively increasing the T_g. This effect is likely mitigated at high concentrations of surfactant due to an increase of surfactant incorporation into the nanoparticles, where they act as plasticizing agents. The ability to modulate T_g of polymer nanoparticles may prove useful in the control of degradation and cargo release for medical applications.

When considering the zeta potential for all the formulations there were no evident trends beyond the observation that for representative formulations with a surfactant (S25-S36) the zeta potential was higher compared to the PLGA nanoparticles without surfactant (-14.3mV) and ranged from -17.4mV to -20.5mV as seen in **figure 20**.

Using the PIN method, nanoparticles of PLGA polymer were obtained though there was some degree of fusion among the particles. This method is particularly advantageous for the encapsulation of sensitive therapeutics such as nucleotides and proteins. The reason being that the other existing methods of nanoparticle fabrication involve a certain degree of stress that is detrimental to these sensitive therapeutic agents rendering them inactive or greatly reducing their activity as a result of damage to the therapeutic agent. For this reason, the PIN method offers a convenient solution for the encapsulation of such sensitive therapeutics since it doesn’t involve any external agitational forces on the active agents and the solvent exposure is very minimal as compared to that encountered in other commonly used methods. Though in the scope of this study, we have seen fusion of particles with each other, discrete particles can be obtained by fine tuning the fabrication method further by using the variables we have used in this study and also by looking at other variables that play a role in the nanoparticle formation. Using the polymer poly (fumaric-co-sebacic anhydride), Furtado et. al. have obtained discrete polymer nanoparticles of a small size and very little to no fusion between particles [19]. Therefore, the PIN method has great potential for the formulation of nanoparticles encapsulating sensitive therapeutic agents.

Nonetheless, within the boundaries of the parameters we tested, the particles obtained in our study were fused to a certain extent. Therefore, we decided not to utilize those particles for *in vivo* studies due to the fact that they have the potential to cause severe aggregation and blockage of blood vessels upon intravenous administration which could be lethal to the animal. Accordingly, we proceeded with other methods for nanoparticle fabrication for our *in vivo* nanoparticle biodegradation studies which are discussed in chapter 4. The particles used for the *in vivo* degradation studies were produced by an emulsion method and nanoprecipitation method. When compared to particles made by PIN method, the nanoparticles fabricated by the two mentioned methods had a smooth surface with little to no fusion between particles. These particles also had a negative surface charge similar to that of the polystyrene nanoparticles that were used in the lung biodistribution studies that are discussed in chapter 2. Furthermore, the particles prepared by PIN method had extremely poor redispersibility in aqueous media unless a solution of 1% pluronic F-127 was used for dispersion of these nanoparticles. On the other hand, the nanoparticles made by the emulsion method and nanoprecipitation method were easily redispersed in normal saline upon sonication. As a result of the excellent properties of the nanoparticles prepared by these two methods (emulsion method and nanoprecipitation), these formulations were used for the *in vivo* biodegradation studies discussed in the following chapter.

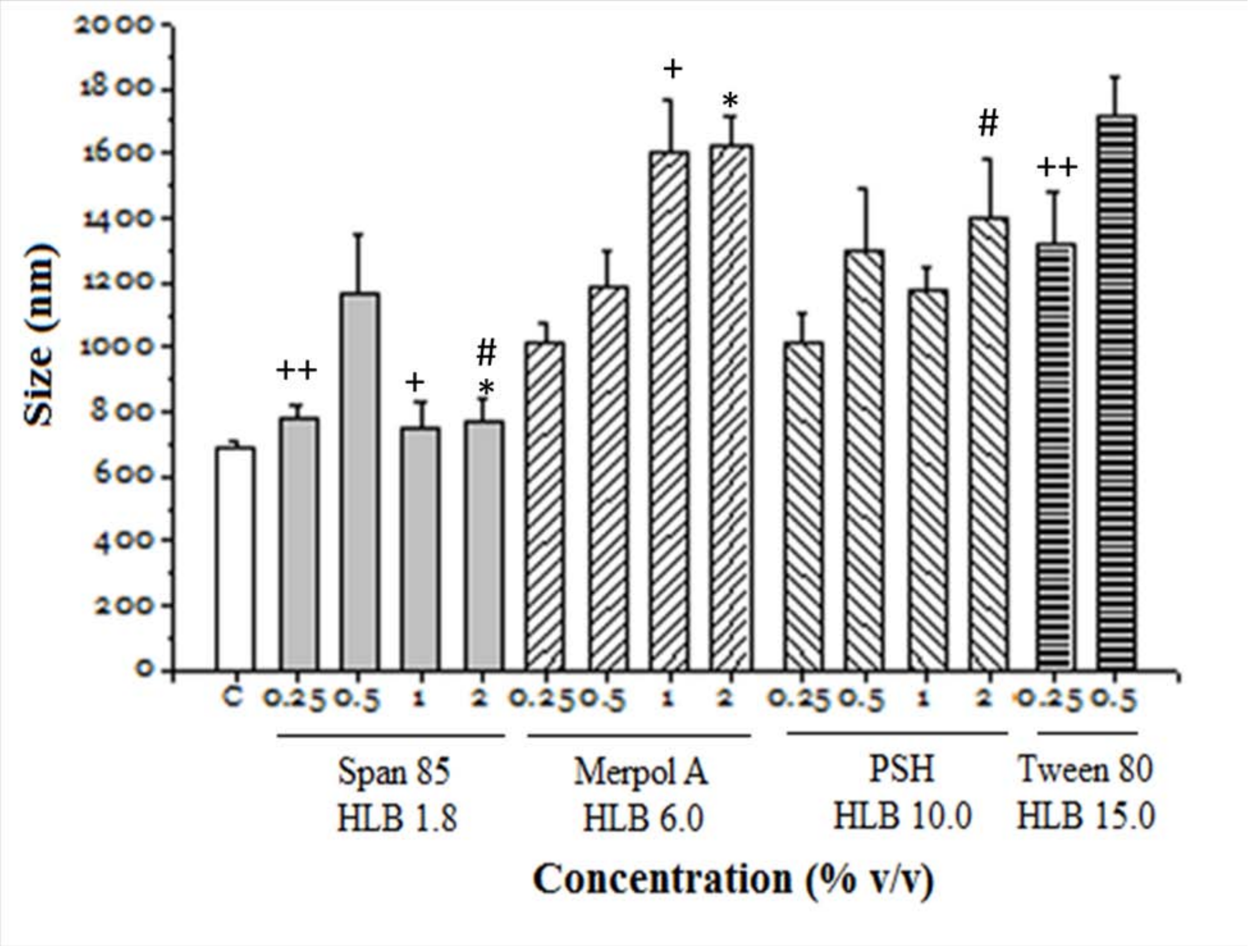

Figure 18. Size of all nanoparticle formulations (n=3, mean±SEM).

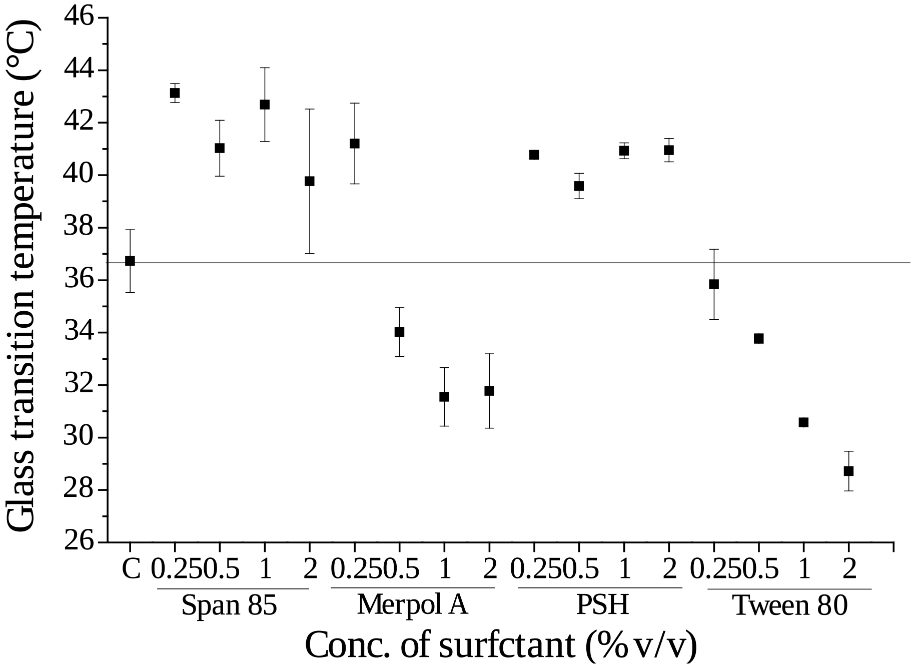

Figure 19. Glass transition temperatures (T_g) for all formulations. The line indicates the T_g for nanoparticles fabricated without surfactant (36.7^{o}C). (n=3, mean±SEM)

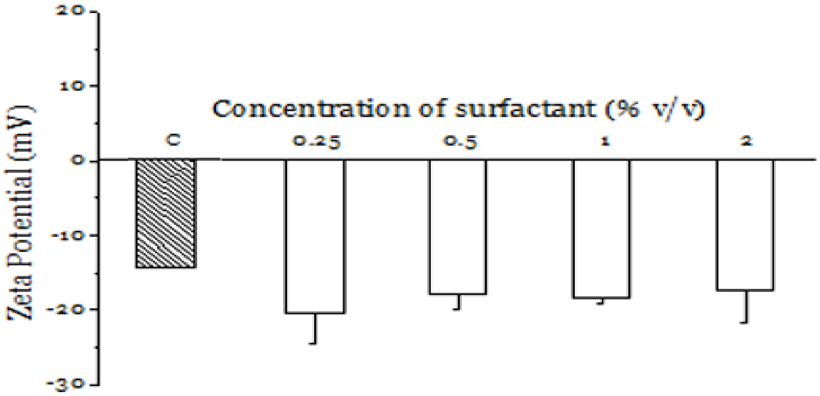

Figure 20. Zeta potentials of nanoparticle formulations with incorporation of PSH. (n=3, mean±SEM)

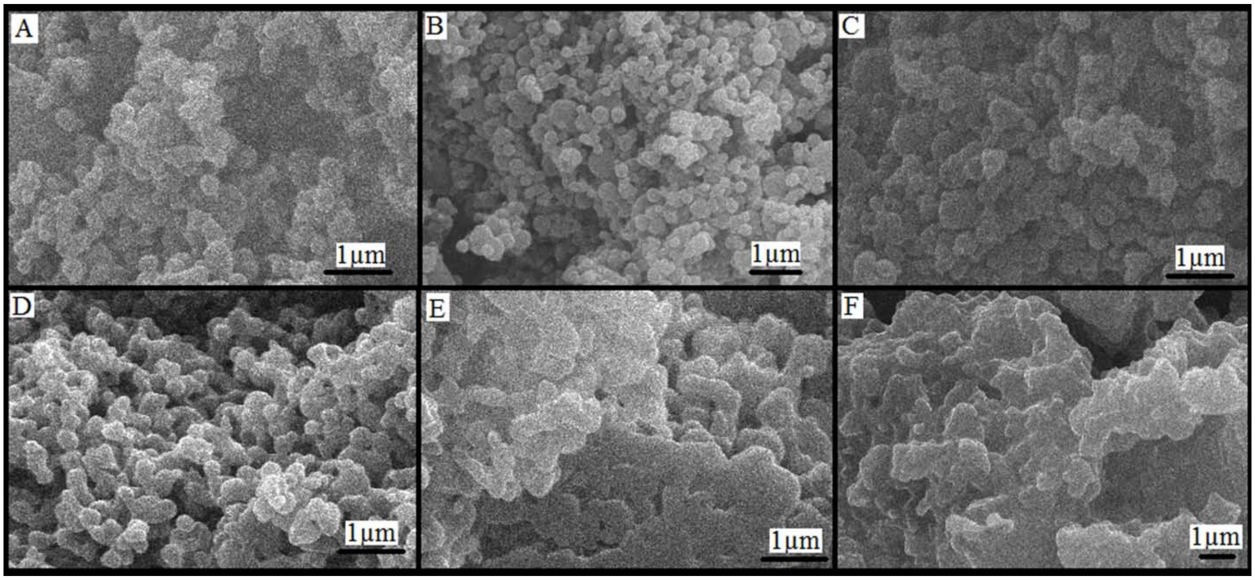

Figure 21. SEM images of the PLGA nanoparticles of formulations (A) C at magnification of 20,000X (B) S11 at a magnification of 15,000X, (C) S22 at a magnification 20,000X; (D) S36 at a magnification 20,000X, (E) S48 at 10,000X, (F) S13 at a magnification of 10,000X.

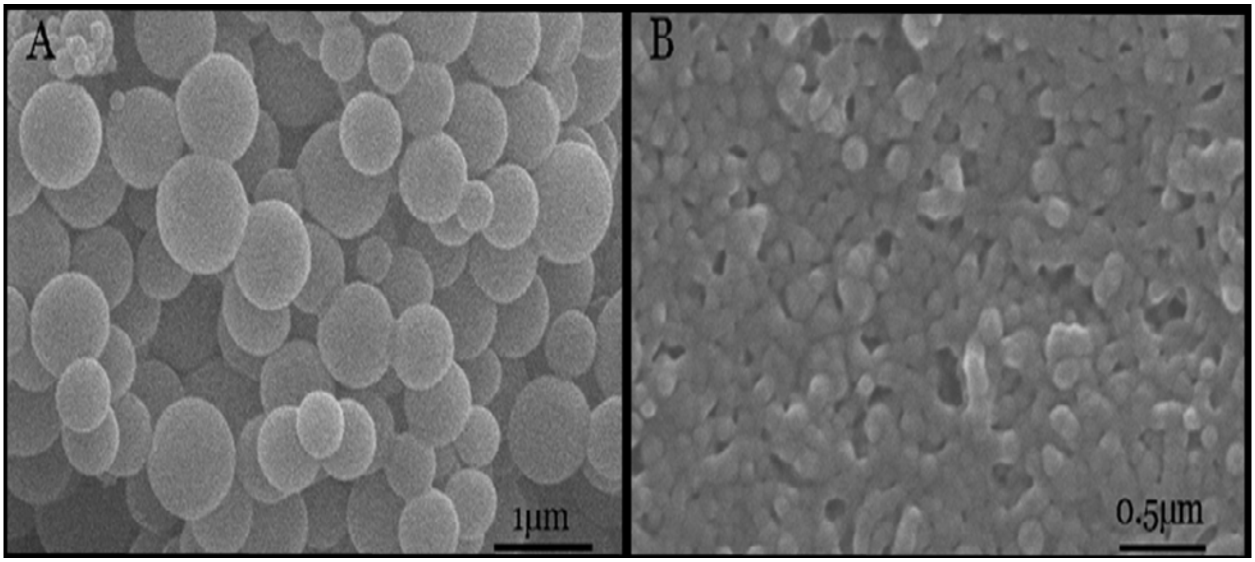

Figure 22. SEM images of PLGA nanoparticles of size (A) 500 nm made by emulsion method and (B) 200 nm made by nanoprecipitation method respectively at magnification of 30,000X.

Surfactant	**HLB**	**Formulation ID**	**Surfactant Conc. (%v/v)**
Span 85	1.8	S1 S2 S3 S4	2.00% 1.00% 0.50% 0.25%
Merpol A	6	S5 S6 S7 S8	2.00% 1.00% 0.50% 0.25%
Polyoxyethylene sorbitol hexaoleate	10	S9 S10 S11 S12	2.00% 1.00% 0.50% 0.25%
Tween 80	15	S13 S14 S15 S16	2.00% 1.00% 0.50% 0.25%
No surfactant		C	None

Table 5. Formulation parameters of PLGA nanoparticles prepared by PIN method.

3.6 Conclusions

The PIN method is a very useful method, particularly when considering the encapsulation of hydrophilic drugs, including proteins and peptides, due to the absence of an aqueous phase and reduced shear stress. It has been demonstrated to effectively encapsulate hydrophobic drugs, insulin and genetic material [10]. We show here that the incorporation of surfactants in the PIN method can modulate nanoparticle size, thermal properties and zeta potential. These parameters were affected by the surfactant HLB and surfactant concentration. Since surfactants likely play a key role in drug loading, drug stabilization and drug release, further studies should be done with this system including the incorporation of various cargos. The PIN method is a versatile nanoparticle fabrication method that can produce polymer nanoparticles of greatly varied properties to suit the desired application. The utilization of surfactants enhances this ability further.

3.7 References

1. Emerich DF, Thanos CG. The pinpoint promise of nanoparticle-based drug delivery and molecular diagnosis. Biomol Eng 2006;23:171-184.

2. Mora-Huertas CE, Fessi H, Elaissari A. Polymer-based nanocapsules for drug delivery. Int J Pharm 2010;385:113-142.

3. Hillaireau H, Couvreur P. Nanocarriers' entry into the cell: relevance to drug delivery. Cell Mol Life Sci 2009;66:2873-2896.

4. Tsukada Y, Hara K, Bando Y, Huang CC, Kousaka Y, Kawashima Y, et al. Particle size control of poly(dl-lactide-co-glycolide) nanospheres for sterile applications. Int J Pharm 2009 ;370:196-201.

5. Aggarwal P, Hall JB, McLeland CB, Dobrovolskaia MA, McNeil SE. Nanoparticle interaction with plasma proteins as it relates to particle biodistribution, biocompatibility and therapeutic efficacy. Adv Drug Deliv Rev 2009;61:428-437.

6. Jain RA. The manufacturing techniques of various drug loaded biodegradable poly(lactide-co-glycolide) (PLGA) devices. Biomaterials 2000;21:2475-2490.

7. Hans ML, Lowman AM. Biodegradable nanoparticles for drug delivery and targeting. Current Opinion in Solid State and Materials Science 2002;6:319-327.

8. Cohen-Sela E, Chorny M, Koroukhov N, Danenberg HD, Golomb G. A new double emulsion solvent diffusion technique for encapsulating hydrophilic molecules in PLGA nanoparticles. J Control Release 2009;133:90-95.

9. Mathiowitz E, Chickering D, Jong YS, Jacob JS. Process for preparing microparticles through phase inversion phenomena. Patent numer: 6616869, 2003.

10. Mathiowitz E, Jacob JS, Jong YS, Carino GP, Chickering DE, Chaturvedi P, et al. Biologically erodable microspheres as potential oral drug delivery systems. Nature 1997;386:410-414.

11. Furtado S, Abramson D, Burrill R, Olivier G, Gourd C, Bubbers E, et al. Oral delivery of insulin loaded poly(fumaric-co-sebacic) anhydride microspheres. Int J Pharm 2008;347:149-155.

12. Lemoine D, Préat V. Polymeric nanoparticles as delivery system for influenza virus glycoproteins. Journal of Controlled Release 1998;54:15-27.

13. Song CX, Labhasetwar V, Murphy H, Qu X, Humphrey WR, Shebuski RJ, et al. Formulation and characterization of biodegradable nanoparticles for intravascular local drug delivery. Journal of Controlled Release 1997;43:197-212.

14. Yallapu MM, Gupta BK, Jaggi M, Chauhan SC. Fabrication of curcumin encapsulated PLGA nanoparticles for improved therapeutic effects in metastatic cancer cells. J Colloid Interface Sci 2010;351:19-29.

15. Mainardes RM, Evangelista RC. PLGA nanoparticles containing praziquantel: effect of formulation variables on size distribution. Int J Pharm 2005;290:137-144.

16. Tadros TF, Vandamme A, Levecke B, Booten K, Stevens CV. Stabilization of emulsions using polymeric surfactants based on inulin. Advances in Colloid and Interface Science 2004;108–109:207-226.

17. Dunne M, Corrigan I, Ramtoola Z. Influence of particle size and dissolution conditions on the degradation properties of polylactide-co-glycolide particles. Biomaterials 2000;21:1659-1668.

18. Ghebremeskel AN, Vemavarapu C, Lodaya M. Use of surfactants as plasticizers in preparing solid dispersions of poorly soluble API: Selection of polymer–surfactant combinations using solubility parameters and testing the processability. International Journal of Pharmaceutics 2007;328:119-129.

19. Furtado S, Abramson D, Simhkay L, Wobbekind D, Mathiowitz E. Subcutaneous delivery of insulin loaded poly(fumaric-co-sebacic anhydride) microspheres to type 1 diabetic rats. Eur J Pharm Biopharm 2006;63:229-236.

CHAPTER 4

4.1 Introduction:

Nanoparticle systems have tremendous potential in clinical applications and there are already several successful nanoparticle systems in use for various diseases [1]. The *in vitro* degradation of PLGA microparticles and nanoparticles has received significant attention from a quantitative as well as qualitative standpoint [2-4]. However, to the best of our knowledge, there are no previous reports quantitatively examining the *in vivo* degradation of biodegradable microparticles or nanoparticles in tissues post systemic administration i.e. distributed nanoparticles or microparticles. The lack of quantitative information on *in vivo* degradation, an important parameter controlling the drug release, makes it difficult to design optimal drug delivery systems with predictable drug release properties in target tissues.

Conventionally, the drug release from PLGA nanoparticles *in vitro* is used as a basis to predict a release *in vivo*. However, it must be noted that *in vitro* drug release need not be the same as that *in vivo*. For instance, the role of enzymes in PLGA degradation is still debated [5-7]. Given the fact that nanoparticle degradation plays a crucial role in sustained drug release [8], we wanted to determine the *in vivo* degradation of PLGA nanoparticles post intravenous administration. This specific aim would provide us with a platform for developing efficient polymeric nanoparticle based drug delivery systems.

Accordingly, we have investigated the *in vivo* biodegradation of PLGA nanoparticles of mean sizes 215±18nm and 501±31nm post intravenous administration; for ease of understanding, these sizes will hereafter be referred to as 200nm and 500nm respectively. After intravenous administration of nanoparticles, the tissues were extracted at time points of 3, 24, 72 hours, and 1 week. The decrease in weight average molecular weight (M_w) is a manifestation of ester bond scission in the polymer backbone which has a positive effect on the drug release from a nanoparticle system encapsulating a drug. This degradation information can also be obtained for other types of PLGA such as that shown in a recent study where PLGA copolymer type (random, sequenced) had a significant effect on its *in vitro* degradation [9]. Apart from PLGA, this method can also be applied to other degradable polymer systems including polyanhydrides, polyamides, polyesters, poly(cyano acrylates), polyurethanes, poly orthoesters, polydihydropyrans, polyacetals etc.

4.2 Materials

PLGA of molecular weight (M_w) 44,000 Da was provided by Purac Biomaterials (USA). Polyvinyl alcohol (PVA) of molecular weight 88,000 Da and phosphate buffered saline (PBS; pH 7.4) was purchased from Fisher Scientific (USA). All other organic solvents were obtained from Fisher Scientific and were of HPLC grade.

4.3 Methods

4.3.1 Fabrication and characterization of PLGA nanoparticles

The methods of preparation of the PLGA nanoparticles used in this study and their characterizations are detailed in section 3.3.2, 3.3.3, and 3.3.4 of chapter 3.

4.3.2 *In vitro* degradation of PLGA nanoparticles

For *in vitro* degradation, 10 mg of the PLGA nanoparticles was suspended in 1.25 ml of PBS and incubated at 37°C on a mixer. The samples were removed from the incubator at pre - determined time points and lyophilized. Dried samples were dissolved in chloroform and subjected to analysis by gel permeation chromatography (GPC) (GPC Max VE 2001, Viscotek Corporation) equipped with a column bank consisting of three columns with size exclusion limits of 4 million, 70,000, and 5,000 Da. A refractive index (RI) detector (VE 3580, Viscotek Corporation) was used for PLGA detection.

4.3.3 Preparation of nanoparticle suspension and intravenous administration

The nanoparticles were suspended in sterilized 0.9% sodium chloride solution at a concentration of 3% w/v and sonicated in a water bath for 30 minutes. Once the nanoparticles were well suspended, they were stored at 4˚C until further use (a maximum of 5 minutes). Before administration of nanoparticles to each animal, the formulation was sonicated for about 10 minutes. Degradation analysis yielded no degradation of nanoparticle formulations following this suspension method. Male Balb/c mice weighing between 20-25 g (Charles River Inc.) were used following acclimation for a week. Food and water were available to the animals ad libitum.

The PLGA nanoparticles in suspension were administered to the mice via tail vein injection. Each animal received 300µl of the nanoparticle suspension. For all the study groups n = 3. All animal experiments were conducted in accordance to the Institutional Animal Care and Use Committee at Wayne State University.

4.3.4 Harvesting tissues and sample preparation

Tissues including liver, spleen, kidneys, heart, brain, lungs, and lymph nodes (axillary, brachial, cervical, and mesenteric lymph nodes) were extracted, processed, and analyzed by a method similar to that described earlier [10]. Briefly, the harvested tissues were homogenized and lyophilized. Chloroform was added to the lyophilized tissue and placed on a mixer for 96 hours at room temperature. This was done to ensure the complete dissolution of PLGA in chloroform. After the extraction step, the mixture was filtered using a 0.2 µm filter and chloroform was frozen and lyophilized. This polymer extract was then subjected to analysis by GPC after dissolving it in THF.

4.3.5 Assay for biodegradation and biodistribution of nanoparticles *in vivo*

Analysis of polymer concentration and molecular weight determination from tissue extracts was performed by GPC as described above for in vitro degradation (section 4.3.2). A refractive index (RI) detector (VE 3580, Viscotek Corporation) was used for PLGA detection. For calculation of the molecular weight of PLGA in tissues, the peak retention time was calculated by the Omni SEC software, and the molecular weight of the polymer *in vivo* was determined by means of a calibration curve of retention time versus log molecular weight of narrow standard polystyrene samples of molecular weights ranging from 1000 to 90000 Da. For biodistribution of nanoparticles *in vivo*, the area under the curve was calculated by Omni SEC software and the amount of nanoparticles present in each tissue was calculated as a percent of the administered dose. In order to ensure that the degradation observed is not as a result of tissue processing, a sample of PLGA nanoparticles were processed directly and no degradation was observed upon GPC analysis of the same.

4.3.6 Statistical analysis

Statistical analysis was performed using one-way ANOVA followed by Tukey's post-hoc analysis where applicable, with OriginPro8 software.

4.4 Results and discussion

4.4.1 *In vivo* biodegradation of PLGA nanoparticles post intravenous administration

For both the tested nanoparticle sizes, the liver was the site of highest nanoparticle deposition followed by spleen and lungs. Therefore, we further determined the degradation of nanoparticles in these most relevant tissues. Among all the tissues studied, degradation in the liver is highest (**figure 23 and 24**). For the 500 nm nanoparticles, the weight-average molecular weight (M_w) by 3 hours and 24 hours was 36,879 Da and 40,427 Da respectively. However, it decreased to 31,377 Da by 72 hours and further decreased to 23,623 Da at the end of 1 week. The next highest degradation of nanoparticles was seen in spleen wherein, at the end of 3 hours and 24 hours, the M_w was 39,557 Da and 38,111 Da respectively. However, it decreased to 35,076 Da by 72 hours and further decreased to 28,153 Da at the end of 1 week. For these three tissues it is interesting to note that the degradation seems to have a lag phase up to at least 24 hours after which we see a decrease in the M_w by 72 hours. For the 200nm size nanoparticles, extensive degradation was observed in the liver. The M_w at the end of 3 hours and 24 hours was 37,970 Da and 37,417 Da respectively. Thereafter, it decreased to 31,192 Da by 72 hours and 24,116 Da at the end of 1 week. In spleen, the M_w at the end of 3 hours and 24 hours was 38,449 Da and 39,704 Da respectively; however by 72 hours the M_w decreased to 31,633 Da; it then increased to 34,557 Da at the end of 1 week (**figure 24**).

From the *in vitro* degradation data, the 500 nm nanoparticles have a faster rate of degradation as compared to 200 nm nanoparticles (**figure 25**). A similar size-based degradation difference has been reported by Dunne and co-workers. This is because in larger sized nanoparticles, the degraded polymer fractions have a longer path to diffuse to the nanoparticle surface resulting in accumulation of these oligomers leading to autocatalysis of PLGA chains. In the case of smaller particles the degraded fractions diffuse out much faster [8]. This is thought to be the reason for larger sized particles having a faster degradation. However *in vivo*, in the liver there is little difference in the degradation pattern of the two nanoparticle sizes with the 500 nm nanoparticles having a slightly higher degradation at the end of one week where the M_w for 500 nm is 23,623 Da whereas that for the 200 nm nanoparticles is 24,116 Da. In the spleen, for the first two time points of 3 hour and 24 hours there is little difference in the Mw between both the sizes. At 3 hours, the M_w for 500 nm and 200 nm nanoparticles was 39,557 Da and 38,449 Da respectively. At the end of 24 hours the M_w was 38,111 Da and 39,704 Da for 500 nm and 200 nm size nanoparticles in spleen, respectively. Furthermore at the 3 day time point, the 200 nm nanoparticles shows a higher degradation where the M_w is 31,633 Da as compared to 35,076 Da for the 500 nm size. However, at the end of 1 week the 500 nm nanoparticles are degraded to a larger extent as compared to the 200 nm nanoparticles with the M_w being 28,153 Da and 34,557 Da respectively. Furthermore, it should be noted that the 500 nm nanoparticles have a higher deposition in the liver, and that the 500 nm nanoparticles in general have shown a slightly higher *in vivo* degradation than the 200 nm nanoparticles. In the liver, the 500 nm nanoparticles have a 35.9% reduction in the M_w at the end of 1 week and the 200 nm nanoparticles had a 36.4% reduction in M_w as compared to that at the initial time point of 3 hours. However, in the spleen, 500 nm nanoparticles had a higher degradation as compared to that for 200 nm size. Relative to the M_w at 3 hours, the 500 nm nanoparticles have a 28.8% reduction in M_w at the end of 1 week whereas the 200 nm nanoparticles only have a decrease of 10.1% at the end of 1 week. Taken together, this suggests that the 500 nm nanoparticles have a much faster *in vivo* degradation rate than that of 200 nm nanoparticles in the spleen. On the other hand, in the liver, the nanoparticle size did not seem to affect its biodegradation pattern. The higher amount of nanoparticle degradation observed in the liver over other tissues may be attributed to the presence of higher concentrations of several esterases in the liver [11]. Therefore, as a result of differences in the enzymatic diversity and concentration in these different tissues, the degree of degradation is expected to vary based on the amount of enzymes in these tissues with liver being the tissue with the highest nanoparticle biodegradation. In addition to the differences in enzymatic make up, the liver has the highest nanoparticle deposition followed by spleen and lungs. Therefore, based on these considerations and the biodegradation observed in tissues, the order of nanoparticle degradation in the three tissues can be generalized as: liver>spleen.

PLGA degrades by hydrolysis of its ester bonds and the polymer degradation results in the decrease of M_w and M_n. As the long polymer chains are broken down, the M_w and M_n decrease except in cases where a considerable proportion of the oligomeric fractions are lost; in such a situation the M_w and M_n increase. If the M_w shows a decrease with time and M_n stays fairly constant, it could be an indication that the oligomeric fractions are resistant to hydrolytic degradation. This observation was made by santos et. al. [12] in the degradation of poly (fumaric-co-sebacic anhydride) microspheres where the M_n stayed fairly constant over the course of the study while the M_w decreased substantially over time. They have attributed this observation to be a result of the oligomers being more stable to hydrolytic attack as compared to longer polymer chains. A similar observation is encountered in our *in vivo* degradation studies. For the 200 nm PLGA nanoparticles in the liver, the M_n is relatively constant up until 24 hours after which it decreases till 7 days. This indicates that in the liver, the oligomeric fractions undergo a pronounced degradation after 24 hours. In spleen the M_n values suggest that the oligomeric fractions degrade after 24 hours up until 3 days and then the M_n remains fairly constant. However, the M_w shows a substantial increase from 3 days to 7 days. This M_w and M_n taken together suggest a possibility of the oligomeric fractions leaving the tissue after 3 days due to which there is an increase in M_w however the M_n remains relatively constant due to new oligomers being created from the long chain polymer degradation.

In the case of 500 nm PLGA nanoparticles in liver, the M_n stays relatively stable until 24 hours after which it decreases until 7 days. This suggests that the oligomeric fractions degrade after 24 hours thereby resulting in a decrease in the M_n, similar to that of 200 nm PLGA nanoparticles in the liver. In spleen the M_n is relatively stable until 3 days after which it decreases by the end of 7 days. This suggests that the oligomers are fairly resistant to hydrolytic attack at least until 3 days after which they degrade further.

The polydispersity index (PDI) (among several other parameters) of PLGA in the liver and spleen is shown in **table 6**. For both the nanoparticles (200 nm and 500 nm), the PDI in spleen in higher than that in the liver. This indicates that the oligomeric fractions may be retained in the spleen to a higher extent whereas in the liver they might be released into circulation and new oligomeric fractions are created which keeps the PDI relatively constant. The amount of PLGA nanoparticles deposited in the liver is significantly higher than that in the spleen. Therefore, though the oligomers leave the liver, there are more oligomers created which would prevent the PDI from increasing. The Mw, Mn, and PDI information for the *in vivo* tissue degradation of PLGA nanoparticles not only elucidates the polymer degradation over time but also provides insights into the finer details of the pattern of degradation happening with time.

On the whole, this type of information on the *in vivo* tissue biodegradation provides critical insights with respect to the extent of polymer degradation in tissues which in turn has an impact on the drug release in the tissues. In addition, such information also gives insights about the toxicity potential of the drug delivery system in tissues. Determination of nanoparticle degradation in tissues could greatly improve the design of drug delivery systems and also lend important insights about nanoparticle toxicity potential in general.

4.4.2 Degradation kinetics of PLGA nanoparticles

It has been demonstrated in several studies that the hydrolytic degradation of poly lactic acid, poly glycolic acid, and their copolymer PLGA follows first order kinetics [13, 14]. The first order degradation pattern can be represented by the following equation:

$$M = M_o (e^{-kt}) \quad \text{Eq. (1)}$$

In the above equation, M is the molecular weight of the degrading polymer at time t, k is the rate constant of degradation, M_o is the initial molecular weight of the polymer. Plotting Ln (M_w) against time for the *in vitro* degradation study gives the profiles depicted in **figure 26**. The data when fitted for linearity gives r^2 values of 0.9969 and 0.9606 for 500 nm and 200 nm size respectively (**table 7**). This indicates that the *in vitro* degradation of PLGA nanoparticles of both the sizes follows first-order linear kinetics. The *in vitro* rate of degradation of 500 nm size nanoparticles is 2 times faster than that of 200 nm nanoparticles (**figure 26**).

In the *in vivo* study, when the Ln (Mw) was plotted against time and the data fitted for linearity, r^2 values were obtained that suggest the *in vivo* degradation in the liver and spleen followed first order degradation pattern. For 500 nm size nanoparticles in liver and spleen the r^2 values were 0.9233 and 0.9954 respectively. Similarly, for the 200 nm size nanoparticles in liver and spleen the r^2 values were 0.9899 and 0.9669 respectively (**table 7**). Important comparisons arise when the degradation rates in tissues *in vivo* and those *in vitro* are compared for each nanoparticle size. The 500 nm nanoparticles in liver have a rate of degradation similar to that of *in vitro*, whereas in spleen the rate of degradation is 0.67 times that *in vitro*. On the other hand, the 200 nm nanoparticles in liver have a degradation rate that is 1.88 times that *in vitro* and the nanoparticles in spleen have a degradation rate that is 2 times higher than that *in vitro* (**table 8**).

Taken together, these observations suggest that smaller size PLGA nanoparticles degrade almost twice as fast in the liver and spleen as compared to their *in vitro* degradation in PBS whereas the 500 nm nanoparticles in liver have similar degradation pattern as that *in vitro.* However in spleen they degrade at a rate slower than that *in vitro*. Furthermore, when comparisons are made between the rate constants between tissues for each size, we see that the rate of degradation for 500 nm nanoparticles is 1.5 times higher than that for 200 nm nanoparticles in the liver. Whereas in the spleen, both the nanoparticle sizes have almost similar rate of degradation where the degradation rate for 500 nm nanoparticles is 0.93 times that for 200 nm nanoparticles (**table 8**). Thus, the molecular weight data and information of degradation kinetics together give important insights into the pattern of nanoparticle degradation in tissues and help establish correlation of *in vivo* degradation with the *in vitro* degradation. Additionally, it allows for the establishment of correlation of degradation between several nanoparticle systems with varying physiochemical properties. Therefore, such mathematical treatment of real time degradation information helps predict the *in vivo* degradation pattern of particular nanoparticle systems in tissues at specific time points. Additionally it also gives an estimate of the amount of drug released by a particular time period since degradation is an important parameter affecting the drug release.

4.4.3 Biodistribution of PLGA nanoparticles following intravenous administration

For both the nanoparticle sizes, liver was the site of highest deposition followed by spleen and lungs (**figures 27 and 28**). This result is in good agreement with the established fact that nanoparticles with hydrophobic surfaces are rapidly sequestered by the organs of reticuloendothelial system (RES) from the circulation [15]. The larger size nanoparticles deposit in the liver in larger amounts as compared to the 200 nm nanoparticles. This is also in agreement with the fact that the optimum size for phagocytic (macrophage) uptake is 250 nm to 3 microns

[16]. The 500 nm PLGA nanoparticles have a higher deposition in liver at 45.9% of the administered dose (**figure 27**) which could be a result of more efficient uptake by Kupffer cells of liver, while the 200nm nanoparticles have a liver deposition of 32.3% at the end of 3 hours (**figure 28**). In accordance with this observation, there have been reports showing larger sized nanoparticles having a higher accumulation in the liver [17, 18]. However, in the spleen, nanoparticles of both sizes have a similar amount of deposition at 10.1% and 10.5% of administered dose at the end of 3 hours (**figures 27** and **28**). The amount of nanoparticles in these tissues decreases with time and is likely a result of degradation and subsequent removal of the monomers from these organs in addition to possible redistribution of nanoparticles to other tissues. The decrease in the amount of nanoparticles over time and the overall mass loss in all the tissues combined are shown (**figures 29** and **30**). Knowledge of biodegradation coupled with that of biodistribution is a powerful tool in designing efficacious drug delivery systems as it throws light on the pharmacokinetics of the nanoparticle systems. As discussed earlier, different organs have different nanoparticle disposition and degradation rates. Therefore, information regarding tissue disposition of the nanoparticles alone does not comprise the full situation of nanoparticle pharmacokinetics. Since the nanoparticles degrade in tissues and are eliminated/excreted, knowing the biodegradation coupled with the biodistribution will give a true understanding of the pharmacokinetics of degradable nanoparticle systems and also the tissue pharmacokinetics of drugs carried by the nanoparticles. All of this information will have a direct positive impact on the design of polymeric drug delivery systems including safety considerations.

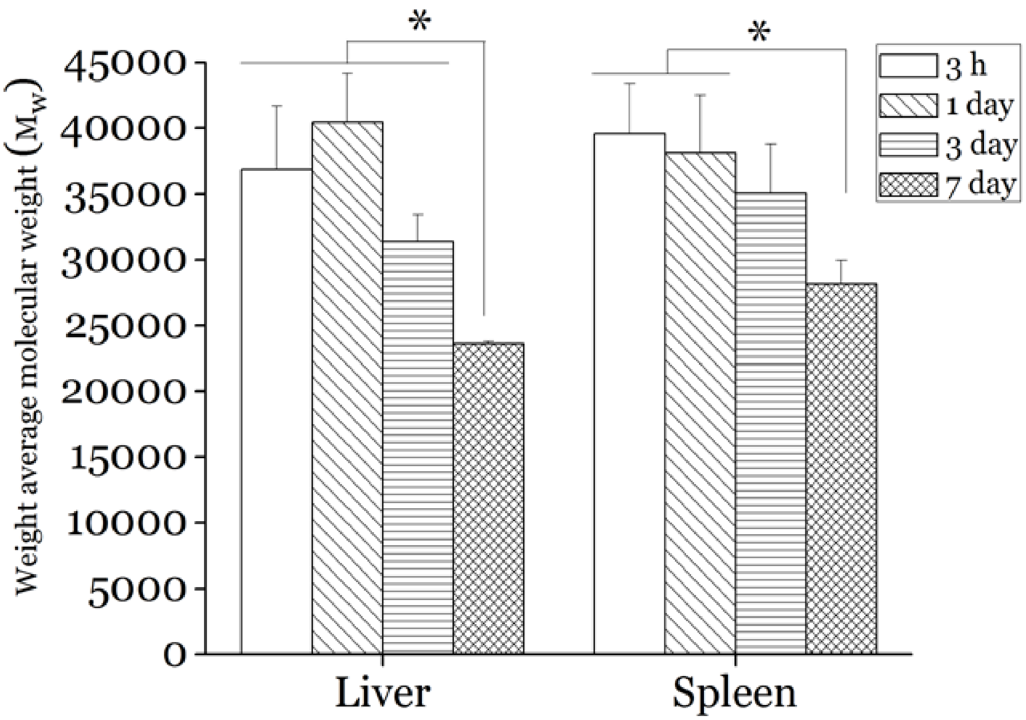

Figure 23. The biodegradation of PLGA nanoparticles of size 500 nm in diameter. (n=3; mean ± s.d). ‘*’ – statistically significant ($p<0.05$). In order to ensure that the degradation observed is not as a result of tissue processing, the PLGA nanoparticles were processed and observed no degradation upon GPC analysis of the same.

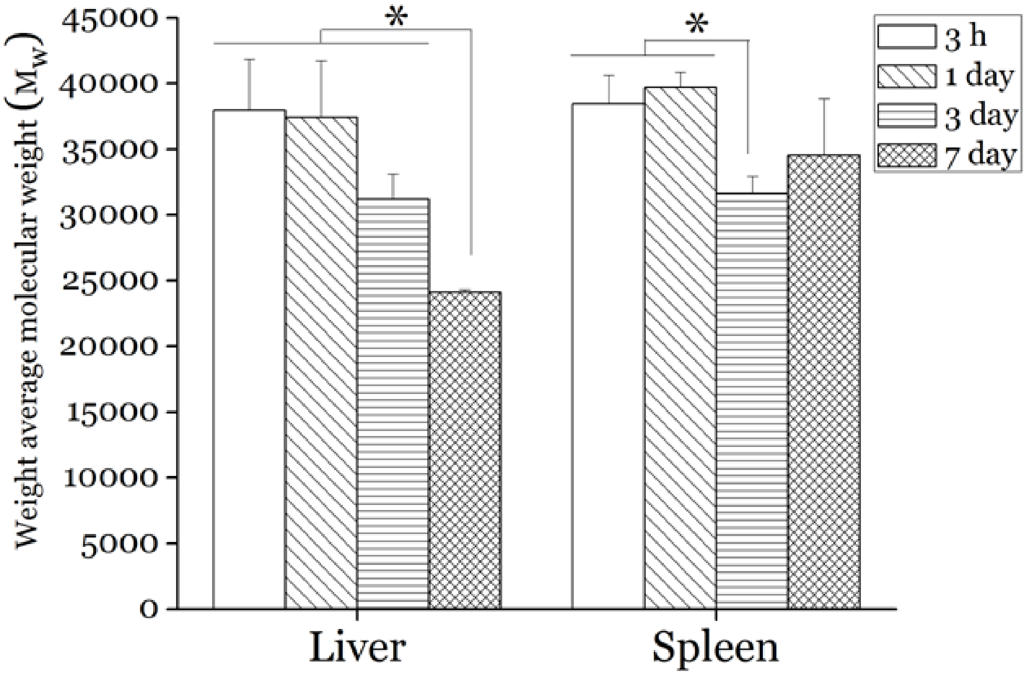

Figure 24. The biodegradation of PLGA nanoparticles of size 200nm in diameter. ‘*’ – statistically significant, $p<0.05$ (n=3;mean ± s.d). In order to ensure that the degradation observed is not as a result of tissue processing, the PLGA nanoparticles were processed and observed no degradation upon GPC analysis of the same.

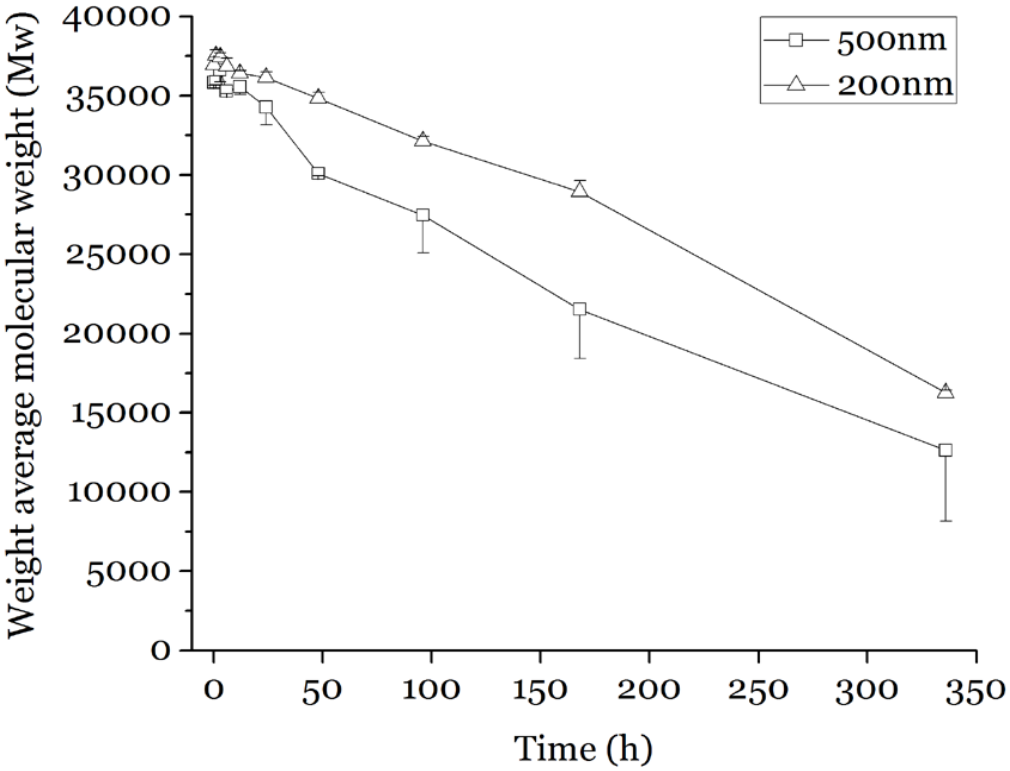

Figure 25. *In vitro* degradation profile of PLGA nanoparticles (n=3;mean ± s.d).

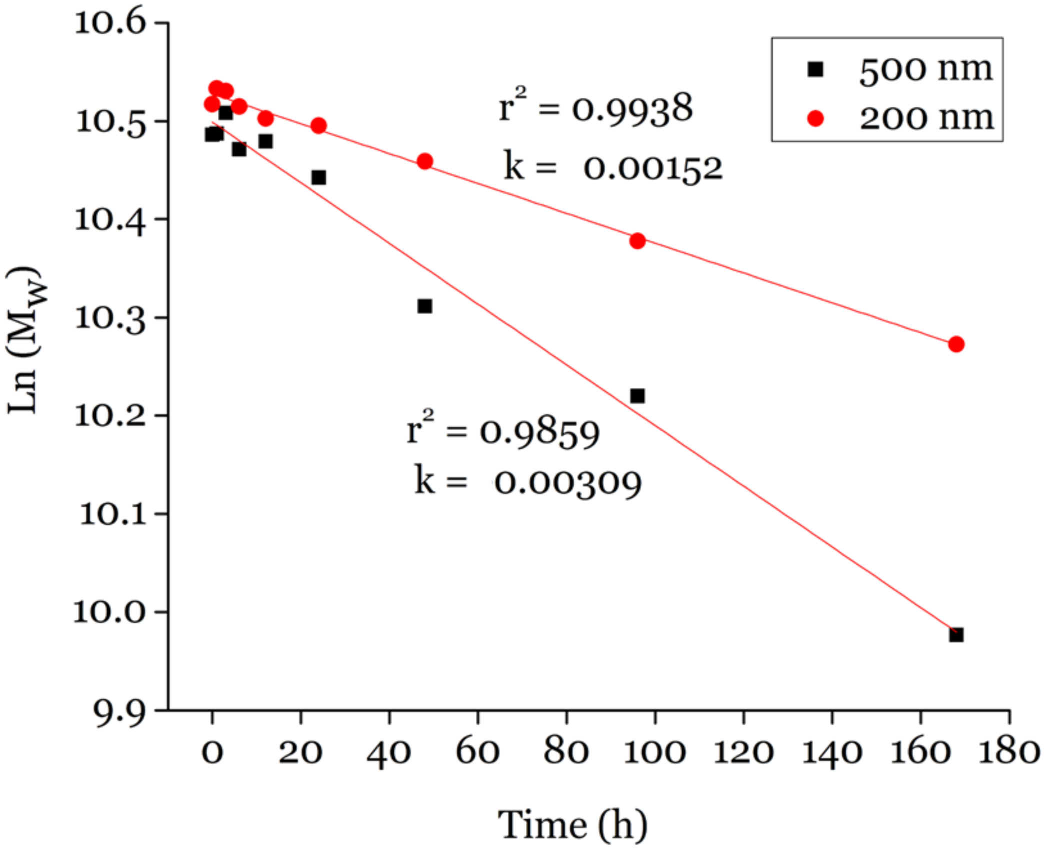

Figure 26. This figure represents a plot of Ln(Mw) versus time for the *in vitro* degradation of nanoparticles of the two sizes. The data was subjected to linear fit and r^2 values confirm the linearity of the data.

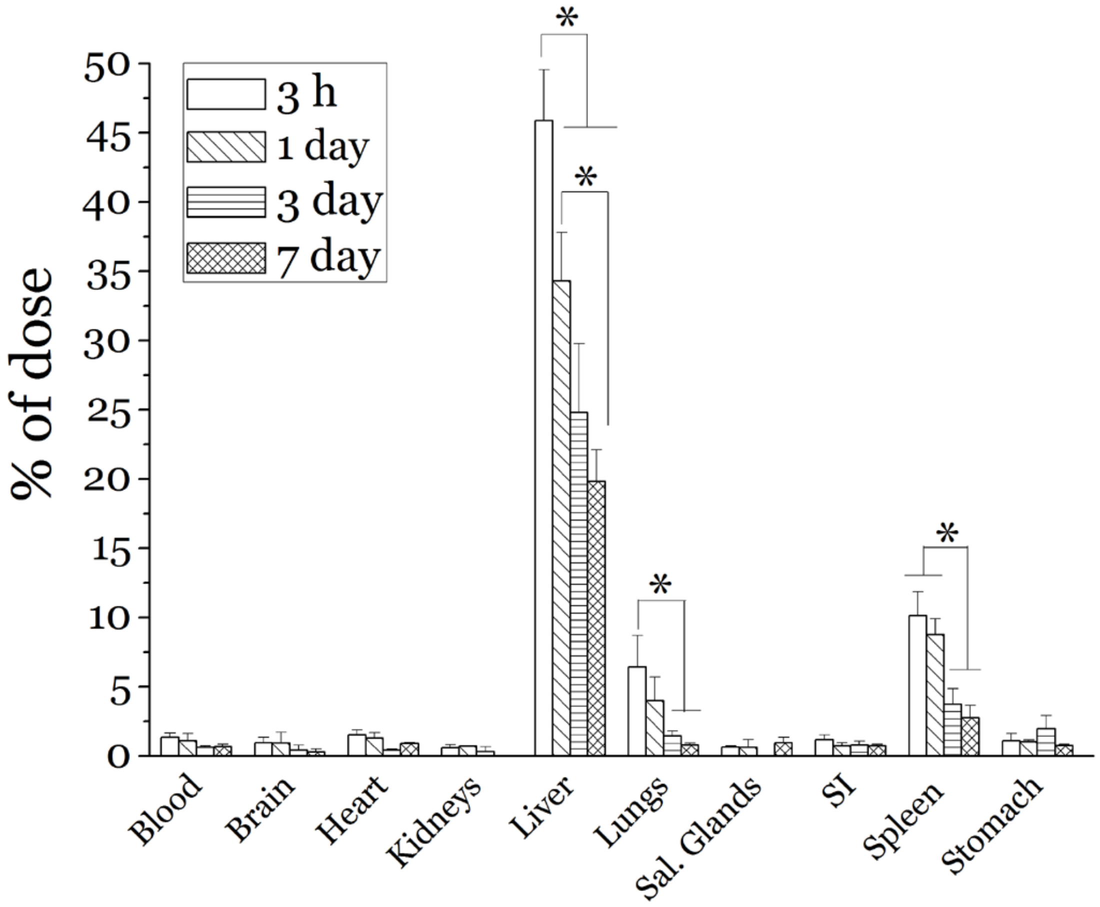

Figure 27. Biodistribution of PLGA nanoparticles of mean size 500nm after intravenous administration. '*' means statistically significant, $p< 0.05$ (n=3; mean ± s.d). SI-Small intestines, Sal. – Salivary.

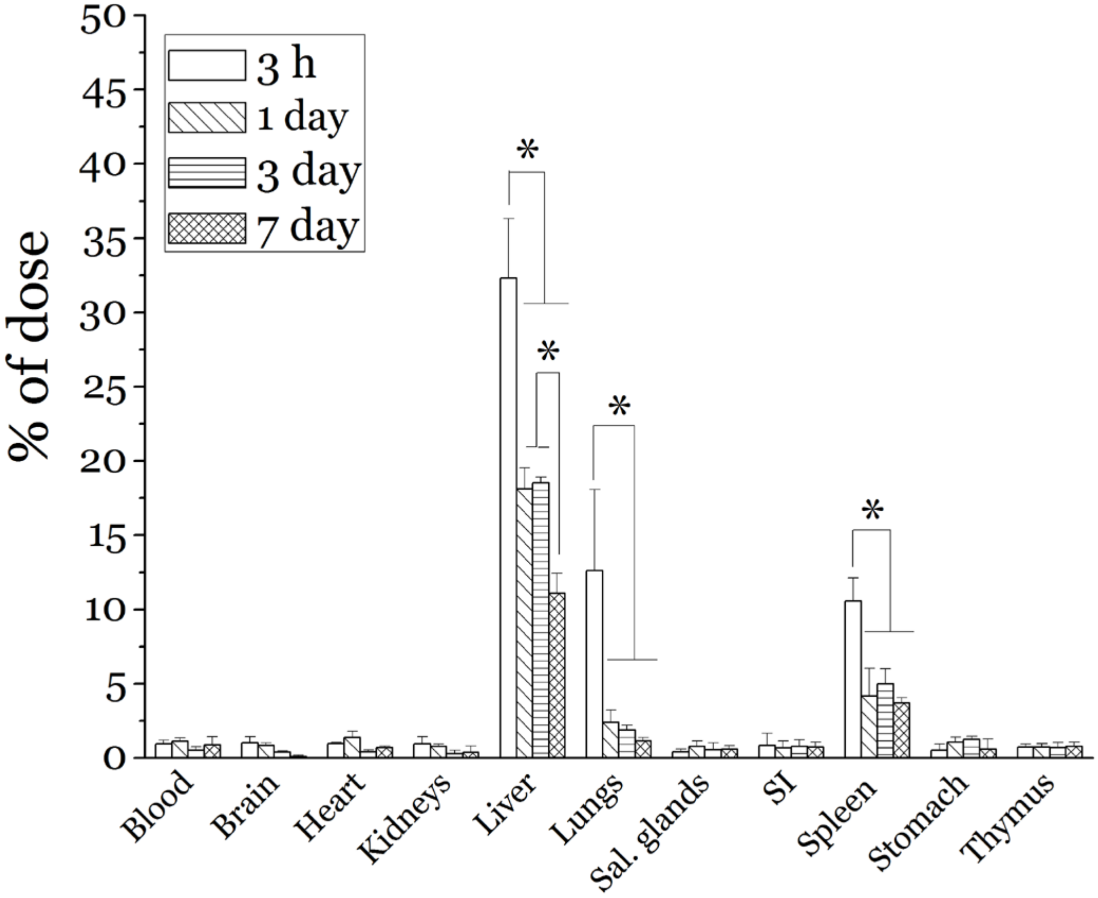

Figure 28. Biodistribution of PLGA nanoparticles of mean size 200 nm after intravenous administration. ‘*’ means statistically significant, $p < 0.05$ (n=3; mean ± s.d).

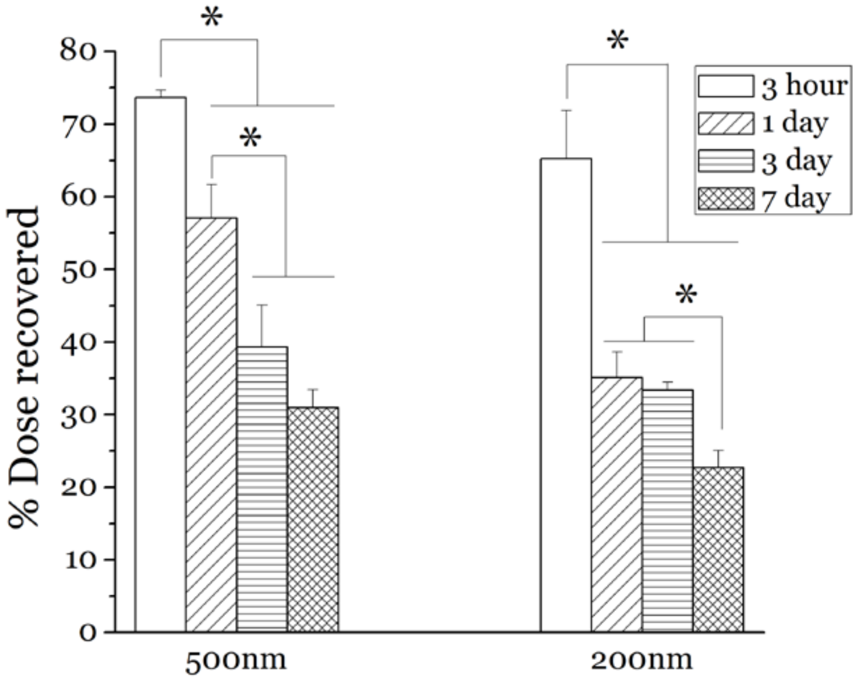

Figure 29. Total amount of nanoparticles detected from all tissues represented as the percentage of the administered dose recovered. ‘*’ means statistically significant, $p < 0.05$ (n=3; mean ± s.d).

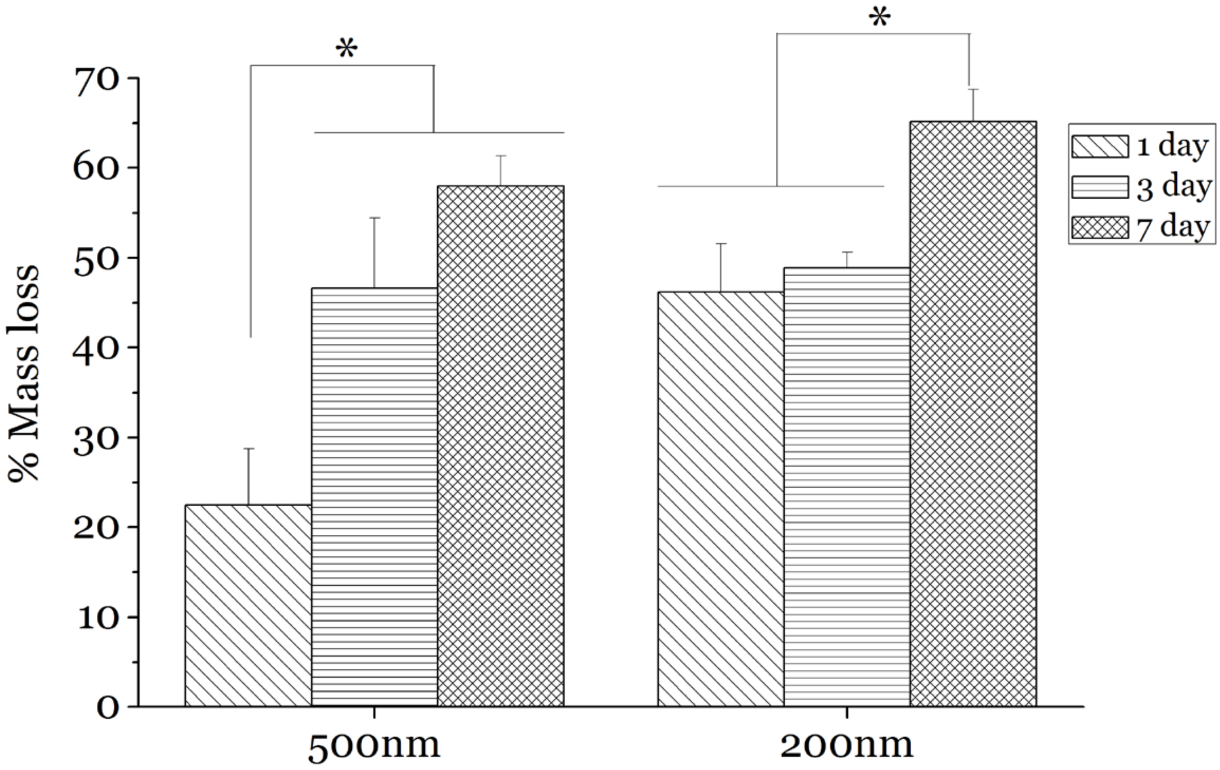

Figure 30. Percent decrease in the total amount of nanoparticles detected from all the tissues at the three time points (1, 3, 7 days) relative to the amount deposited at 3 hours. '*' means statistically significant, p< 0.05 (n=3; mean ± s.d).

Size (nm)	**Tissues**	**Time (h)**	**M_w (Da)**	**M_n (Da)**	**M_p (Da)**	**M_z (Da)**	**PDI**
200	Liver	3	37970±3870	29472±2686	28086±1881	52871±8184	1.29±0.02
		24	37417±4285	29960±4651	24960±5802	48914±3910	1.25±0.05
		72	31192±1925	25321±884	24784±624	40485±5110	1.23±0.04
		168	24116±155	20922±210	15415±2460	28633±590	1.15±0.01
	Spleen	3	35547±4330	22855±6789	35697±1138	52938±1624	1.48±0.22
		24	30891±1601	14228±2180	33361±1087	59964±6107	1.41±0.13
		72	25934±1371	15074±1315	27915±1575	42224±905	1.35±0.06
		168	30318±4058	21386±1183	16439±4957	49348±12776	1.51±0.15
500	Liver	3	36879±4801	29708±3881	27210±1064	48222±7853	1.24±0.02
		24	40427±3742	31728±2200	29139±4253	55697±7987	1.27±0.03
		72	31377±2059	26535±2220	22245±3179	38509±2469	1.18±0.03
		168	23623±169	20272±373	18547±434	28170±345	1.16±0.01
	Spleen	3	39557±3811	27190±4057	34530±2423	58663±8400	1.46±0.11
		24	38111±4371	25213±4552	34166±2283	65864±13231	1.53±0.16
		72	35076±3718	25068±906	27315±2965	52779±10770	1.40±0.10
		168	28153±1816	21155±265	21799±2271	41299±6650	1.33±0.09

Table 6. Molecular weight information of PLGA nanoparticle degradation in the liver and spleen at the respective time points after administration intravenously (n=3; mean ± s.d).

Size (nm)	**r^2**		
	Liver	**Spleen**	***In vitro***
500	0.9233	0.9954	0.9969
200	0.9899	0.9669	0.9606

Table 7. Calculated r^2 values from the plot of Ln(M_w) versus time for the degradation in liver, spleen, and *in vitro* degradation.

Size (nm)	**Rate constant (k) (x 10^{-3})**		
	Liver	**Spleen**	***In vitro***
500	3.1	2.1	3.1
200	2.9	2.8	1.5

Table 8. First order rate constants of degradation of polymer nanoparticles in tissues and *in vitro*. The rate constants were calculated by plotting Ln(M_w) versus time (t) and the data was fitted linearly which then gives slope (k) of the line for each data set.

4.5 Conclusions

In this work, we have successfully shown for the first time the *in vivo* degradation of PLGA nanoparticles in the liver and spleen at several time points after intravenous administration. We have been able to show the differences in PLGA nanoparticle degradation by tissues and by nanoparticle size. We have been able to obtain the degradation data in tissues for parameters such as Mw, Mn, Mz, Mp, and polydispersity index (**table 6**). For the 500 nm size nanoparticles, the *in vivo* degradation in the liver was shown to occur at a slower rate as compared to the *in vitro* degradation. Whereas in the spleen, the rate of degradation was faster than that *in vitro*. For the 200 nm size nanoparticles, the rate of degradation in both the liver and spleen were twice as fast as *in vitro*. Being able to determine the dynamic degradation of nanoparticles in tissues will advance our knowledge of *in vivo* degradation of nanoparticles with regards to properties like size, chemistry, molecular weight etc. Furthermore, from the *in vivo* tissue degradation of nanoparticles and the drug release from nanoparticles in a particular tissue, it would be possible to establish a correlation between polymer degradation and drug release. This will enable the design of nanoparticle drug delivery systems with precisely predictable amounts of drug release in any target tissue. Understanding *in vivo* biodegradation kinetics of polymer nanoparticles will have major implications on drug delivery involving biodegradable polymer nanoparticles and microparticles. This method can further be improved and applied not only to PLGA based delivery devices, but to any degradable polymers used in biological systems. We believe that the combined knowledge of biodistribution and *in vivo* biodegradation of polymeric nanoparticle systems will have a significant impact on the understanding of nanoparticle pharmacokinetics and the dynamic property change of nanoparticles *in vivo*.

Further, the application of this work may aid in the rational design of tailored drug delivery systems to a target tissue where drug release is degradation dependent.

4.6 References

1. Couvreur P, Vauthier C. Nanotechnology: intelligent design to treat complex disease. Pharm Res 2006;23:1417-50.

2. Zolnik BS, Burgess DJ. Effect of acidic pH on PLGA microsphere degradation and release. J Control Release 2007;122:338-44.

3. Panyam J, Dali MM, Sahoo SK, Ma W, Chakravarthi SS, Amidon GL, et al. Polymer degradation and *in vitro* release of a model protein from poly(D,L-lactide-co-glycolide) nano- and microparticles. J Control Release 2003;92:173-87.

4. Wang J, Wang BM, Schwendeman SP. Characterization of the initial burst release of a model peptide from poly(D,L-lactide-co-glycolide) microspheres. J Control Release 2002;82:289-307.

5. Shive MS, Anderson JM. Biodegradation and biocompatibility of PLA and PLGA microspheres. Adv Drug Deliv Rev 1997;28:5-24.

6. Cai Q, Shi G, Bei J, Wang S. Enzymatic degradation behavior and mechanism of poly(lactide-co-glycolide) foams by trypsin. Biomaterials 2003;24:629-38.

7. Pan H, Jiang H, Chen W. The biodegradability of electrospun Dextran/PLGA scaffold in a fibroblast/macrophage co-culture. Biomaterials 2008;29:1583-92.

8. Dunne M, Corrigan OI, Ramtoola Z. Influence of particle size and dissolution conditions on the degradation properties of polylactide-co-glycolide particles. Biomaterials 2000;21:1659-68.

9. Li J, Stayshich RM, Meyer TY. Exploiting Sequence To Control the Hydrolysis Behavior of Biodegradable PLGA Copolymers. J Am Chem Soc 2011.

10. Florence AT, Hillery AM, Hussain N, Jani PU. Nanoparticles as carriers for oral peptide absorption: Studies on particle uptake and fate. Journal of Controlled Release 1995;36:39-46.

11. Markert CL, Hunter RL. The distribution of esterases in mouse tissues. J Histochem Cytochem 1959;7:42-9.

12. Santos CA, Freedman BD, Leach KJ, Press DL, Scarpulla M, Mathiowitz E. Poly(fumaric-co-sebacic anhydride). A degradation study as evaluated by FTIR, DSC, GPC and X-ray diffraction. J Control Release 1999;60:11-22.

13. Deng M, Chen G, Burkley D, Zhou J, Jamiolkowski D, Xu Y, et al. A study on *in vitro* degradation behavior of a poly(glycolide-co-L-lactide) monofilament. Acta Biomater 2008;4:1382-91.

14. Farrar DF, Gillson RK. Hydrolytic degradation of polyglyconate B: the relationship between degradation time, strength and molecular weight. Biomaterials 2002;23:3905-12.

15. Li SD, Huang L. Pharmacokinetics and biodistribution of nanoparticles. Mol Pharm 2008;5:496-504.

16. Korn ED, Weisman RA. Phagocytosis of latex beads by Acanthamoeba. II. Electron microscopic study of the initial events. J Cell Biol 1967;34:219-27.

17. He C, Hu Y, Yin L, Tang C, Yin C. Effects of particle size and surface charge on cellular uptake and biodistribution of polymeric nanoparticles. Biomaterials 2010;31:3657-66.

18. Decuzzi P, Godin B, Tanaka T, Lee SY, Chiappini C, Liu X, et al. Size and shape effects in the biodistribution of intravascularly injected particles. Journal of Controlled Release 2010;141:320-7.

CHAPTER 5

5.1 Introduction

Curcumin, a hydrophobic polyphenol derived from turmeric has been found to have several therapeutic applications especially in many types of cancers [1, 2]. It has been shown to have an inhibitory effect on the proliferation of several cancer cells [3]. However, due to its highly hydrophobic nature which means poor solubility, its bioavailability is poor. Furthermore, it is also rapidly metabolized in the body. As a result of these issues, it has found limited success in the clinic [4]. Recently, a novel curcumin analogue 3, 4-difluorobenzo curcumin also known as Difluorinatedcurcumin (CDF) was sysnthesized by Padhye et. al [5]. The curcumin analogue CDF has shown inhibitory activity in cancer cell lines (especially in pancreatic cancer cells) apart from inducing apoptosis [5]. Furthermore, it has been shown to possess relatively greater bioavailability in systemic circulation and in the pancreas as compared to its precursor curcumin [6].

Since CDF has been shown to be a chemosensitizer for cancer cells, we had envisioned the development of a formulation with co-encapsulation of CDF and doxorubicin (a potent anticancer drug with immunomodulatory potential) for treatment of breast cancer. However, due to the non-availability of the free base form of doxorubicin, we have encapsulated CDF into polymeric nanoparticles made of PLGA with different loading capacities (%w/w) as follows: 24% (F1), 33% (F2), and 38% (F3). Of these four formulations, the formulation F2 was tested for its antiproliferative activity on MDA-MB-231 (breast cancer) and BxPC3 (pancreatic cancer) cell lines. In addition to the formulation F2, the antiproliferative activity of free CDF and empty PLGA nanoparticles was evaluated. The formulation F2 showed potent antiproliferative activity similar to the free CDF. This is notable since at the tested time points, the formulation would only be able to release part of the drug encapsulate. This means that the cell growth inhibition observed from the formulation is only resulting from part of the encapsulate drug being released. Therefore this observation indicates that the encapsulation of CDF into nanoparticles improves the efficiency of CDF in terms of its antiproliferative potential.

5.2 Materials

PLGA (Resomer RG 502H, 50:50) with an inherent viscosity of 0.16-0.24 dL/g was obtained from Boehringer Ingelheim (Germany). CDF was gifted by Dr. Fazlul Sarkar, Department of Pathology, Barbara Ann Karmanos Cancer Center. Poly (vinyl alcohol) of molecular weight 88,000 Da was purchased from Fisher Scientific (USA). All other organic solvents were purchased from fisher scientific and were of HPLC grade.

Breast cancer cell line MDA-MB-231 and pancreatic cancer cell line BxPC-3 were obtained from ATCC (Manassas, VA). Both of these cell lines were maintained in DMEM (Invitrogen, Carlsbad, CA) supplemented with 10% fetal bovine serum (FBS), 100 units/ml penicillin and 100 µg/ml streptomycin. Cells were cultured in a 5% CO_2–humidified atmosphere at 37°C.

5.3 Methods

5.3.1 Formulation of CDF loaded nanoparticles

The CDF loaded nanoparticles were fabricated by the oil-in-water emulsion method. For formulation F1, 50 mg of PLGA and 33.3 mg of CDF was dissolved in 2 ml THF. This solution was added to 10ml of 2% PVA solution, vortexed and then sonicated for 5 minutes at an output of 30 W. This mixture was added to 40 ml of 0.25% PVA solution and left to stir overnight at 600 rpm. The nanoparticles were centrifuged at 40,000 x g for 90 minutes and were then washed with 30ml deionized water thrice following which they were resuspended in 15ml of deionized water, frozen and lyophilized.

For formulation F2, 50mg of PLGA and 21.5 mg of CDF was dissolved in a mixture of 0.5 ml DMSO and 1.75 ml Ethyl acetate. This solution was added drop wise to 4 ml of 4% PVA while the PVA solution was being vortexed at the highest speed setting. This mixture was then sonicated over an ice bath for 3 minutes at an output of 30W. This mixture was then added to 100 ml of 0.25% PVA at 800 rpm overnight on a magnetic stir plate. The nanoparticles were centrifuged at 40,000 x g for 90 minutes and were then washed with 30ml deionized water thrice following which they were resuspended in 15ml of deionized water, frozen and lyophilized.

In the case of formulation F3, 50 mg of PLGA and 33.3 mg of CDF was dissolved in a mixture of 1 ml of Ethyl acetate and 1 ml of DMSO. This mixture was added drop wise to 4 ml of 4% PVA solution while it was being vortexed. The mixture was then sonicated on an ice bath for 3 minutes at an output of 30 W. this was added to 100 ml of 0.25% PVA solution at a stirring speed of 600 rpm overnight.

5.3.2 Determination of drug loading

In order to determine drug loading in the nanoparticle and microparticle formulations, a known amount of the formulation was dissolved in acetone and the absorbance was determined at a wavelength of 360 nm. The drug loading was calculated according to the formula:

Loading = (Amt. of drug in formulation/Total amt. of the formulation)*100

5.3.3 Determination of particle size

The formulations were either sized directly right after preparation or were lyophilized and reconstituted with 1% PVA solution to make 1% w/v dispersion and sonicated for 30-60 seconds in a bath sonicator to disperse the nanoparticles. The dispersion was then subject to size analysis on a 90Plus Particle Size Analyzer (Brookhaven Instrument Corporation). Mean values following 5 runs for each formulation were recorded.

5.3.4 Determination of drug release

A known amount of the formulation was dispersed in PBS containing 2.5% Tween 80 and incubated at 37˚C. Tween 80 was used in the release media as CDF had very poor solubility in water and determination of release was not feasible if the release was conducted in PBS alone. At pre-determined time point of 1, 3, 6, 12, 24, 36 hours, and then 2, 3, 4, 5, 6, and 7 days the sample was centrifuged, supernatant was collected and analyzed by UV spectrometry to determine the amount of drug released. Fresh media (PBS containing 2.5% Tween 80) was replaced with the same volume withdrawn at each time point.

5.3.5 Cell Growth Inhibition studies by MTT assay

The two cancer cell lines were seeded at a density of 3 x 10^3 cells per well in 96-well microtiter culture plates. After overnight incubation, the medium was removed and replaced with a fresh medium containing vehicle control or indicated concentrations of drug. After appropriate incubation (as indicated in the results), 25ml of 3-(4,5-dimethylthiazol-2-yl)-2,5-diphenyltetrazolium bromide (MTT) solution (5mg/ml in phosphate-buffered saline, PBS) was added to each well and incubated further for 2 h at 37°C. Upon termination, the supernatant was aspirated and the MTT formazan, formed by metabolically viable cells, was dissolved in DMSO (100ml). The plates were mixed for 30 min on a gyratory shaker, and the absorbance was measured at 595 nm on Ultra Multifunctional Microplate Reader (TECAN, Durham, NC). Each treatment had eight replicate wells and the mean values are reported.

5.3.6 Cell fixing for confocal microscopy imaging of the cancer cells

MDA-MB-231 and BxPC-3 cells (5 x 10^5) were seeded on collagen-coated cover-slips placed inside 100 mm cell culture dishes. The cells were allowed to attach overnight and the FITC conjugated PLGA nanoparticles were added to the cell cultures the next day at working concentrations of 25 nM, 250 nM and 2.5 μM diluted directly from a 1 mM stock preparation. The incubation with formulations was done for 24 hours. Cover-slips with attached cells were washed twice with warm PBS at the end of incubation time, followed by fixing in 3.7% formaldehyde in PBS for 10 minutes at room temperature. This was followed by two more PBS washes and extraction with 0.1% Triton X-100 in PBS for 5 minutes. Cells were again washed twice with PBS before staining with fluorescent phallotoxin (Invitrogen). For staining, 5 μl methanolic stock of commercial phallotoxin was diluted into 200 μl PBS for each individual cover-slip. Staining was allowed to proceed at room temperature for 20 minutes before washing with PBS two more times. A drop of DAPI was placed on the cover-slips before they were mounted on slides for confocal observations. The confocal imaging was carried out on a Leica TCS SP5 confocal microscope with an inverted lens.

5.4 Results and discussion

Nanoparticles encapsulating curcumin were fabricated with three different loading capacities: 24% (F1), 33% (F2), and 38% (F3) w/w. The size and zeta potential of the nanoparticle formulations is shown in **table 9**. The nanoparticle size for all three formulations was below 500 nm, a size well suited for intracellular uptake. The zeta potential was positive for all formulations and ranged from 1.9 to 7.5 mV. The release profile of the three nanoparticle formulations is represented in **figure 31**. Of the three nanoparticle formulations, the formulation F2 had the fastest rate and highest amount of drug release. Therefore, this formulation was chosen to test its antiproliferative activity on two cancer cell lines: MDA-MB-231 (Breast cancer) and BxPC3 (Pancreatic cancer). From here on, the CDF-loaded nanoparticle formulation F2 will be referred to as CDFNP.

The cell growth inhibition studies show a time dependent and dose dependent effect of the formulation on both the cell lines.

5.4.1 Cell growth inhibition of BxPC3 cells

The antiproliferative effect of free CDF, CDFNP, and empty PLGA nanoparticles on BxPC3 cells was evaluated at the end of 24, 48, and 120 hours of incubation. The IC50 values for each of the formulations are represented in **table 10**.

Figure 32A shows the cell proliferation profile of BxPC3 cells incubated for 24 hours with several concentrations of PLGA (nanoparticle control), CDF, CDFNP respectively. The blank PLGA nanoparticles have little to no toxicity on the cells at this time point. The CDF and CDFNP show a similar antiproliferative effect at all concentrations used. There is a concentration dependant antiproliferative effect displayed by both the free CDF and CDFNP.

The activity of the free CDF and CDFNP after 48 hours of incubation is represented in **figure 32B**. At this time point, at CDF concentrations of 0.15 µM and higher, the antiproliferative effect of both the CDF and CDFNP increased significantly as compared to that at 24 hours. The IC_{50} for free CDF was 0.53 µM and that for CDFNP was 0.74 µM. Though the IC_{50} for CDFNP is higher than that for free CDF, it is to be noted that only about 57% of the encapsulated drug is released from the nanoparticle formulation as per the *in vitro* release profile. Therefore, the cell growth inhibition resulting from the CDFNP is remarkable as it takes much less free drug to elicit a similar antiproliferative response in the cancer cells when the drug is encapsulated in nanoparticles. In other words the encapsulation of CDF in nanoparticles improves the efficiency of the antiproliferative ability of CDF.

At the end of 5 days, the inhibitory activity of both the CDF and CDFNP was more pronounced wherein more than 90% of the cell population was killed at a CDF concentration of

0.5 µM and above. The IC_{50} for free CDF was 0.09 µM whereas for the PLGA encapsulated CDF it was 0.12 µM. It is noteworthy that for the free CDF, the growth inhibition after a concentration of 0.25 µM remains the same for all higher concentrations after that. However, for the nanoparticle encapsulated CDF, the cell killing effect keeps increasing up to the concentration of 2.5 µM in a concentration dependent manner. This highlights the importance and advantage of encapsulating the drug in nanoparticles where they release the drug over an extended period of time thereby resulting in better antiproliferative activity as compared to free drug, especially over extended periods of time.

5.4.2 Cell growth inhibition of MDA-MB-231 cells

Similar cell growth inhibition studies as that on the BxPC3 cells were conducted on the breast cancer cells, MDA-MB-231. In general there was a concentration dependent increase in the antiproliferative activity observed wherein with a increase in the drug concentration there was an increase in the cell growth inhibitory activity. The IC_{50} values are displayed in **table 11**. The empty PLGA nanoparticles had insignificant to no effect on the cell proliferation at the tested time points.

When compared to the BxPC3 cells, the MDA-MB-231 cells have higher IC_{50} values at all concentrations for both the CDF and CDFNP. This indicates that the BxPC3 cells are more responsive to treatment with CDF as compared to the breast cancer cells.

Figure 33A shows the antiproliferative activity of CDF, CDFNP, and empty PLGA nanoparticles when incubated with MDA-MB-231 cells. The empty PLGA nanoparticles show no antiproliferative activity on these cancer cells. The free CDF shows a concentration dependent antiproliferative activity wherein with an increase in the drug concentration there is an increase in the antiproliferative activity. Similarly, the CDFNP shows concentration dependant antiproliferative activity though after a concentration of 0.75 μM there is no significant increase in cell growth inhibition with an increase in concentration. One possible reason for this observation with the CDFNP could be that at this early time point there might not be a significant polymer degradation occurring due to which the drug release from nanoparticles might be similar. The IC$_{50}$ for free CDF was 1.66 μM whereas for the CDFNP it was 0.87 μM. The fact that only 43% of the drug is released at this time point further highlights the improved potency of the drug when encapsulated in PLGA nanoparticles. Taking this into consideration the actual IC$_{50}$ for the CDFNP will be less than 0.87 μM. In either case, at this time point the IC$_{50}$ value for the CDFNP is much less as compared to free CDF.

At the end of 48 hours, the antiproliferative activity of both the CDF and CDF encapsulated nanoparticles is further increased as can be seen from **figure 33B**. At this time point the IC$_{50}$ for free CDF is 0.47 μM whereas for the CDFNP it is 0.74 μM. There is a concentration dependent and a time dependent antiproliferative effect of the free CDF and CDF loaded nanoparticles on the breast cancer cells. At this time point the IC$_{50}$ values for CDF and CDFNP decrease as compared to that for 24 hours.

The antiproliferative potential further increased upon incubation for 5 days. As shown in **figure 33C**, after a concentration of 0.25 μM there is no significant increase in the antiproliferative activity with the CDF, however for the CDFNP the antiproliferative effect increases with concentration all the way up to the highest concentration of 2.5 μM. This observation suggests that the drug when encapsulated in nanoparticles due to its release over time produces effective antiproliferative activity as compared to free CDF. In the case of free CDF, after the concentration of 0.25 μM, any higher amount of free drug did not improve the antiproliferative activity implying that higher drug amounts does not add to the improvement in antiproliferative activity. However when encapsulated in nanoparticles, the same excess of drug results in a continued increase in antiproliferative activity. This highlights the advantage of drug encapsulation in nanoparticles with regards to its improvement in antiproliferative effect

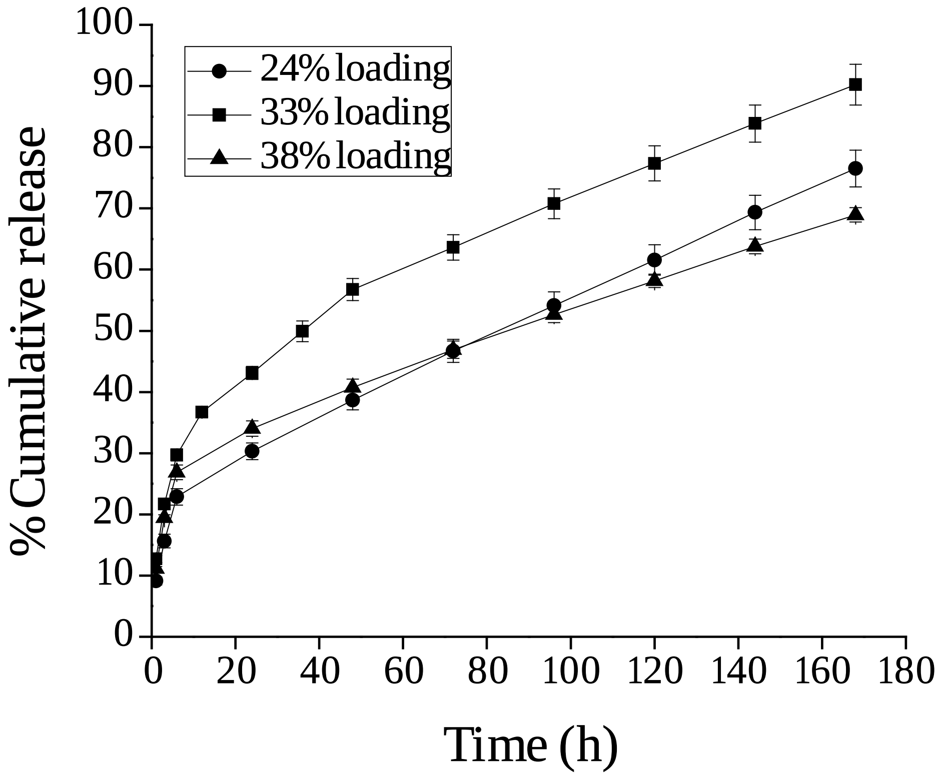

Figure 31. The cumulative release of CDF from PLGA nanoparticle formulations with three different loading capacities (n=3; mean±s.d.).

A)

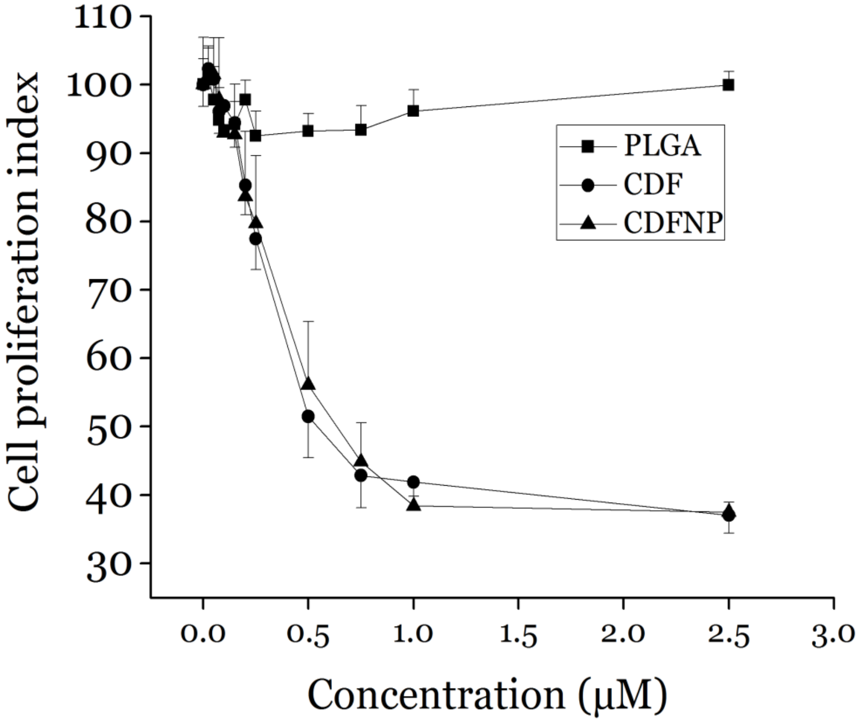
Cell proliferation index
110
100
90
80
70
60
50
40
30
0.0
0.5
1.0
1.5
2.0
2.5
3.0
Concentration (μM)
PLGA
CDF
CDFNP

B)

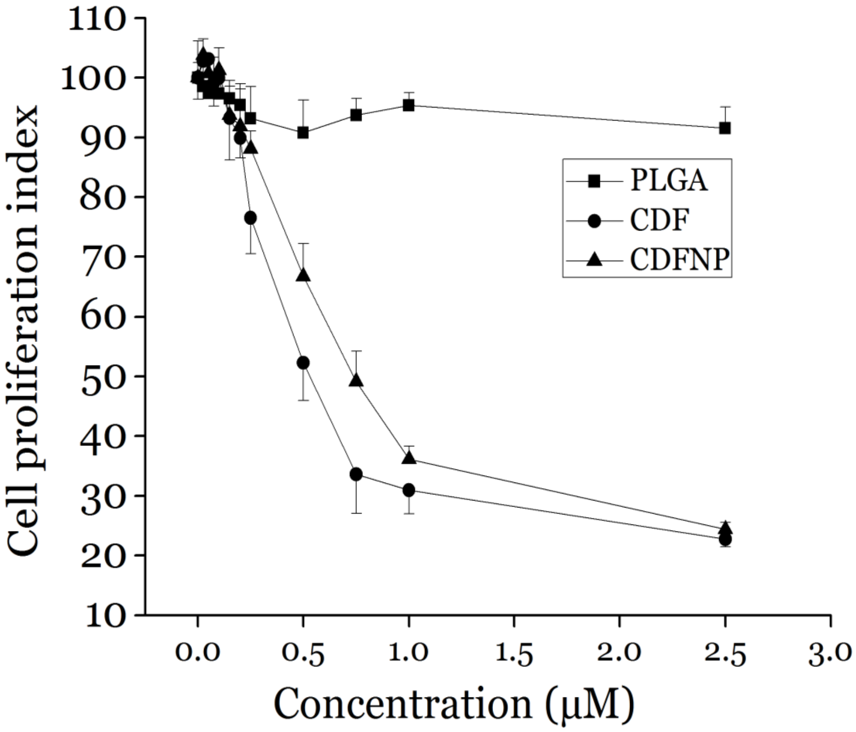
Cell proliferation index
110
100
90
80
70
60
50
40
30
20
10
0.0
0.5
1.0
1.5
2.0
2.5
3.0
Concentration (μM)
PLGA
CDF
CDFNP

C)

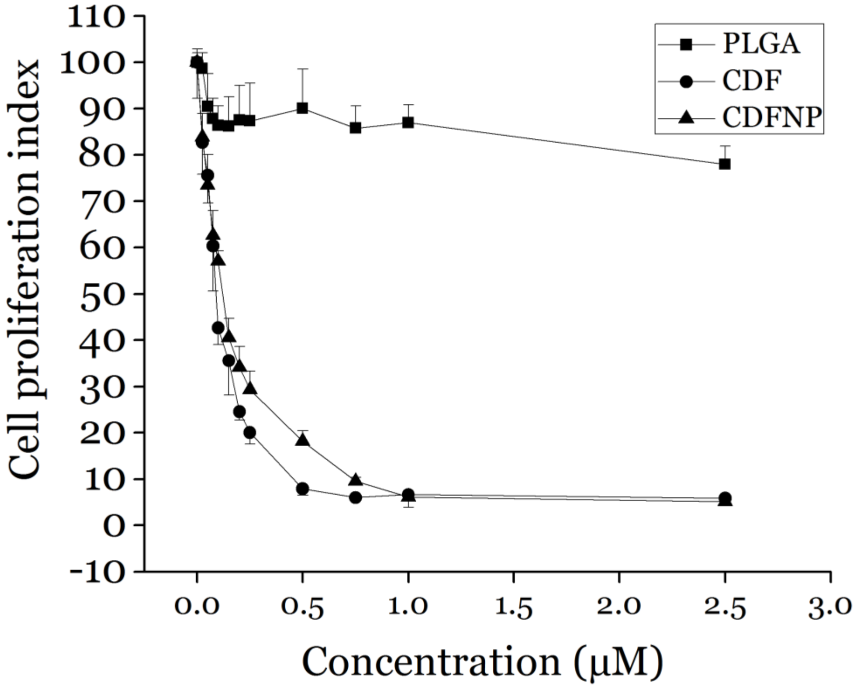

Figure 32. Cell proliferation profile of BxPC3 cells (pancreatic cancer cell line) upon incubation with PLGA nanoparticles, free CDF, and CDFNP at the end of (A) 24 hours (B) 48 hours, and (C) 5 days (n=8; mean±s.d.). Empty PLGA nanoparticles (PLGA) were used as nanoparticle control to assess the toxicity of the carrier itself.

A)

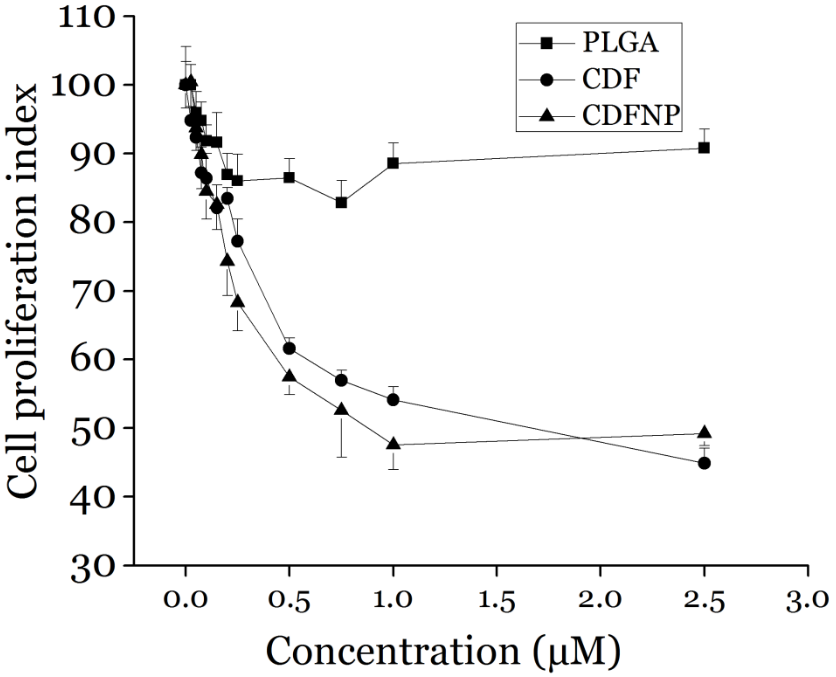
PLGA
CDF
CDFNP
Cell proliferation index
110
100
90
80
70
60
50
40
30
0.0
0.5
1.0
1.5
2.0
2.5
3.0
Concentration (µM)

B)

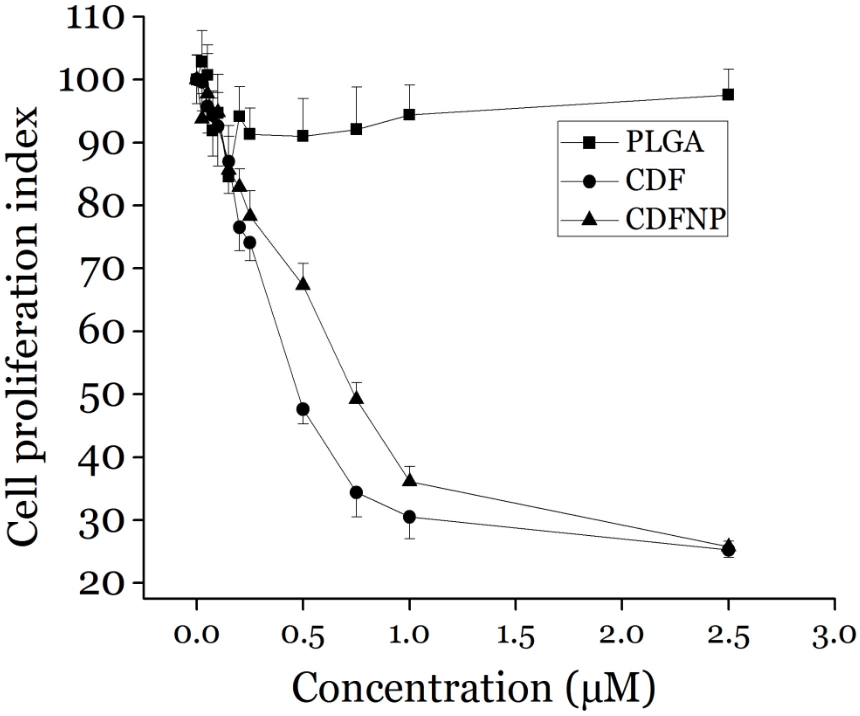
PLGA
CDF
CDFNP
Cell proliferation index
110
100
90
80
70
60
50
40
30
20
0.0
0.5
1.0
1.5
2.0
2.5
3.0
Concentration (µM)

C)

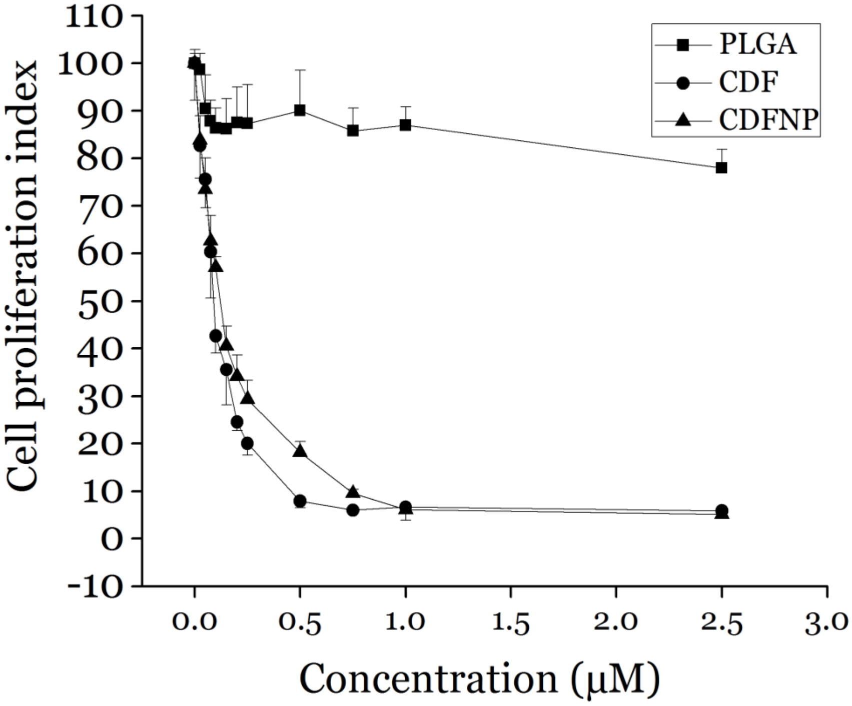

Figure 33. Cell proliferation profile of MDA-MB-231 cells (breast cancer cell line) upon incubation with PLGA nanoparticles, free CDF, and CDFNP at the end of (A) 24 hours (B) 48 hours, and (C) 5 days (n=8; mean±s.d.). Empty PLGA nanoparticles (PLGA) were used as nanoparticle control to assess the toxicity of the carrier itself.

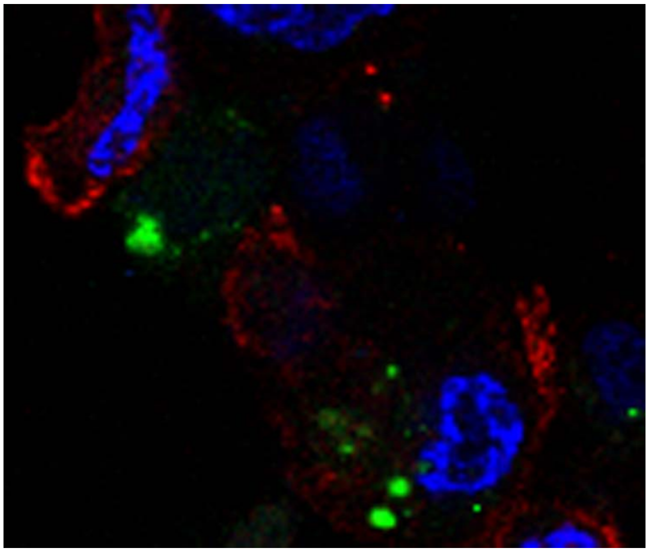

Figure 34. Confocal microscopy image of MDA-MB-231 cells after incubation with FITC conjugated PLGA nanoparticles (green fluorescence) for 24 hours. The cell nuclei were labeled with DAPI and the cytoskeleton of the cell was labeled red with Rhodamine-Phalloidin. The green fluorescence pertains to the FITC-conjugated PLGA nanoparticles.

Formulation	Loading (%w/w)	Size (nm)	Zeta potential (mV)
F1	24%	362.7±29.1	1.93±2.77
F2	33%	283.3±13.2	7.45±2.09
F3	38%	415.7±17.2	6.11±4.03

Table 9. Size and zeta potential measurements of the nanoparticle formulations encapsulating CDF with different loading capacities.

Time (h)	IC_{50}(μM)	
	CDF	**CDFNP**
24	0.54	0.63
48	0.53	0.74
120	0.09	0.12

Table 10. IC_{50} values of CDF and CDF-loaded PLGA nanoparticles (CDFNP) against BxPC3 cells (pancreatic cancer).

Time (h)	IC_{50} (μM)	
	CDF	**CDFNP**
24	1.66	0.87
48	0.47	0.74
120	0.15	0.22

Table 11. IC_{50} values of CDF and CDF-loaded PLGA nanoparticles (CDFNP) against MDA-MB-231 cells (breast cancer).

5.5 Conclusions

The novel curcumin analogue, CDF was encapsulated in PLGA nanoparticles with different loading capacities of 24%, 33%, and 38%. *In vitro* release studies were performed in which the formulation with 33% loading showed the fastest rate and the highest amount of drug release compared to the other formulations. This formulation was chosen to test its antiproliferative potential on BxPC3 cells (pancreatic cancer) and MDA-MB-231 cells (breast cancer). The pancreatic cancer cells were more sensitive to drug treatment as compared to the breast cancer cells. This is evident from the IC_{50} values of the free CDF and the CDFNP.

In both the cell lines there was a clear time- and concentration-dependent cell growth inhibition. In case of the BxPC3 cells, free CDF had a IC_{50} value less than that for the CDF encapsulated nanoparticles. However, it is to be noted that at the time points tested, only a part of the drug is released from the nanoparticles. Therefore, the cell killing that is observed is from the released drug and not the total amount that was encapsulated. With this fact taken into consideration, the actual IC_{50} value of the CDFNP is less than the calculated value from the cell proliferative index profile. The same holds true for the IC_{50} values of the CDFNP with respect to breast cancer cells. The free drug had shown a saturation antiproliferative effect where after a certain concentration there was no enhancement in the antiproliferative activity whereas with the CDFNP, there was a continual increase in the antiproliferative effect with an increase in concentration. This underscores the advantage of drug encapsulation in nanoparticles where the drug is released slowly over a period of time, thereby increasing the antiproliferative potential of the drug in this case. Furthermore, the confocal microscopy images of the FITC labeled PLGA nanoparticles incubated with MDA-MB-231 cells show the nanoparticles present in the cells (**figure 34**). This suggests that the CDFNP are likely being internalized by the cells thereby resulting in improved antiproliferative efficiency by way of releasing the drug intracellularly though some drug may be released extracellularly. Taken together, the data from this work clearly emphasizes the advantage of nanoparticle encapsulated drug delivery of CDF to improve the potency and efficiency of the drug reflected by its antiproliferative activity. Based on the excellent activity of CDF in the cancer cell lines, a future goal of the lab is to encapsulate CDF plus doxorubicin and study the degradation and pharmacokinetics for development of this formulation for application in an *in vivo* model of metastatic breast cancer by pulmonary administration.

5.6 References

1. Anand P, Sundaram C, Jhurani S, Kunnumakkara AB, Aggarwal BB. Curcumin and cancer: an "old-age" disease with an "age-old" solution. Cancer letters. 2008;267:133-64.

2. Srivastava RM, Singh S, Dubey SK, Misra K, Khar A. Immunomodulatory and therapeutic activity of curcumin. International immunopharmacology. 2011;11:331-41.

3. Ravindran J, Prasad S, Aggarwal BB. Curcumin and cancer cells: how many ways can curry kill tumor cells selectively? The AAPS journal. 2009;11:495-510.

4. Anand P, Kunnumakkara AB, Newman RA, Aggarwal BB. Bioavailability of curcumin: problems and promises. Molecular pharmaceutics. 2007;4:807-18.

5. Padhye S, Yang H, Jamadar A, Cui QC, Chavan D, Dominiak K, et al. New difluoro Knoevenagel condensates of curcumin, their Schiff bases and copper complexes as proteasome inhibitors and apoptosis inducers in cancer cells. Pharmaceutical research. 2009;26:1874-80.

6. Padhye S, Banerjee S, Chavan D, Pandye S, Swamy KV, Ali S, et al. Fluorocurcumins as cyclooxygenase-2 inhibitor: molecular docking, pharmacokinetics and tissue distribution in mice. Pharmaceutical research. 2009;26:2438-45.

CHAPTER 6

CONCLUSIONS AND FUTURE DIRECTIONS

It is well established in the literature that the lungs are permeable to proteins and small molecules, however, few studies systematically investigate the pulmonary biodistribution of nanoparticles from a drug delivery standpoint. The first specific aim of my work focused on the extrapulmonary transit of polystyrene nanoparticles and their biodistribution throughout the body, following administration to the lungs via pharyngeal aspiration. This research has uncovered the possible potential of nanoparticle-based pulmonary drug delivery systems for several important therapeutic applications. From these studies, it is evident that nanoparticle translocation out of the lungs occurs in a size dependent and a time dependent manner. Interesting kinetics are observed, wherein large size (900 nm) nanoparticles have a higher total uptake at the early time point of 1 hour whereas the 50 nm size nanoparticles had the highest total uptake at 5 hours. Biodistribution studies demonstrate that a greater percentage of nanoparticles deposit in the lymph nodes surrounding the neck and thoracic region, however some deposition is also observed in the spleen and heart. Lymph node deposition was also found to occur in a size dependent manner, wherein the smallest nanoparticles deposited in larger amounts at the end of 5 hours as compared to the larger sized nanoparticles. This finding is of great interest due to the role lymph nodes are known to play in generation of immune response. Therefore, the observation of nanoparticle transit to lymph nodes might be of potential interest for effectively administering vaccine based therapies. Additionally, axillary lymph nodes (involved in metastatic spread of breast cancers) were found to have the highest nanoparticle deposition compared to all lymph nodes investigated. Therefore, pulmonary delivery of nanoparticle-based anti-cancer drugs may serve as an effective alternative in the treatment of metastatic breast cancers with nodal involvement.

Though this study has highlighted the extrapulmonary biodistribution potential of nanoparticles after administration to the lungs. The study would be far from complete with regards to a translational perspective without studies looking at the tissue degradation of polymeric nanoparticle systems. Moreover, in this study, polystyrene nanoparticles were used to investigate nanoparticle translocation from the lungs. However, for purposes of drug delivery, a biodegradable nanocarrier system is desired. For this purpose, PLGA is one of the most widely used biodegradable polymers for drug delivery applications. The degradation of PLGA plays an important role in the release of drug from the nanoparticle system. Therefore, knowledge of the *in vivo* tissue degradation characteristics of PLGA nanoparticles is necessary in order to design effective drug delivery systems with predictable drug release properties. Therefore, my second specific aim was to investigate the *in vivo* tissue degradation and distribution of 200 nm and 500 nm PLGA nanoparticles. The *in vitro* degradation of the PLGA nanoparticles suggests that it follows a first order degradation pattern as observed from the data fit with good regression coefficient (>0.9) in the equation for first order degradation. Interestingly, the degradation *in vivo* in the liver and spleen also reflected a first order process. However, differences were observed in the rate of degradation *in vivo* as compared to that *in vitro* in liver and spleen for 200 nm and in spleen for 500 nm nanoparticles. Additionally, this research revealed differences in nanoparticle degradation among the tissues (liver and spleen) for each size apart from giving information about the degradation in tissues over time. Knowledge of the rate and extent of polymer degradation in tissues has significant implications in the design of polymer based drug delivery systems, as it provides a quantitative means indicative of a predictable drug release thereby resulting in improvement of treatment efficacy.

CDF encapsulated PLGA nanoparticles (CDFNP) were formulated and tested for their activity in two cancer cell lines which formed the specific aim 3. CDF when encapsulated into PLGA nanoparticles has shown better activity as compared to free CDF in both the cell lines. The activity of CDF encapsulated PLGA nanoparticles results from only part of the encapsulated drug that is being released at the specific time points. Taking this into consideration, the results suggest that encapsulation of CDF into PLGA nanoparticles improves the activity of the drug considerably. Based on the effectiveness of CDFNP, it would be worthwhile to co-encapsulate CDF and doxorubicin into PLGA nanoparticles for improved anticancer activity. Therefore, results from the third specific aim set the stage for the development of PLGA nanoparticles encapsulating CDF and doxorubicin as a combination treatment in an *in vivo* model of metastatic breast cancer.

On the whole, our work investigating the extrapulmonary transit of nanoparticles has significant implications in several clinically relevant pathologic conditions such as breast cancer with nodal involvement (specifically ALN), lymph node related disorders and in vaccine delivery. This body of work provides a platform for investigating a new approach in the treatment of metastatic breast cancer achieved by targeted lymph node delivery of the active agent post pulmonary administration. Specifically, results from this work will be used in the future to investigate the pulmonary administration of PLGA nanoparticles encapsulating CDF and doxorubicin in an animal model of metastatic breast cancer.

Finally, based on knowledge gained from all my work, I hope that an effective drug delivery system can be designed in order to achieve lymph node deposition and subsequent cytotoxic and immunomodulatory effect following administration from the lungs. I believe that this work has provided a possible new insight into metastatic breast cancer therapy in addition to providing a platform for a robust and calculated design of polymeric nanoparticle delivery systems intended to achieve the desired and pre-determined performance characteristics from a therapeutic standpoint.

ABSTRACT

INVESTIGATION OF THE ABSORPTIVE POTENTIAL OF POLYMERIC NANOPARTICLES ACROSS THE LUNGS AND THEIR DEVELOPMENT FOR EFFICIENT SYSTEMIC DELIVERY FOLLOWING PULMONARY ADMINISTRATION

by

ABDUL KHADER MOHAMMAD

August 2012

Advisor: Dr. Joshua Reineke

Major: Pharmaceutical Sciences

Degree: Doctor of Philosophy

The lungs are an attractive route for drug delivery due to their high epithelial surface area available for absorption, a thin epithelium and extensive vasculature to name a few. Accordingly, a vast number of small molecule drugs, peptides, and proteins have been used to investigate their translocation across the lungs with many of the tested candidates showing excellent pharmacokinetics following pulmonary administration. Findings from all these studies over the years have strongly established the lungs as a route for drug delivery of small molecules and proteins. Nanoparticles on the other hand have gained increasing interest in drug delivery due to the wide variety of advantages they possess that allow for temporal, spatial and targeted delivery of therapeutics that can be fine tuned for various applications. Further, the pulmonary administration of polymeric nanoparticle based drug delivery systems is of great interest for both systemic and localized therapies. However, little is understood about the relationship between nanoparticle size and its effect on pulmonary absorption from a drug delivery perspective. Therefore the aim of this study was to investigate the effect of nanoparticle size on their

biodistribution from lungs after pulmonary administration with a special emphasis on their lymph node distribution. Interesting observations were made wherein polystyrene nanoparticles demonstrated significant translocation out of the lungs into extrapulmonary organs. Nanoparticles predominantly deposited in the regional lymph nodes surrounding the lungs as compared to that in other tissues. Furthermore, lymph node deposition of nanoparticles occurred in a time dependent and size dependent manner. The smallest size nanoparticles (50 nm) demonstrated the highest lymph node deposition among all sizes tested and increased with time. Results from this study suggest that nanoparticles may potentially be employed in the treatment of lymph related diseases following pulmonary administration.

AUTOBIOGRAPHICAL STATEMENT

Education:

- PhD Pharmaceutics, June 2012, Wayne State University, Pharmaceutical Sciences Detroit, MI.
- Bachelor of Pharmacy (Honors), June 2006, Birla Institute of Technology and Science, Pilani, India.

Awards:

- Graduate Exhibition, 2nd place poster, Wayne State University, 2010
- Summer Dissertation Fellowship, Wayne State University, 2011
- NOBCChE Travel Award, NOBCChE Conference, 2011

Publications:

- **Abdul Khader Mohammad**, John Maxwell Mazzara, Joshua James Reineke. Lymph accumulation of polystyrene nanoparticles following pulmonary administration. *Submitted*.
- **Abdul Khader Mohammad** and Joshua Reineke. Detecting *in vivo* tissue degradation of PLGA nanoparticles following intravenous administration. *Submitted*.
- **Abdul Khader Mohammad** and Joshua James Reineke. Effect of Surfactant HLB and phase on nanoparticles fabricated by phase inversion. *Submitted*.
- **Abdul Khader Mohammad** and Joshua James Reineke. Quantitative nanoparticle organ disposition by gel permeation chromatography. In: Methods in Nanotoxicology. *In Press*
- Balaji Bharatwaj, **Abdul Khader Mohammad**, Radovan Dimovski, Fernando L Cassio, Reinaldo Bazito, Denise Conti, Joshua Reineke, and Sandro R. P. da Rocha. Dendrimer Nanocarriers for transport modulation across the pulmonary epithelium. *Ready to submit*.